

**AUTOMATIC CHARACTERIZATION OF LUNG AIRWAYS BASED
ON CT IMAGES**

AN AUTOMATIC METHOD
FOR
THE CHARACTERIZATION OF LUNG AIRWAYS
BASED ON CT IMAGES

BY
MOHAMMADREZA HEYDARIAN FIROUZ ABADI, M.Sc., B.Eng.

A Thesis
Submitted to the school of Graduate Studies
in Partial Fulfillment of the Requirements
for the Degree
PhD

McMaster University

© Copyright by Mohammadreza Heydarian, September 2009

PhD (2009)

McMaster University

(Computer Science)

Hamilton, Ontario

TITLE: An Automatic Method for the Characterization of Lung Airways based on CT
Images

AUTHOR: Mohammadreza Heydarian Firouz Abadi, M.Sc.

SUPERVISORS: Dr. Skip Poehlman and Dr. Markad Kamath

NUMBER OF PAGES: xii, 100

Abstract

Disease identification is one of the most important aspects of a physician's duties. Radiologists play a very important role in disease recognition based on the increasing use of diagnostic images. Nowadays, medical scanning devices such as MRI and CT produce thousands of images per patient which makes the radiologist's job even more onerous; indeed radiologists look at approximately 50,000 images per day leading to fatigue and a higher probability for missing smaller lesions. Therefore it is critical to assist radiologists in their duties.

In this PhD work, research is focused on developing segmentation-based mathematical algorithms and computer programs for automatically characterizing lung CT images. There are two kinds of segmentation methods; the first group contains the methods that find edges of all objects in the image and the second group contains the methods that focus on one object in the image. By assessing many segmentation methods and based on the concept of this project, the *level set method*, from the second group, has the capability to accurately find the boundary of an object in medical images. Although this method does not need any threshold for segmenting an object in an image, it does require the setting of seven parameters. Genetic algorithms were employed to optimize seven parameters of the *level set method* for use as a boundary detection method. A streamlined automatic mechanism, essential for successful and fast segmenting processes, provided the *level set method* with a good initial contour.

This segmentation step was fundamental for further measurements such as bronchial lumen diameter and wall thickness measurement. The developed program automatically measures airway lumen diameter with exceptional repeatability. Also, by simulating manual methods used by radiologists for measuring luminal wall thickness, the automated fitting method consistently finds the wall thickness at the thinnest part, minimizing partial volume problems. The current standard for measuring luminal wall thickness is the full-width at half-maximum method. The technique formulated here is more accurate and reproducible and can be performed automatically.

To find the lumen airway tapering, in order to recognize some prominent lung diseases, a method for tracing of an airway through various CT slices was developed. These measurements are of critical importance in the understanding of a number of lung diseases including asthma and COPD; this tracing step was fundamental for bronchial bifurcation angle measurement. This tracing method was extended to detect and follow bifurcation branches. Then, an estimation method for finding a fitted line through airway center points was developed. For the last portion of this PhD work an approach for measuring lung airway bifurcation angle from CT datasets, which is important in lung diseases such as asthma, was created.

The current goal, characterizing lung CT images, was achieved as a working form of this software development. This mathematical approach has been shown to be accurate with phantom studies. The ultimate goal of this work was to develop software for recognizing key lung diseases and to compare serially (weeks or months apart) acquired images to assess any progress, regression, or stability in a disease.

ACKNOWLEDGEMENTS

First of all, I would like to sincerely thank my supervisors, Dr. Skip Poehlman and Dr. Markad Kamath, for all their support academically and personally. They not only provided technical guidance and understanding during the course of my research but also provided direction for my personal development. I would also thank Dr. Mike Noseworthy, a member of my supervisory committee, who provided a great opportunity for me to be as a member of his lab (IRC), which makes my interdisciplinary research more sensible and reachable. I would also like to thank other members of my supervisory committee, Prof. Tamas Terlaky, Prof. Ivan Bruha, and Dr. Jan Modersitzki, who provided invaluable tips whenever we had the chance to talk about my research.

I owe a great gratitude to Dr. Colm Boylan, who was a true mentor during this entire project. Although he was very busy with his clinical tasks, he spent a great deal of time explaining the research aims from a radiologist's perspective, and for providing me with real medical images from patients. Also thanks to Prof. Myrna Dolovich who helped familiarize me with the respiratory system, from an engineering point of view, and for updating me with new articles in this field.

I would also like to thank all MRI and CT technologists at Imaging Research Center. A special thank you to Jay Neadles, Cheryl Contant, Janet Burr and Steve Madison. Thank you also to Norm Konyer who provided a great deal of help, especially with making phantoms.

I would also like to thank my lab mates at ACsG: Nicholas, David, Asghar, and Jie, and my lab mates at IRC: Graeme, Sergei, Ali, Alyaa, Adrian, Paul, Gavin, Aravinthan, Andrew, Oilei, Peter, Mohammed, Brendan, and Jeff, who shared their own experiences and helped me answer the many questions I asked. I would also like to thank all my friends and compatriots, especially Ali, Eissa, Mohammadali, Mahnaz, Nima, Reza, and Hossein, who helped me get familiar with living in Canada, from the time that I started my study here.

I must also thank the staff at CAS, especially Laurie who always helped out with any administrative problems. Thanks also to Dr. Sartipi whose advice was helpful for completing the comprehensive exam and for continuing my research.

Last, but definitely not least, there are those to whom I simply cannot express my gratitude in words. My wife, parents, sister, nephew, niece, father in law, mother in law, brothers in law, and sisters in law have always provided encouragement and a belief in my abilities; which has enabled me to pursue my studies. My wife and my parents sacrifice and hard work is the reason for my successful achievements. My appreciation for them is unending. Also thanks to my wife Fatemeh and my little boy Arvin, who made home a lovely and beautiful place to live. Their emotional support made me a strong man to pursue my research and achieve good results. I want to thank each one of you for being there for me and for the encouragement that you provided (and still do). I am truly grateful for all your support. Thank you.

It is impossible to provide an exhaustive list of all the other people with whom I have had the pleasure of interacting with during the completion of my studies. I would like to thank all of them for the unique ways in which they helped.

To my wife Fatemeh and my little boy Arvin

Table of Contents

Chapter 1: Introduction	1
Chapter 2: Medical Image Processing	4
2.1: Computed Tomography (CT)	4
2.2: Magnetic Resonance Imaging (MRI)	4
2.3: Segmentation (Clustering)	6
2.4: Classification	7
2.5: Filtering	7
2.6: Registration	8
2.7: DICOM Standard	9
2.8: Some examples of comparing serial images in time	9
References	10
Chapter 3: Using Artificial Intelligence in Medical Image Processing	11
3.1: Expert Systems	11
3.1.1: Introduction	11
3.1.2: Applications	13
3.2: Fuzzy Logic	14
3.2.1: Introduction	14
3.2.2: Applications	15
3.3: Genetic Algorithms	16
3.3.1: Introduction	16
3.3.2: Applications	17
References	18
Chapter 4: Optimizing the Level Set Method using Genetic Algorithm	21
4.1: Overview on Article	21
4.2: Optimizing the Level Set Algorithm for Detecting Object Edges in MR and CT Images	22
4.3: Summary to article	45
Chapter 5: Measuring Airway Luminal Diameter and Wall Thickness	46
5.1: Overview on Article	46
5.2: A Multi.step Algorithm for Measuring Airway Luminal Diameter and Wall Thickness on Lung CT Images	47
5.3: Summary to article	71
Chapter 6: Measuring Angle of Lung Airway Branches	74
6.1: Overview on Article	74
6.2: A Morphological Algorithm for Measuring Angle of Airway Branches in Lung CT Images	75
6.3: Summary to article	93

Chapter 7: Conclusion and Future Work	94
7.1: Introduction	94
7.2: Knowledge Base System	95
7.3: Suggestions for Future Work	97
7.4: summary	99

List of Illustrations, Charts, Diagrams

Chapter 3:

Fig. 1: Complete structure of a rule-based expert system	13
--	----

Chapter 4:

Table I: Different sets of parameter to set the level set method. The first three rows are from [12] and the rest are the result of GA	24
--	----

Table II: The range of the parameters for the level set method (derived from Li <i>et al.</i> 2005 [12]). k is used to calculate μ	25
--	----

Fig. 1: A flowchart of the software system that uses a GA to optimize the parameters of the level set method	26
--	----

Fig. 2: An example of an evaluation function to show the progress of the genetic algorithm	31
--	----

Fig. 3: Plot A shows the progress of the genetic algorithm with 19 individuals in the population. Plot B shows the progress of our dynamic genetic algorithm with 27 individuals in the population	32
--	----

Fig. 4: The MR image on the left (A) shows the initial contour that was selected manually by nine mouse clicks and the right image (B) shows the result of the level set method after 400 iterations	35
--	----

Fig. 5: The initial contour (A) and the result of the level set method (B) after 400 iterations (15 seconds of computation time)	36
--	----

Fig. 6: The initial contour, B. The result of the level set method after 960 iterations (17 seconds of computation time)	37
--	----

Fig. 7: Result of the level set method on resized lung CT image through a small airway (black)	38
--	----

Fig. 8: Result of the level set method on high-resolution lung CT image, reconstructed from raw data	38
--	----

Fig. 9: Left image (A) shows the initial contour that covers one kidney and the right image (B) shows the result of the level set method after 3000 iterations	40
--	----

Fig. 10: Left image (A) shows that there are two different tissues between the initial contour and border of the kidney and the right image (B) shows the result of the level set method after 3000 iterations	41
--	----

Fig. 11: Left image (A) shows the initial contour that is selected inside the kidney with some vessels connected to that kidney and the right image (B) shows the result of the level set method after 320 iterations	42
---	----

Chapter 5:

Table I: Shows the measurement of glass pipettes and one plastic syringe inner diameter and wall thickness in both methods, using caliper and the algorithm on CT images	65
--	----

Fig. 1: (a) Shows the whole lung, (b) shows part of the lung illustrating vessels connected to the airway	50
Fig. 2: (a, b, c, d, e, f, g) show the expanding level of a lumen contour by one pixel, respectively, while (h) shows the inner and outer border of airway wall	55
Fig. 3: (a, b, c, d, e, f, g) show the corresponding histogram of pixels on the border illustrated in figures 2 a-g, respectively	56
Fig. 4: (a) shows the inner and outer border of the airway wall. Both (b,c) are histograms from pixels in the inner and outer boundary of the luminal wall, respectfully	57
Fig. 5: Results of different slices acquired from different patients showing all pixels on expanded borders (after the third expansion) which are in the interval $[0, k+40]$ as well as all pixels on the first (inner) airway border wall (where k is the minimum intensity of inner border wall pixels)	58
Fig. 6: (a) initial contour for LSM, (b, c, d) contours after 100, 420, and 800 iterations of the LSM, respectively	60
Fig. 7: The top curve shows lumen area (mm^2), middle curve shows lumen diameter (mm), and the bottom curve shows the airway wall thickness (mm)	61
Fig. 8: 3D view of pixels on the lumen boundary over slices	62
Fig. 9: (a) shows one axial slice of the phantom, through the Styrofoam, (b) shows the result of lumen segmentation and wall thickness measurement	63
Fig. 10: (Top) shows an x-ray of our phantom from coronal view, (bottom) shows a photo of our phantom	72
Fig. 11: shows a photo of a syringe that was cut in the middle	73

Chapter 6:

Table I: Shows the result of angle measurements on Y-Shape pipes with 6.0mm inner diameter while considering all, or some percentage of slices	91
Table II: Shows the result of angle measurements where the actual angle for types 1-3 are 60 degree (with 3.0mm, 5.0mm, and 6.0mm inner diameter for types 1,2, and 3, respectively) and for type 4 is 120 degree. Method-1 uses thinning function and Method-2 uses top-down-left-right method for finding lumen center	91
Fig. 1: Shows different steps on lumen center specification: (a) result of level set method, (b) result of thinning function, (c) end points of part c, (d, e, f, g, h, i) result of several steps for deleting end points	78
Fig. 2: Top curve shows the lumen area (mm^2), middle curve shows the lumen diameter (mm), and the bottom curve shows the airway wall thickness (mm)	79
Fig. 3: Shows several steps of localizing the center of both branches at a bifurcation	80

Fig. 4: Shows a case that the result of thinning lumen boundary has more than two end-points	81
Fig. 5: Shows the position of lumen center points in X-Y axis	82
Fig. 6: Shows the result of estimating lumen center-line as a straight line	84
Fig. 7: (a) 3D view of the result of tracing and segmenting airway lumen through one of the branches at a bifurcation, (b) 3D view of the result of tracing and segmenting airway lumen through one of the branches at a bifurcation	85
Fig. 8: shows the result of estimating center-line for both branches of a bifurcation	86
Fig. 9: Shows a photo of phantom	67
Fig. 10: Shows a CT slice of this phantom, where this slice positioned near to the bifurcation area of most of pipes	88

Chapter 7:

Table I: The result of luminal diameter and wall thickness measurements and computed ratio of them	96
Fig. 1: provides a plot based on the TDR column of Table I	97
Fig. 2: shows the average of deviation of TDR from 1/6 for each case	98

M. Heydarian's contributions to this work

In order to confirm to the style required for this thesis document (which is in Sandwich Format), it is necessary to clarify the role of each author in the enclosed articles. The authors of all three papers are exactly the same and their role in all of them is also the same (repeated). The underlying project was introduced and explained by Dr. Noseworthy and Dr. Boylan. The author checked the results of the project at each step through weekly meetings with Dr. Noseworthy and when needed with Dr. Boylan. Along with results were included other medical issues such as some imaging scanner limitations (e.g. image resolution). While reviewing the literature (implementing and testing existing methods) and working on developing the proposed method (for achieving the expected result for characterizing the lung airways), Dr. Poehlman was supervising all steps of the project (in weekly meetings) and was there to advise on all computer science aspects of the project. We discussed details of the proposed method in different forms (considering computation time (algorithm complexity), memory usage, accuracy of results, implementation possibility, amount of data needed, etc.). Dr. Kamath, with experience in both medicine and engineering area, was also supervising and discussing the result of each step of the project. Not only was the author, working on developing and implementing new methods, but also in so doing was serving as a connection bridge between co-authors, transferring and explaining their opinion for changing/continuing the project. Dr. Poehlman, Dr. Noseworthy, and Dr. Kamath edited articles at different steps of preparation and submission while Dr. Boylan and Dr. Noseworthy provided articles with special imaging characteristics of CT and MRI scanners, respectively.

Chapter 1: Introduction

Disease identification/recognition is an important part of a physician's job. The more high quality data available from patients, the higher the probability of more accurate diagnosis. Radiologists play a very important role in disease recognition based on anatomical variations obtained through various forms of medical imaging technologies.

Nowadays, medical imaging devices such as magnetic resonance imaging (MRI), computed tomography (CT), positron emission tomography (PET), and single photon emission computed tomography (SPECT) are able to produce very high quality images of internal body structures and their function. By high quality it is inferred many imaging methods have reached sub-millimeter isotropic voxel resolution. Furthermore the images very accurately represent the true anatomic geometry. This technology provides physicians the ability to localize and classify small abnormalities in organs (lesions), which is invaluable in the non-invasive (or minimally invasive) assessment of disease progress and/or regression (i.e. therapeutic monitoring).

The explosion in medical imaging advancement has led to one serious difficulty: radiologists 20 years ago may have worked with 1000 images per day. Now with high resolution MRI and multi-detector spiral CT they are burdened with evaluation required on up to 50,000 images per day. (Not all images are examined in detail, but some can obviously be simply perused to add collaborating evidence to verify any disease identification already made.) With this immense volume of data it has now quite difficult for radiologists to rapidly identify and subsequently characterize small lesions consistently over their day. Furthermore it is even more difficult to compare differences between high resolution images from the same patient taken at multiple time points. This demand is tiring for anyone and thus leads to inaccuracy during the last hours of work. This "operator overload" of information is accelerating and no end is in sight in the foreseeable future. Therefore it is critical to develop some form of assistance to radiologists in their work, especially where tasks are repetitive and potentially automated.

There are many ongoing efforts to provide useful radiological software packages. These may provide some measurements, for example, which are useful in the diagnostic process. Although radiologists themselves could do most of these measurements, computer software packages are usually faster, more accurate, and consistent. In addition to the traditional usage of the computer for analysis such as edge detection or different measurements on segmented objects, artificial intelligence methods (i.e. expert systems and fuzzy expert systems) provide a good environment for simulating the physician's behavior in identifying and classifying diseases. These methods can also be automated to diagnose diseases by utilizing numerous types of input data and rules, both numeric and linguistic.

Disease recognition as well as temporal image comparisons (to evaluate progress or regression of disease) are ongoing research topics which usually employ some form of image preprocessing work, such as filtering, segmentation, classification, and

registration. This area of research is dependent on human-decision making; by this it is meant there is need for a radiologist's knowledge and experience to explain image texture and properties as related to certain diseases. By using expert systems, it is possible to add a radiologist's knowledge and experience (implemented by developing a set of rules) to a decision-making system.

There are several medical image processing utilities already available for radiologists. Most of these packages come with imaging systems (i.e. MRI, CT, PET, etc.) and are only able to do some very simple and preliminary image processing such as resizing and filtering. On other hand, there are some open source medical image processing packages (e.g. AFNI, ITK/VTK, Osirix) which are general purpose packages with an illustration ability (i.e. 3D view), that are primarily capable of basic processing such as resizing, filtering, basic segmentation, as well as limited registration (e.g. on the brain). As these packages have not been designed for any specific radiological task (e.g. automatically measuring the luminal diameter of airway), there is need to design and implement new algorithms in order to perform specific processes on the images of an individual anatomic regions of the body (e.g. segmenting lung airways using CT images).

The objectives for development of a software package required the following properties:

- 1- Software should aid the radiologist in analyzing diagnostic images.
- 2- Software ideally would minimize the amount of input required interactively by the radiologist in generation of appropriate results.
- 3- Software needs to output radiologically meaningful results.
- 4- The software needs to operate in a timely manner for the radiologist. However, for the preliminary version of this software, we have used Matlab (The Mathworks, Natick VA) environment for implementation (this was for convenience, albeit slower than implementation in languages such as C or C++).

For this work Matlab was the development environment of choice as it allows for rapid revision of software for investigative operations. Furthermore many functions are built in that allow reading and manipulation of medical image formatted data (i.e. DICOM standard is easily read into Matlab with header information characterized automatically). However, use of Matlab does not lend itself to a rapid production run. Conversion to a dedicated compiler based computational language would comprise the final step for this work.

The work done in this thesis focused on MRI data from human kidneys and CT data from human lungs. Thoracic and abdominal organs, such as kidney, liver, heart, and lungs are non-rigid and as such deform during slower forms of medical imaging. Furthermore these organs also move during the normal breathing cycle. As such medical imaging technologists ask patients to hold their breath for several seconds (20-30s) during these types of scans.

In this project, the primary goal was to develop software for recognizing certain lung diseases as well as to compare two serially acquired images (from the same patient's different visits) in order to find any progress, regression, or stability of a disease. To perform disease recognition and comparison, extraction of several lung CT image properties, used by radiologists, were required. Working closely with a radiologist (Dr. Colm Boylan, Diagnostic Imaging, St. Joseph's Healthcare), several useful properties for recognizing and classifying disease progression or regression were identified. Features successfully measured were: airway luminal diameter and wall thickness (with both measurements performed over an airway from one branch to the next branch), and angle of airway bifurcation (based on automatically tracing both branches at each airway bifurcation).

In order to measure airway luminal diameter, segmentation of the lumen area from its wall was needed. The first peer-reviewed paper from this thesis (chapter 4) explains an optimization method which was employed to adapt the level set method for segmenting airway lumen. For measuring airway luminal wall thickness, instead of a segmentation method in order to find the outer border of airway luminal wall, a fitting method (which expands the lumen border until a termination condition meets) was developed. The second peer reviewed article in this thesis (chapter 5) explains this fitting method as well as a streamlining mechanism that provides the level set method with a better algorithm initial conditions (here a good initial contour), essential for successful and fast segmenting processes. In order to recognize some prominent lung diseases, the lumen airway tapers in size rather than remaining relatively consistent in diameter which necessitates the tracing of an airway through various CT slices. Chapter 5 also explains a method which performs such tracing in more detail. For measuring the bifurcation angle, the algorithm needs to detect and follow the branches at a bifurcation. The third paper in this thesis (chapter 6) explains the tracing algorithm as well as the estimation method for finding a fitted line on the center points of the airways. Algorithms developed in this thesis could be employed in detecting and identifying lung diseases from sample CT images. The last chapter of this thesis summarizes the research and lists suggested future research foci. It also includes a discussion on how these lung characterization could be employed in recognizing some of lung diseases and what are practical problems in this area.

To give relevant background to topics detailed in peer reviewed papers, chapters 2 and 3 provide rudimentary information on medical imaging (chapter 2) including terminology and describe some of the techniques in applications of artificial intelligence in medicine (chapter 3). The work presented in this thesis was done in collaboration with clinicians, engineers, medical physicists, and computer scientists.

Chapter 2: Medical Image Processing

2.1 Computed Tomography (CT)

Computed Tomography (CT) or Computer Axial (Assisted) Tomography (CAT) uses X-rays to generate cross-sectional images of the body. To acquire images, the X-ray tube rotates 360° around the patient, and the transmitted radiation is measured by a ring of detectors located on the gantry around the patient. The data can be projected as a three-dimensional model to display spatial information or surface characteristics, utilizing the basic principle that the internal structure of the body can be reconstructed from multiple X-ray projections [1].

Area of Usage: These images allow the radiologist and medical doctors to examine the inside of the body. This type of special x-ray, in a sense, takes "pictures" of slices of the body so doctors can view the area of interest in three dimensions. CT scans are frequently used to evaluate the brain, neck, spine, chest, abdomen, pelvis, and sinuses [2].

Advantages: CT is available in most tertiary care hospitals in North America and Europe. It is an increasingly rapid imaging modality with excellent image resolution, enabling faster and more accurate diagnostic evaluation of patients over a wide spectrum of clinical indications. The data acquired in one scan can subsequently be manipulated to provide multi-planar and 3D reconstructions [1].

Disadvantages: “Although CT scans account for only 4% of X-ray examinations, they contribute to more than 20% of the radiation dose to the population by ‘medical X-rays’ [1]. Similar to all other imaging modalities, artifacts do occur in CT images. An artifact is an appearance in the image that does not actually exist. Compared with MRI, it has poor contrast between different types of tissues (in adults and in children with the lack of intra abdominal fat for separating various tissue planes) [1]. Also, CT has a high cost and limited portability compared to the other image modalities except MRI and PET. Sometimes the patient may be required to have a contrast injection to distinguish abnormal tissues from normal tissues.

2.2 Magnetic Resonance Imaging (MRI)

Magnetic Resonance Imaging (MRI) is an imaging technique to produce high quality images inside the human body. It was called Nuclear Magnetic Resonance imaging (NMR) when it was introduced for the first time, but because of fears that people wrongly thought that people are subjected to nuclear radiation was involved, the “nuclear” part was dropped from its name [3] [4].

Functional Analysis: The MRI scanner consists of a very strong magnet (usually 1.5 - 3 Tesla) in which the patient is placed. A radio wave coil is used to send and receive radio frequency (RF) signals to the body. These returning signals are converted into

pictures. The radio frequency pulse is frequency selective, which means that only the spins within the frequency range covered by the RF pulse are excited and results provide an image based only on the spins within this slice. By changing the direction of the gradient applied during the RF pulse, it is possible to cut slices in any direction. This is one of the strengths of MRI. Thus one is not limited to acquiring images in any single plane. Three magnetic field gradients must be applied to obtain spatial encoding of the data [5].

There are different types of data acquisition in MRI, each of which uses different features of spins and gives different gray intensity for different tissues of the body [4] (e.g. CSF of brain is darker in a T1 weighted image than in a T2 weighted image).

T1 weighted images: The return of excited nuclei (by RF) from the high energy state to the low energy or ground state is associated with a loss of energy to the surrounding nuclei. Macroscopically, T1 relaxation is characterized by the longitudinal return of the net magnetization to its ground state of maximum length in the direction of the main magnetic field. The T1 relaxation time is the time for the magnetization to return to 63% of its original length. Spins are considered completely relaxed after 3-5 T1 times. Higher magnetic fields are associated with longer T1 times [6].

T2 weighted images: Microscopically, T2 relaxation or spin-spin relaxation occurs when spins in the high and low energy state exchange energy but do not lose energy to the surrounding lattice. This results macroscopically in loss of the transverse magnetization. In body tissues, the T2 time is considerably shorter than the T1 time. For example, CSF has T1 and T2 equal to 1.9 seconds and 0.25 seconds respectively. T2 relaxation occurs exponentially such as in T1 relaxation with 63% of the transverse magnetization gone after one T2 period. A T2 weighted image is produced by using long TR (Repetition Time for image acquisition) and long TE (Echo Time) pulse trains when the T1 weighted image is produced by using short TR and short TE. The longer the TR and/or the longer the TE, results in the more T2 weighted of the image, but the penalty for longer TR is time of acquiring images and the penalty for long TE is noisier images that cause a reduced signal to noise ratio (SNR) [6].

Proton Density (PD) image: The PD image can be thought of as an image that is halfway between the T1 weighted and the T2 weighted image. It is produced using long TR and short TE. Spin density, balanced image, and mixed image are other names for this kind of MRI [6].

By changing parameters used during examination (i.e. TR, TE), the MRI system can cause body tissues to take on different appearances even for the same kind of image such as T1, T2, or PD images.

Area of Usage: Pictures of almost any part of the body can be captured at any particular angle. MRI is good for examining the soft tissues (non-bony parts) of the body. In particular, the brain, spinal cord and nerves are seen much more clearly with MRI than other techniques. MRI scans are commonly used to examine and evaluate knees and shoulders following injuries because muscles, ligaments and tendons can be seen very

well using MRI, and to look at cystic disease inside the liver or kidney as the cysts are separable from those organs using MRI [3] [6].

Another use of MRI is functional MRI (fMRI), which is acquiring a series of images from specific slices of the body to find differences in an organ between imaging times. For example, in the blood-oxygen level dependent (BOLD) method, a series of baseline images are taken of the region of interest, when the subject is at rest. When the subject performs a task, a second series of images are taken; then the first set of images is subtracted from the second, and the areas that are most visible in the resulting image are presumed to have been activated by the task. Other fMRI methods exploit the fact that the bulk movement of hydrogen nuclei causes changes in the MRI signal. Such methods could image CSF flow, blood flow, or diffusion of water through tissue [6].

Safety: MRI is a very safe and reliable imaging technique with very few side-effects or dangers, because MRI does not use X-rays or other radiation. All hazards can be overcome by training of the staff and increased vigilance (due to the powerful magnet) prior to and during the examination. Although MRI is quite safe for most patients, patients with implanted medical devices, or patients with pieces of metal close to or in an important organ such as the eye, may not be scanned. Sometimes the presence of metal, which is close to the part being scanned, can cause poor pictures [7].

Costs of an MRI scan: Generally speaking, the cost of an MRI scan depends on the duration of the scan, which is a result of the types of sequences required to generate images that are most suitable for diagnosing a certain disease. Estimated figures for a routine diagnostic MRI scan range from \$1000 - \$4000 in Canada. The cost of an MRI scan is approximately 150% of a CT scan [6].

Disadvantages: A disadvantage of MRI is its higher cost compared to a regular x-ray or CT. Also, CT scans are better for looking at bones than MRI [7]. Finally MRI is not practically useful for imaging lungs where as CT is.

2.3 Segmentation (Clustering)

Image Segmentation, also called Image Clustering, is grouping a collection of pixels into multiple unlabeled regions such that pixels within each group are more similar to each other than pixels assigned to other groups according to a given criterion. The goal is typically to locate objects of interest inside the image and is sometimes considered a computer vision problem. Each pixel of a medical image corresponds to a cubic volume of the body and is called a voxel.

Selection criterion of regions is based on different features such as gray intensities, texture, and edge information. When working on a specific image modality such as MRI, other overall features of varying complexity would also be important. For example, features such as voxel size, gap, plane of acquisition (e.g. Axial, Sagittal, Coronal), chemical composition of the tissue, presence of a contrast agent, machine parameters such as TR and TE, magnetic field power, and the subject's age and physical condition may be important in processing an MRI output.

Saeed [8] categorized segmentation algorithms into two categories: low-to-intermediate-level and high-level. The first category, which operates at pixel level, includes five popular methods: gray intensity histogram analysis, texture analysis, edge enhancement and linking, region growing, and contour following. The second category, which is anatomical segmentation, needs prior (expert) knowledge. Fuzzy classifiers and neural network procedures may be useful in the first category, while expert systems can be used to supply prior (expert) knowledge for segmentation, all originating from Artificial Intelligence applications. More will be said about this area of work in a subsequent chapter.

2.4 Classification

Classification is the assignment of clusters to predefined classes. It can be obtained by numerical and non-numerical methods. The numerical methods include geometrical and statistical classifiers, while the non-numerical methods are the rule-based classifiers (i.e. expert systems), which are defined by a set of rules and a grammar. To classify volume data, the grammar must be designed to describe 3D rules. Statistical classifiers (e.g., K Nearest Neighbor algorithm) must map a feature space to a set of labels. Another group of statistical classification algorithms first applies unsupervised clustering to the feature space, then attempts to label each of the clusters or regions.

Examples of classification algorithms include: linear classifiers (i.e. Fisher's linear discriminant, logistic regression, Naive Bayes classifier, perceptron), quadratic classifiers, k-nearest neighbor, boosting, decision trees, artificial neural networks, Bayesian networks, support vector machines, and hidden Markov models.

2.5 Filtering

Image filters are used to remove noise, sharpen contrast, or highlight contours in images. One common classification of filters categorizes them into two classes: linear filters and frequency-based filters.

Linear filters, also known as convolution filters, are mathematical functions that replace each pixel by a weighted sum of its neighbors. This could be accomplished by a matrix multiplication.

Frequency-based filters attenuate or amplify certain frequency ranges. For images, low-pass or high-pass filters are used. Low-pass filters are used for operations like noise removal or image smoothing. High-pass filters respond to abrupt changes in light intensity in an image, so they are used to enhance details in the image, but they enhance high-frequency noise too. Frequency-based filters are easy to design and implement, but they can introduce artifacts into the image when the inverse transform is applied. These artifacts typically appear as "ringing" or ripples that come from edges in the image.

2.6 Registration

Image registration is the process of aligning different sets of images into one coordinate system (see [3], Pages 65-82). We need registration when comparing images obtained from different measurements that may have global translation, rotation, or scaling. Transformation of 2D images may include two translations and one rotation, where as transformation of 3D images may include three translations and three rotations. The Image Registration algorithm uses a "cost function" and then adjusts the alignment iteratively until it reaches a maximum or minimum amount of a cost function. For example, when we have several images from the same patient at different perspectives, or when we have several images from the same patient at different points in time in the same or different modality (e.g. MRI, CT, PET), or when we have images from different patients in the same modality such as aligning a patient's images to atlas images. Medical imaging registration also involves non-rigid registration to cope with images that undergo deformation in parts of the body. One of the images is referred to as the reference image and the other one, that is mapped onto the reference image, is referred to as the target image. Based on varying criteria, there are different ways of classifying registration algorithms [9].

Depending on the kind of information that we extract from an image, there are two main types: area based methods and feature based methods. The area based methods look at the structure of the image via correlation metrics, Fourier properties and other means of structural analysis, while feature based methods use the correlation of image features such as lines, curves, points, line intersections, boundaries, etc, which are intrinsic features. Also, sometimes an external object (extrinsic feature), which is attached to the subject during all scans, is used as a reference point for registration. Extrinsic features cannot be used for time series medical scans where there may be a long temporal gap between acquisitions.

Based on the search method used to find the parameters for a transformation function, registration methods can be categorized into search-based methods and direct methods. In the search-based methods the effect of different image transformations is evaluated to determine the best one. In direct methods an estimate of the image deformation is computed using image statistics.

Based on the transformation model (used to transform the target image to the reference image), there are two categories: linear transformations, which are a combination of translation, rotation, global scaling, shear and perspective components, and elastic or nonrigid transformations methods. Since linear transformations are methods that are not able to model local deformations, then elastic ones are used to allow local warping of image features, and hence support local deformations.

According to the nature of images that are used as input to the registration algorithms, there are single-modality and multi-modality registration algorithms. The

former algorithms register images of the same modality (e.g. MRI, CT, PET), while the latter algorithms register images of different modalities (e.g. MRI/CT, PET/CT).

As a metric to determine the appropriateness of the resultant registration, similarity methods are usually used in medical image registration. Mutual information and its variant are commonly used as image similarity measures for registration of multimodality images, where cross-correlation, mean square difference, and ratio image uniformity are commonly used as image similarity measures for registration of images of the same modality.

2.7 DICOM Standard

Although Digital Imaging and Communications in Medicine (DICOM) commonly refers to image files, it is more correctly a standard that was created to aid in the distribution and viewing of medical images, such as CT and MRI. The distribution ability of DICOM is used to store/retrieve data to/from a PACS (picture archiving and communication systems), which are composed of computers in networks that are used for storage, retrieval, distribution and presentation of images.

A part of this standard explains the file format of images. A DICOM file contains both a header and the image data. The header contains information about the scan such as date, patient's name, the type of scan, the amount of parameters such as TR and TE, image dimensions, etc. The image data contains the image pixel data in three dimensions.

2.8 Some examples of comparing serial images in time

In this section we will review some medical image processing work that has been applied on MRI. Curati *et al.* [10] used registration and subtraction to improve demonstration of contrast enhancement in MRI of the brain. They first used segmentation to separate the brain from surrounding skull and soft tissue, then registered the before and after injection images. After registration, they subtract the earlier images from the later images. Finally two radiologists independently assessed the original, registered, and subtracted images. Beier *et al.* [11] developed a system that registered CT, MR, and coronary angiography images prior to the subtraction in order to have an enhanced visualization of the contrast agent. Their focus was on developing a good registration, and comparison of subtraction images was humanly done. Ionescu *et al.* [12] applied subtraction on registered time series MRI to make evident pulsing brain arteries movements associated with heart activity. This work could be categorized as functional MRI analysis as all time series images were acquired in one scan. There are many other works on functional MRI. Rory *et al.* [13] compared several methods for presenting 4D space-time data (temporal images), which have the potential to compress large quantities of images into a single image. They also examined several derived scalar and vector quantities. The problems that they faced during their work were mentioned as: choosing quantities that are most informative, limited resolution in voxel size, and long time for

acquiring more slices. Connor *et al.* [14] compared image registration and subtraction techniques in their ability to improve the detection of minor changes in low grade glioma volume when applied to standard T2 and FLAIR (Fluid Attenuated Inversion Recovery) images. Three independent neuroradiologists rated the resulted images. They reported a statistically significant improvement to detect changes in tumor volume while using registration/subtraction related to unregistered images.

References:

- [1] www.fleshandbones.com/readingroom/pdf/940.pdf, visited on Dec. 2006.
- [2] www.emedicinehealth.com/ct_scan/article_em.htm, visited on Dec. 2006.
- [3] Arnulf Oppelt, Imaging systems for Medical Diagnostic, Publicis Corporate Publishing, 2005.
- [4] A. D. Elster, J. H. Burdette, Questions and Answers in Magnetic Resonance Imaging, Second Edition, Mosby Inc. 2001.
- [5] www.cis.rit.edu/htbooks/mri/inside.htm, visited on Oct. 2006.
- [6] www.markschenk.com/tudelft/et4129/introduction_to_MRI.pdf, visited on Dec. 2006.
- [7] www.mritutor.org/mritutor/, visited on Dec. 2006.
- [8] N. Saeed, Magnetic Resonance Image segmentation using pattern recognition, and applied to image registration and quantization, NMR in biomedicine, NMR Biomed 11, 157-168, John Wiley & Sons, Ltd, 1998.
- [9] <http://www.wikipedia.org/>, visited on Nov. 2006.
- [10] W. L. Curati, E. J. Williams, A. Oatridge, J. V. Hajnal, N. Saeed, G. M. Bydder, Use of subvoxel registration and subtraction to improve demonstration of contrast enhancement in MRI of the brain, Diagnostic Neuroradiology, 38: 717–723, Springer-Verlag 1996.
- [11] J. Beier, H. Oellinger, C. S. Richter, E. Fleck, R. Felix, Registered image subtraction for CT-, MR- and coronary angiography, European Radiology, 7, 82–89, Springer-Verlag 1997.
- [12] R. Ionescu, C. Alarcon, F. Langevin, Brain Arteries Movement Detection with gated Gradient Echo Sequence: Standardization, Registration and Subtraction of Serial Magnetic Resonance Images, Proceeding of the 23rd Annual EMBS International Conference, Oct. 25-28, 2001, Istanbul, Turkey.
- [13] M. Tory, N. Röber, T. Möller, A. Celler, and M. Stella Atkins, 4D Space-Time Techniques: A Medical Imaging Case Study, Presented at IEEE Visualization, Oct. 21-26, 2001, San Diego Paradise Point Resort, San Diego.
- [14] S. E. J. Connor, R. Gunny, T. Hampton, R. O’Gorman, Magnetic resonance image registration and subtraction in the assessment of minor changes in low grade glioma volume, European Radiology 2004, 14:2061–2066, DOI 10.1007/s00330-004-2391-4.

Chapter 3:

Using Artificial Intelligence in Medical Image Processing

The phrase, “Artificial intelligence” has different meanings to experts from disparate disciplines. Even a precise definition for the word “intelligence” is rather elusive. In practice, finding a good and feasible answer for unseen questions could, in this case, be a test to determine how intelligent a person is, but many other parameters have an effect on the human ability, termed as “intelligence”. The most important virtue of those who display high level of intelligence is their educational preparation while other parameters such as good definition of the problem, being familiar with similar problems, being in a good frame of mind, and other similar parameters are required to solve a problem. The ultimate goal in AI is developing a computer that can solve problems like a human being. However, the first step of this long process is to just imagine that the machine one designs has features which simulate some of the features of the human thinking process or simply as an assistant to the human being in solving certain types of problem. However for deeper definitions which go beyond more logical activities are extremely difficult.

Thinking at the level of a human being involves the formulation of a software which has strong components of AI, but one can imagine weaker AI techniques that try to simulate some human behaviors that are feasible for implementation. Along this way, we can invoke involving different mathematical methods for such simulation, some of which involve a certain “intelligent” behavior of a human being. For example, Artificial Neural networks (ANN) simulate human expertise in training and recognition of certain types of patterns in data. Another example is Fuzzy Logic that simulates the decision-making ability of a human as well as providing a way to manipulate linguistic terms. Genetic Algorithms simulate evolution of certain types of population during generations, which is distinctly different from human intelligence. Expert Systems are another AI technique that employs rule-based system to simulate the decision-making ability of human.

3.1 Expert Systems

3.1.1 Introduction

Although there are many definitions for Expert Systems (ES), all of them share the common concept that ES is an Artificial Intelligence (AI) system that simulates human behavior of making decisions based on certain logic, rules, and probability. The ES is a replacement of a human expert by a computer application to perform a specific task although, more often, especially in medical image processing, ES is designed to assist a human expert at his/her job. From the view of constructing an ES, programmer studies how the human expert makes decisions while performing his/her specialized task and then translates such information into a program code that a computer can understand [1,2].

Since the human expert decision process more often translated to IF-THEN rules, we call the expert system a rule-based Expert System [2]. Another type of ES is called frame-based ES, where the frame is a data structure with the knowledge about a particular object or concept [2]. The most difficult part of designing an ES is to acquire, a process called “mining”, data in the form of IF-THEN rules, from the human expert and then translate it to the computerized format, which is usually done by knowledge engineers or human experts themselves. One big problem in simulating human expert behaviour is to deal with incomplete, inconsistent, and uncertain information; the ES does not cope with these defects easily. Uncertain information can also be interpreted and manipulated by Fuzzy logic (section 3.2), where pure ES can use statistical techniques to deal with uncertain information. The combination of ES and Fuzzy Logic is called Fuzzy Expert System, which is really a powerful tool with actions similar to human behaviors.

Rule-base ES may use both or either *goal driven* or *data driven* strategies. The former strategy uses a *backward chaining* inference engine that tries to conclude the goal of a rule by establishing the truth of its premise. When the ultimate goal is known, this strategy is faster because it fires the relevant rules and just asks the questions related to the fired rules. The latter strategy uses *forward chaining* inference engine, using known facts or values, tries to fire all rules when their premise matches known facts and values. New facts and values obtained from fired rules are then used to fire more rules. This procedure ends when the goal is obtained or no more rules can be fired using new facts and values. This strategy is used when the problem can have more than one possible answer.

Figure 3.1 [1] shows the complete structure of a rule-base expert system. Each component of the ES is explained briefly: The *knowledge base* contains a set of rules, while the *database* contains a set of facts and values of certain benchmark parameters that are used in IF-THEN rules. The *inference engine* links the rules and the facts to do the reasoning whereby the ES reaches a solution. The *explanation facilities* part shows which rules were fired and how the ES reached a particular result. The *user interface* should be meaningful and as user-friendly as possible, so that the end user, who may be an expert or non-expert, could use it as easily as possible. Some of the components in the figure 3.1 may not form a part of all ESs.

The interface to external database and external program makes ESs more powerful when they can use external knowledge and methods. The *developer interface* is a facility that knowledge engineers and experts use to make changes in the ES, using a knowledge base editor and I/O facilities.

To develop an ES, there are two kinds of tools: high-level programming languages and ES Shells. The former tools are more flexible and powerful if the developer has good programming skills, where an ES shell with built-in inference engine, explanation facilities, and user interface parts make the development of an ES more easy and cost-effective without the need of any programming skills; but each existing shell is designed only for a narrow family of problems and so we may not meet all project

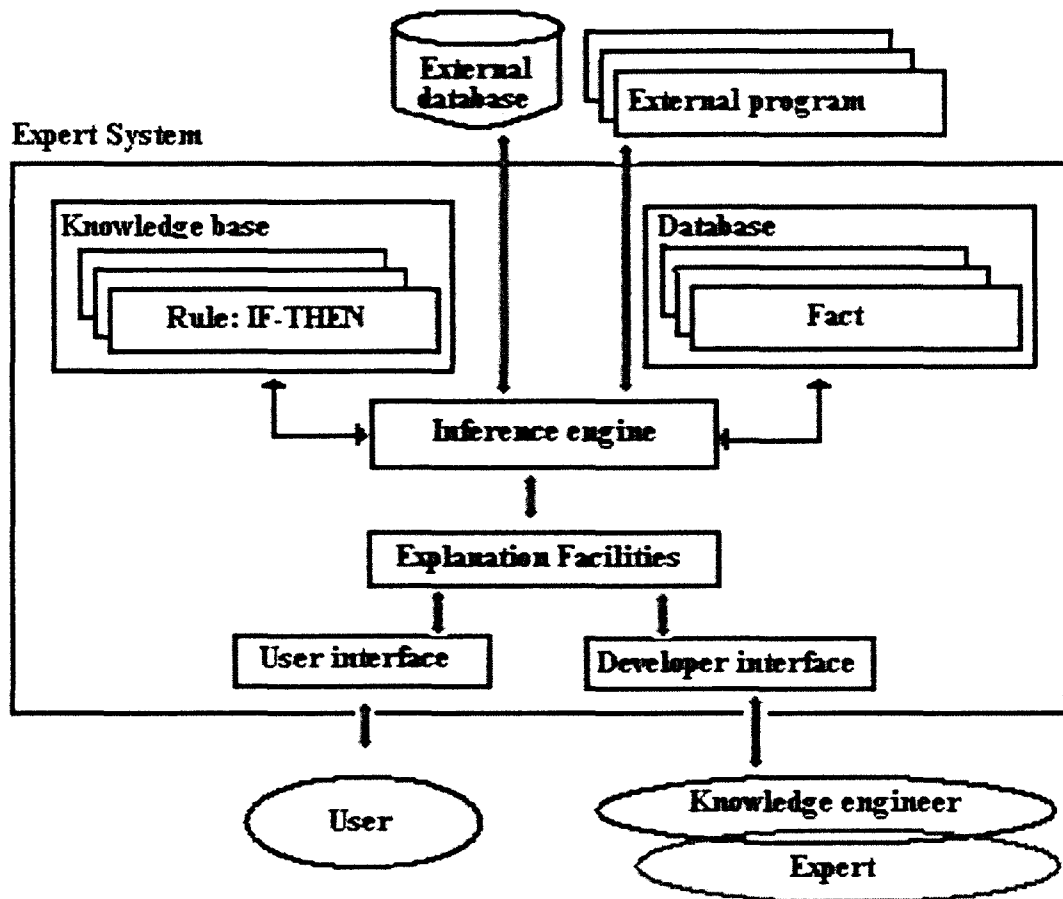


Fig 3.1: Complete structure of a rule-based expert system [1].

requirements with a particular shell. There are other issues to be considered, such as availability of human experts, while designing an ES.

3.1.2 Applications

A wide range of problems in different areas such as medicine, engineering, computer science, mathematics, business, and education has been solved using Expert Systems. However, approaches to solve problems tend to be problem specific rather than domain specific [2]. For instance, an ES might support planning activities such as developing a marketing strategy for a new product. Instructional ES are used to diagnose student weaknesses and to customize instruction. ES also have been developed to control necessary components for installation of customized equipment.

Several laboratories have spent considerable time and resources on medical diagnosis. As an example, Mycin is an ES that was developed at Stanford University in 1970s to diagnose and recommend treatment for certain blood infections. While, its performance was good during its test by members of the Stanford medical school, physicians could not turn over the responsibility of treating their patients to a piece of software and hence the software did not gain acceptance in the real world medical practice.

Zhang *et al.* [3] (2000) used a four-step segmentation method in which the key part of algorithm is a rule-based fuzzy expert system. The method, which is a combination of several segmentation algorithms and an ES, will be discussed in section 3-2-2 below.

Ruggiero *et al.* [4] (1992) developed an ES to confirm or assess the presence of pathology on the basis of morphological data, coming from radiological source. Their ES contained three kinds of information: A knowledge base involving anatomical structure of the organs and their pathologies, a set of rules, and a set of clinical data for the current patient. They used their ES at three levels: recognizing pathology in real images, providing expected images for some pathologies, and getting consultation on the anatomical region.

Kowarski [5] (1990) developed a radiology diagnostic ES that creates a ranked list of possible diagnoses from selected radiographic and clinical features. The ES came with access to a correlated image and text database to use for inference and description steps. This ES was designed for diagnosing pathology within the adrenal gland (in kidney, liver, pancreas).

Wells *et al.* [6] (1989) developed an ES for identification of common regions like cerebral hemispheres, ventricles, eyes, and ocular fat within MR brain images. They used the developed ES to identify normal and abnormal anatomical or physiological regions within MRI.

3.2 Fuzzy Logic

3.2.1 Introduction

Many linguistic phrases, which are specific to a particular subject area, are used during a professional discussion. These phrases, albeit are vague in their meaning and context, are often repeated when a non-expert requires an expert to explain how they make decisions in their domain of specialty. Words such as 'big', 'less', 'more', and 'very' are ambiguous phrases that cannot be accommodated by classical set theory in mathematics. For example, to find if the grade B+ is good or not, using a two state definition seems inaccurate. Fuzzy sets, introduced by professor Lotfi Zadeh 1965, were proposed to deal with such vague words and phrases [7]. Unlike classic (crisp) sets that designate a crisp membership of 1 or 0 to an element as belonging or not belonging to a specific set, a fuzzy system gives different degrees of membership of an element to different fuzzy sets. Memberships are a number in the range from 0 to 1 that show the

similarity of an element to the specific set, where 0.0 represents no similarity and 1.0 represents absolute similarity [8]. Although the range [0,1] brings the idea of probability, fuzzy sets theory uses a similarity concept for degree of membership instead of probability [9]. We use the symbol $\mu_A(x)$ to show membership of element x to fuzzy set A .

The next attempt in Fuzzy set theory, was to model decision-making of human subjects, while dealing with ambiguous terms (e.g. big, pretty) and linguistic quantifiers (e.g. usually, almost always). Fuzzy logic [10] brings a mathematical definition for reasoning, arriving at a conclusion, and decision-making in an uncertain situation. "It aims at modeling the imprecise modes of reasoning that play an essential role in the remarkable human ability to make rational decisions in an environment of uncertainty and imprecision" [10]. Fuzzy logic uses IF-THEN format for its inference rules. This is the basis for Fuzzy Controllers, which are often categorized as expert systems [1]. Fuzzy Controllers are used for simulating human operator's behavior, and a very important reason to use Fuzzy Logic Controllers (FLC) is to capture expert's experience in as precise terms as possible

3.2.2 Applications

Fuzzy c-mean (FCM), a clustering algorithm which uses fuzzy logic concept, has been used for clustering medical images. There are several FCM algorithms such as Kernelized FCM (KFCM) [11,12], Hierarchical FCM [13], and Alternative FCM [14] that change a part of the FCM algorithm for a better result. Zhang *et al.* [11] replaced the original Euclidian distance in the FCM by a kernel-induced distance, so it was named kernelized FCM. This version, kFCM, has better clustering performance and is more robust than FCM for incomplete data clustering. They showed that KFCM is robust to noise and outliers, and also tolerates unequal sized clusters. Zhang *et al.* [12] also developed a KFCM for clustering MRI. In their method, labeling a pixel is influenced by its neighbors in the image. They showed that the proposed algorithm has better performance when noise and other artifacts are present.

Kwon *et al.* [13] proposed Hierarchical FCM that processes FCM in a small volume that is hierarchically divided from the original 3D data set and calculates the degree of membership for each volume. They showed that HFCM is able to process nonstationary images such as a high field MR image with RF nonuniformity, because small volumes can be approximated as stationary even if the original image is not stationary.

Ruan *et al.* [15] presented a fuzzy Markovian method to deal with partial volume effects. Berks *et al.* [16] used fuzzy c-mean clustering to assign symptoms to the different types of aphasia categories by exploring a medical database. Mohammed *et al.* [17] used a modified FCM classification algorithm to provide a fuzzy partition. They reported that their method, inspired from the Markov Random Field (MRF), is less sensitive to noise as

it filters the image while clustering, and the filter parameters are enhanced in each iteration by the clustering process.

Although FCM has a better performance than other unsupervised clustering algorithms in medical imaging field, as medical images are fuzzy especially around the edge of tissues and in the area around the tumors or cysts, the algorithm does not provide acceptable clustering of tissues. It needs modification or is to be enhanced by combining other algorithms or methods, especially with expert systems. An example of this combination was employed by Zhang *et al.* [3] who used four steps of segmentation to get better results. In the first step they used FCM for extracting “brain mask” and “extra-cranial mask” from the image to separate “bone, skin, fat” and “brain matter”. Then they used FCM to divide masked brain matter into eight clusters. Next using statistical and morphological characteristics of clusters, they produced a set of fuzzy rules to generate representative sets for White matter, Gray matter, and CSF. In the next step they used another set of fuzzy rules combining with K-mean algorithm to add more pixels of an image to representative classes. Finally, they used K-Nearest-Neighborhood to add the rest of the pixels to representative classes. Suna *et al.* [18] tried to use FCM for automatically determining the number of clusters in an image.

3.3 Genetic Algorithms

3.3.1 Introduction

Intelligent behavior of the human being is obvious and a necessity in every day life. Human intelligence is a product of evolution and therefore, it would be reasonable to incorporate simulation of evolution in mathematical algorithms in order to create intelligent production systems. The Genetic simulation is a kind of optimization method based on a set of evolutionary rules. All evolutionary methods simulate natural evolution, generally by creating an initial population, evaluating the fitness of each individual related to other members in the population, selecting individuals with high fitness value, generating a new population using genetic operations (i.e. crossover and mutation), and repeating this process from the evaluation step until reaching some termination criterion.

Genetic Algorithm (GA) is a type of evolutionary system that simulates evolution over generations. In nature, a chromosome represents the features of an individual. Each chromosome consists of a number of genes each of which represents a specific feature of an individual. Each gene consists of several alleles that are built using one of the four nitrogenous bases: adenine, cytosine, Guanine, or thymine. In simulation, each chromosome is represented by a string of genes. Genes can be made using different types of alleles such as characters, digits, or numbers. A brief explanation of each step in the GA approach follows below.

Initial population: each individual (chromosome) is a solution for the system being designed. The number and type of features from the system being developed is used to calculate the length of chromosomes, but there is no deterministic method to choose the number of individuals in the initial population. The size of the population will

stay fixed during the run time of the GA. It uses random statistics with a normal distribution to produce the initial population. Randomness makes the GA a non-deterministic method that may end with different answers on different runs for the same problem.

Selection: in the current population, some of the individuals are better than others, and therefore, the GA selects them for generating a new population. Finding a good and efficient evaluation function is the most important and difficult part of designing a GA. Also applying this function to evaluate individuals is the most time consuming part of the GA. For example, in a previous study [19] conducted by the author, identifying, designing an evaluation function required more than 95% of the computation time and on average took more than three days to reach termination criteria on a machine with Intel 486 DX5/133 and 64MB memory. This was due to the GA simulation of the pH level controller to see its behaviors and each individual simulation took 2-3 minutes. Therefore, a smaller population is often chosen, although the bigger one has a better probability of finding a globally optimal result.

Crossover: is the most important operation to produce a new population. At this step, the GA combines elements (chromosomes) of existing solutions (current population) to create new solutions by inheriting some features from their parents (current solutions).

Mutation: is a random change in some genes to generate a new solution, which may be better or worse than the previous solution. As it is random and may yield a worse solution, the GA applies it with a low probability (say, less than 1% for each allele). Mutation helps the GA to avoid becoming trapped at a local optimum, when all individuals in population are in the same region around the local optimum and crossover will not generate any new solutions in other areas.

Repetition and termination criteria: after generating each new population, the GA repeats the steps involving selection, crossover, and mutation to produce a new population, unless a termination condition is met. Genetic algorithms use different termination criteria such as a specific number of generations, finding an acceptable solution, or finding no change in fitness of the best individual, during several generations.

3.3.2 Applications

Although there is no mathematical proof for finding a global maximum, relying on statistical facts, one allows the GA to find an optimal answer by choosing the best individuals in a population when producing a new generation. GA can be used when the search domain is wide or complex, expert knowledge is difficult to encode, mathematical analysis is not available, or traditional search algorithms are not useful. Examples of optimization problems that could be solved by GA approaches include the Traveling Salesman Problem, Circuit Design, and Job Shop Scheduling. In the area of Machine Learning, GA has been used to design Neural Networks, to evolve rules for learning classifier systems, and to design Fuzzy Logic Controllers [20].

In previous work, we [19] used GA to design Fuzzy sets and Fuzzy rules for a Fuzzy Controller simultaneously to control the pH of wastewater when no human expert was accessible. Other applications include Gudmundsson *et al.* [21] who used the GA to detect well-localized, un-fragmented thin edges in medical images (MRI, CT, and Ultrasound); Xue *et al.* [22] who applied region-wise classification using GA based on fuzzy modeling of knowledge to segment brain structures in MRI, and then they applied a voxel-wise refinement using parallel region growing to generate a more accurate result; Widz *et al.* [23] who used GA to segment brain tissues in MRI; and Selvathi *et al.* [24] who compared Fuzzy C-Mean and GA for clustering brain tissues in MRI. They found that Fuzzy C-Mean gives higher precision and accuracy than GA.

Rajapakse *et al.* [25] used GA to register functional MRI time-series images of the human brain. Chow *et al.* [26] used GA for finding the transformation between two 3D medical images of heart, vertebra, and fetus models. Lee *et al.* [27] used Adaptive GA to register CT images of brain. They changed the usual method of mutation to an adaptive mutation to control the speed of convergence of the GA. Zhang *et al.* [28] proposed an improved GA to register multi modal medical images (MRI, CT, and PET). They used a wavelet decomposition algorithm as a preprocessing step to find mutual information from different image modalities. Peng *et al.* [29] used Niche GA for medical image registration. Niche GA differs from usual GA by changing in producing new generation. It keeps a copy of some of the best individuals in the current population and after applying GA operations chooses the new generation individuals from this group and result of GA operations.

References:

- [1] M. Negenevitsky, Artificial Intelligence, A Guide to Intelligent Systems, Addison Wesley, Second Edition, 2005.
- [2] A. Cawsey, Essence of Artificial Intelligence, Prentice Hall, 1997.
- [3] S. Zhang, J Maeda, A Rule-Based Expert System for Automatic Segmentation of Cerebral MRI Images, World Computer Congress 2000- ICSP 2000.
- [4] C. Ruggiero, M. Giacomini, An Expert System for Radiological Images, Engineering in Medicine and Biology Society, Vol.14. Proceedings of the Annual International Conference of the IEEE, Volume 3, October 29- November 1, 1992 Page(s):918 - 919.
- [5] D. Kowarski, A Low-Cost Personal Computer-Based Radiology Diagnostic Expert System and Image and Text Database, IEEE Artificial Intelligence and Neural Nets, 1990
- [6] M. Wells, A. Law, A Allen, An Expert System for the Identification of Meaningful Region within MR Brain Images, IEE Third International Conference on Image Processing and its Applications, 18-20 Jul 1989 Page(s):378 - 383.
- [7] L. A. Zadeh, Fuzzy Sets, Inform. Contr. Vol. 8, pp. 338-353, 1965.
- [8] K. Tanaka, An Introduction to Fuzzy Logic for practical Applications: with 82 illustrations, Springer, 1997.

- [9] L. A. Zadeh, Fuzzy sets versus probability, proceeding of IEEE, Vol. 68, No. 3, March 1980.
- [10] L. A. Zadeh, Fuzzy Logic, IEEE Computer, Vol. 21, Issue 4, pp 83-93, April 1998.
- [11] D. Zhanga, B. Chen, A Novel Kernelized Fuzzy C-means algorithm with application in medical image segmentation, Artificial Intelligence in Medicine 2004.
- [12] D. Zhanga, B. Chen, Clustering Incomplete Data Using Kernel-Based Fuzzy C-mean Algorithm, Neural Processing Letter 18: 155-162, 2003.
- [13] M. Kwon, Y. Han, I. Shin, H. Park, Hierarchical Fuzzy Segmentation of Brain MR Images, International Journal of Imaging Systems and Technology Vol. 13, Issue: 2, 2003, pp.115–125.
- [14] M. Yanga, Y. Hua, K.Linb, C.Linc, Segmentation techniques for tissue differentiation in MRI of Ophthalmology using fuzzy clustering algorithms, Magnetic Imaging 20, 173-179, 2002.
- [15] S. Ruan, B. Moretti, J. Fadili, D. Bloye, Fuzzy Markovian Segmentation in Application of Magnetic Resonance Images, Computer Vision and Image Understanding 85, 54-69, 2002.
- [16] G. Berks, D. Keyserlingk, J. Jantzen, and M. Dololi, Fuzzy Clustering- A Versatile Mean to Explore Medical database, ESIT 2000, 14-15 September 2000, Auchen, Germany.
- [17] N. Mohammed, M. Ahmed, Modified FCM in Medical Image Segmentation, 1999.
- [18] H. Suna, S. Wanga, Q. Jiangb, FCM-Based Model Selection Algorithms for Determining the Number of Clusters, Pattern Recognition 37, 2004.
- [19] M. Heydarian, Adaptive Fuzzy Logic Controllers Design, Using Genetic Algorithms, M.Sc. thesis document, Computer Department, Shiraz University, 1997.
- [20] www.doc.ic.ac.uk/~nd/surprise_96/journal/vol4/tcw2/report.html#WhoGain, visited on Oct. 2006.
- [21] M. Gudmundsson, E. El-Kwae, M. Kabuka, Edge Detection in Medical Images Using a Genetic Algorithm, IEEE Transaction on Medical Imaging, Vol. 17, No. 3, June 1998.
- [22] J. Xue, S. Ruan, B. Moretti, M. Revenu, D. Bloyet, W. Philips, Fuzzy Modeling of Knowledge for MRI Brain Structure Segmentation, International Conference on Image Processing, Volume 1, 10-13 Sept. 2000, Page(s): 617-620.
- [23] S. Widz, D. Slezak, K. Revett, Application of Rough Set Based Dynamic Parameter Optimization to MRI Segmentation, IEEE Annual Meeting of the Fuzzy Information, Vol. 1, 27-30 June 2004, Page(s): 440-445.
- [24] D. Selvathi, A. Arulmurgan, S. Thamarai Selvi, S. Alagappan, MRI Image Segmentation Using Unsupervised Clustering Techniques, Proceedings of the Sixth International Conference on Computational Intelligence and Multimedia Applications, IEEE 2005.
- [25] Jagath C. Rajapakse, Bao Guojun, Functional MR Image Registration Using a Genetic Algorithm, 6th International Conference on Neural Information Processing, Volume 3, 16-20 Nov. 1999 Page(s): 922-927.

- [26] C. Chow, H. Tsu, T. Lee, T. La, Medical Image Registration and Model Construction using Genetic Algorithms, International Workshop on Medical Imaging and Augmented Reality, 10-12 June 2001 Page(s): 174-179.
- [27] Jiann-Der Lee, Chung-Hsien Huang and Jau-Hua Huang, Registration of CT Image and Facial Surface Data Using Adaptive Genetic Algorithm, IEEE Region 10 Conference TENCON 2004, Volume B, 21-24 Nov. 2004 Page(s): 203-206 Vol. 2.
- [28] Hongying Zhang, Xiaozhou Zhou, Jizhou Sun, Jiawan Zhang, A Novel Medical Image Registration Method Based on Mutual Information and Genetic Algorithm, Proceedings of the Computer Graphics, Imaging, and Vision, IEEE 2005.
- [29] Wen Peng, Ruofeng Tong, Guiping Qian, Jinxiang Dong, A Local Registration Approach of Medical Images with Niche Genetic Algorithm, 10th International Conference on Computer Supported Cooperative Work in Design, May 2006 Page(s):1-6.

Chapter 4:

Optimizing the Level Set Method using Genetic Algorithms

4.1 Overview of article

In this chapter we present the first article from our research, published in IEEE Transactions on Nuclear Science, VOL. 56, NO. 1, FEBRUARY 2009. Before going to the article (section 4.2), we need to briefly explain its position in this research-work as well as providing some information which is not included in the article itself (i.e. limited size for articles). We will add one more section to the end of this chapter to give a summary of this part of the project.

At the first stage of the project, we needed to segment organ/cysts in images. Having the segmented tissue, we are able to apply some post-processing operations such as area measurement, diameter measurement, shape estimation, etc. We used the results of this article at the next step of the project which comes in the next chapter under the second article. Also, using the segmented object in an image, it is easier and faster to obtain more accurate registration. For example, if we plan to register a kidney in two serial images in time, when we have the segmented kidney in both images, the registration operation will be faster as we ignore the data from the rest of the images. Also registration will be more accurate as we ignore the part of the images that contain the liver, which is an easily deformable body organ.

To choose a suitable segmentation method, we examined many references, from which we can generate two categories. The first category includes methods which find all edges in the entire image (e.g. Fourier Transform High pass Filter, Canny Filter, Sobbel Filter, etc.). The second category includes methods which find edges of a tissue/organ in the image (e.g. Seeded Region Growing Algorithm (SRGA), Active Contour methods such as Level Set Method (LSM) and Snakes). According to our goal, segmenting a specific organ/tissue in the image, the second category matches our application, but the problem is that none of these methods are ready to use for segmenting any specific object. The SRGA is too sensitive to a chosen threshold, and the LSM/Snakes parameters need to be optimized for specific object in different image modalities.

The following article explains the optimization method (Genetic Algorithms) that we used in order to find the optimal parameters of the LSM for segmenting three different objects in the body. We used the GA approach to search for optimal parameters of the LSM in order to segment Kidney/Cyst in abdominal MRI and the airway lumen in CT images.

4.2 Article

Optimizing the Level Set Algorithm for Detecting Object Edges in MR and CT Images¹

Mohammadreza Heydarian, Michael D. Noseworthy, Markad V. Kamath, Colm Boylan, and W. F. S. Poehlman, *Senior Member, IEEE*

Abstract—Specifying the boundary of tissues or an organ is one of the most frequently required tasks for a radiologist. It is a first step for further processing, such as comparing two serial images in time, volume measurements, etc. In the present work, we use genetic algorithms (GA) and where necessary apply a “dynamic genetic algorithm” (dGA) procedure, which (we believe) is a unique application, to assess different values for finding an optimal set of parameters that characterize the level set method, a geometric active contour, for use as a boundary detection method. Four quantitative measures are used in calculating geometric differences between the object boundaries, as determined by the level set method and the desired object boundaries. A semi-automated method is also developed to find the desired boundary for the object. A two-step method requires the user to manipulate the object boundaries obtained by applying an edge detection method based on the Canny filter. By setting the level set method parameters using the output of the GA we obtain accurate boundaries of organs automatically and rapidly.

Index Terms—computed tomography, genetic algorithms, geometric active contour, level set method, magnetic resonance imaging

¹ Manuscript received June 19, 2008; revised September 4, 2008. Current version published February 04, 2009. This work was supported through a fellowship to Mr. Heydarian. Dr. Kamath’s work was supported in part by a Discovery Grant from Natural Sciences and Engineering Research Council (NSERC; Canada).

M. Heydarian is with the Department of Computing and Software, McMaster University, Hamilton, ON L8S 4K1 Canada, and also with the Brain-Body Institute, St. Joseph’s Healthcare, Hamilton, ON L8N 4A6 Canada (e-mail: heydarmr@mcmaster.ca).

M. D. Noseworthy is with the Department of Electrical and Computer Engineering, School of Biomedical Engineering, and Department of Medical Physics, McMaster University, Hamilton, ON L8S 4L8 Canada, and also with the Brain-Body Institute and Diagnostic Imaging, St. Joseph’s Healthcare, Hamilton, ON L8N 4A6 Canada (e-mail: nosewor@mcmaster.ca).

M. V. Kamath is with the Department of Medicine, Department of Electrical and Computer Engineering, Department of Computing and Software, Department of Kinesiology, and School of Biomedical Engineering, McMaster University, Hamilton, ON L8S 4L8 Canada, and also with the Brain-Body Institute, St. Joseph’s Healthcare, Hamilton, ON L8N 4A6 Canada (e-mail: kamathm@mcmaster.ca).

C. Boylan is with the Department of Radiology, McMaster University, Hamilton, ON L8S 4L8 Canada, and also with Diagnostic Imaging, St. Joseph’s Healthcare, Hamilton, ON L8N 4A6 Canada (e-mail: cboyland@stjosham.on.ca).

W. F. S. Poehlman is with the Department of Computing and Software, McMaster University, Hamilton, ON L8S 4K1 Canada (corresponding author to provide phone: 905-525-9140 x22891; fax: 905-524-0340; e-mail: skip@mcmaster.ca).

I. INTRODUCTION

ACCURATELY locating the edges of an organ or cyst is important when radiologists need to measure tissue/pathology volume or compare two images from the same patient acquired at different times. Image segmentation [1] refers to grouping a collection of pixels (voxels) into multiple unlabeled regions such that pixels within each group are more similar to each other than pixels assigned to other groups according to a given criterion. Our goal is to locate objects of interest inside computed tomography (CT) or magnetic resonance (MR) images, an issue considered a problem in the computer vision field.

The selection criterion of regions is based on different features such as gray intensities, texture, and edge information. When working on a specific image modality such as MRI [2], other overall features of varying complexity are also important. For example, image features such as voxel size, gap between slices, plane of acquisition (e.g. axial, sagittal, coronal), the presence of an injected contrast agent, and system acquisition parameters (i.e. repeat time (TR), echo time (TE), RF flip angle, magnetic field strength) all can modulate image features. Furthermore, tissue chemical composition and even subject-specific factors such as age and physical condition may also be relevant while processing an MRI output.

Segmentation algorithms can be classified into two categories: low-to-intermediate level and high-level [3]. The first category, which operates at the pixel level, includes five popular methods: gray intensity histogram analysis, texture analysis, edge enhancement and linking, region growing, and contour following [3]. The second category, which is anatomical segmentation, needs prior knowledge, which is usually supplied by an expert radiologist [3].

There are two different classes of active contour models, parametric active contour [4] and geometric active contour models[5]. The level set method [6]-[11], a geometric active contour model, can be used to isolate and build a coherent mathematical description of a particular shape. Li *et al.* [12], using the higher level language MATLAB, introduced a variational formulation of geometric active contours to eliminate the need for a re-initialization procedure. Although their method is mathematically sound and may work with a variety of images, it requires the specification of a set of seven parameters (detailed in part II). Unfortunately, there is no one set of parameters that works on all types of images. For example, using the parameters from Li *et al.* [12], on high-resolution MR images of the abdomen, we were not able to obtain acceptable results. Also, the number of iterations that are required in order for the level set method to converge on MR images is much larger than that needed for the sample images used in [12]. Images of size 100x200, 64x80, and 110x130 shown in their paper [12] required 650, 800, and 300 iterations of the level set method, respectively, in order for convergence to occur. In addition, different sets of seven parameters, as shown in Table I, were used to implement the level set method on the various images in [12]. In other words, every kind of image needed a specific set of parameters. Unfortunately, there

TABLE I

Different sets of parameter to set the level set method. The first three rows are from [12] and the rest are the result of GA.

	λ	ν	ϵ	τ	μ	ρ	σ
First set from [5]	5.0	3.0	1.5	5.0	0.04	6	1.5
Second set from [5]	5.0	1.5	1.5	5.0	0.04	6	1.5
Third set from [5]	6.0	-3.0	1.5	2.0	0.1	6	1.5
GA on Kidney	21	-4.6	0.7	96	0.0022	10	1.7
GA on Kidney-ROI	36	-5.0	1.7	94	0.0024	13	1.4
GA on Cysts	62	-3.9	1.4	93	0.0014	5	1.8
GA Lung-Airways	50	-5.1	1.7	95	0.0010	9	0.9

seem to be no possible ‘rules of thumb’ for generalization.

Since the solution domain of those seven parameters for the level set method is very large, as shown in Table II, scanning the whole solution-domain or using a “trial and error” method is not suitable for finding optimal parameters. One may, traditionally, use the GA to find the optimal position for the contour points at each iteration of the active contour which involves primarily a parametric method usually with Snakes [13]-[17]. However, more recently the GA is used to optimize a specific energy function [18]-[23] (and the contour position in each iteration of the Snakes [18]-[21]). In this paper we present the use of genetic algorithms (GA) [24] as a heuristic search method to optimize parameters of the level set method in order to obtain more accurate results within a short time. Fig. 1 shows a flowchart of the software system that uses a GA to optimize the parameters of the level set method.

Genetic algorithms are an optimization method based on a set of evolutionary rules. They simulate evolution by: 1. Natural selection through the creation of an initial population; 2. Evaluating the fitness of each individual related to other members in the population; 3. Selecting individuals with high fitness value; 4. Generating a new population using genetic operations (i.e. crossover and mutation); and 5. Repeating this process from the evaluation step until some termination criterion is reached.

One of the most powerful features of the GA is that it can deal with the underlying system (i.e. the level set method) as a black box with several parameters that need to be optimized. The GA needs to know the desired outputs related to the sample inputs. In our case, optimizing the level set method, the box has seven parameters and the input to this box is an image with a polygon inside an image object, and the output is the boundary of that object which is known to an expert in the area (the radiologist). Thus,

TABLE II

The range of the parameters for the level set method (derived from Li *et al.* 2005 [12]). k is used to calculate μ .

	λ	ν	ε	τ	$k = \mu\tau$	ρ	σ
Minimum	1	- 6.4	0.1	1	0.01	1	0.1
Maximum	64	- 0.1	6.4	100	0.24	16	6.4
Precision	1	0.1	0.1	1	0.01	1	0.1
no. of choices	64	64	64	100	24	16	64
no. of bits in gene	6	6	6	7	5	4	6
Size of the solution domain	$64 \times 64 \times 64 \times 100 \times 24 \times 16 \times 64 = 644 \times 10^9$						

optimizing a system using the GA, one does not need to find the mathematical model of the underlying system. This makes it generally an easy to use optimization method. Also, the function (system), which needs to be optimized by the GA, does not need to be a continuous function since the GA does not involve the differentiation of the function.

We developed an evaluation function as a part of the GA to assess the output of the level set algorithm. The evaluation is based on comparing the result of the level set method to a manually selected desired result. Each chromosome in the current population of the GA is decoded to seven parameters for setting the level set algorithm. Then the level set method is applied on sample images and the evaluation function provides the result. The GA uses this result of the assessment for selecting the best individuals in the current population. Then these are used in the production of the subsequent population. The experimental results show that this evaluation method correctly assesses geometrical properties of the contour as the result of the level set method. To evaluate the result of the level set method, we need to define the desired boundary of the underlying object for comparison purposes. Since the edges of organs in medical images are fuzzy, selecting them is often difficult, variable, and time consuming. To assist with edge detection, we developed a semi-automated method by modifying the output of a Canny filter [1] to select desired boundaries.

In this paper we present some of the issues associated with medical image segmentation, explain our proposed evaluation function of the GA, define our proposed dGA, and explain the semi-automated method for selecting a desired boundary. We finally demonstrate the success of our approach using MR images of the kidney, cysts, and CT images of lung airways.

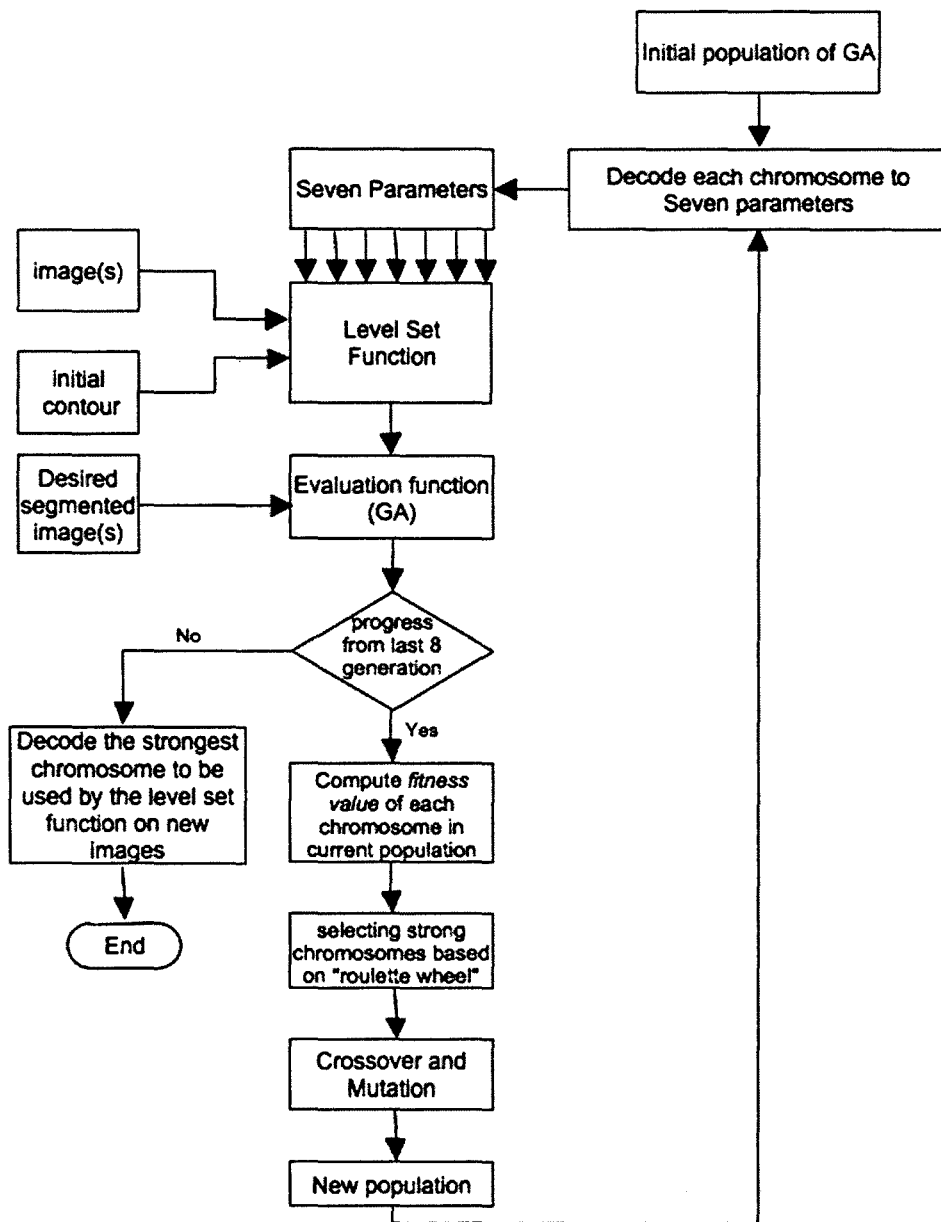


Fig. 1. A flowchart of the software system that uses a GA to optimize the parameters of the level set method.

II. BACKGROUND

A. Medical Image Segmentation

MRI and CT produce very precise images of the body, which have currently reached sub-millimeter isotropic voxel resolution. This imaging capability allows radiologists to find minute changes in organs or lesions, which is helpful in evaluating the progress or regression of disease. However, it is sometimes difficult for radiologists to identify a lesion, which is hardly discernable to the naked eye or to evaluate temporal differences between two images taken in a time sequence. It is considerably more difficult to detect, localize, and identify changes in successive temporal image sequences while working with 3D data sets which may often contain hundreds of images, and even hundreds of lesions (e.g. polycystic disease is one example where hundreds of lesions may or may not vary spatially and/or temporally). Also, for a physician/radiologist who typically examines tens of thousands of images a day, the process of repeated assessment of lesions (size, intensity, and location, over time) is not only tiresome but more importantly highly prone to inaccuracies. Thus, assisting a radiologist in identifying a boundary and localizing a pathological tissue/cyst confined to a volume helps to speed up the process of identification of any temporal variation.

In 3-D image data, a certain part of an organ may not be circumscribed by smooth curves which often leads to partial volumes in certain voxels. This, in turn, results in edges which are elusive to be determined by certain computer algorithms. This problem is more acute when the voxel size is relatively larger, which occurs when fast imaging modalities are employed, for example, in the abdomen. Also, the slice gap thickness is important when dealing with partial volumes or during the process of measurement of volumes in 3-D image data. Some MRI scanner settings such as the repeat time (TR), echo time (TE), and RF pulse flip angle cause modulation of tissue contrast, so the segmentation algorithms that work based on a concrete intensity range or threshold are more likely to fail or produce variable results. Furthermore, the presence of an injected contrast agent should be taken into consideration as this will also modulate tissue contrast.

B. Level set method

The level set method is a shape detection method, which isolates a particular shape of an object inside the image. The object must correspond to a region whose pixels have different grayness intensity from neighboring regions [11]. Introduced by Malladi [25], the use of the level set methods for shape recovery makes it insensitive to noise at boundaries but enables convergence on the object boundary. The algorithm naturally executes topological change and stops based on the image gradient. The idea is to define a filter for finding the image gradient, the results of which show, no change in the gradient away from boundaries, and, sharp changes near boundaries [11]. Using the level

set method, numerical computation for curves and surfaces on a fixed Cartesian grid can be performed with no need to parameterize these objects.

Li *et al.* [12] developed a new variational formulation for geometric active contours that eliminates the need for the re-initialization step. Their method is based on a variational energy function, consisting of an internal energy term to penalize the direction of the level set method from a signed distance function and an external energy term to derive the motion of the zero level set to the object boundaries [12]. This was accomplished by introducing the following total energy function:

$$E(\phi) = \mu P(\phi) + E_{g,\lambda,\nu}(\phi) \quad (1)$$

where P and $E_{g,\lambda,\nu}$ are internal and external energy functions of the level set method, respectively, and are defined as

$$P(\phi) = \int_{\Omega} \frac{1}{2} (|\nabla \phi| - 1)^2 dx dy \quad (2)$$

$$E_{g,\lambda,\nu}(\phi) = \lambda L_g(\phi) + \nu A_g(\phi) \quad (3)$$

where $\Omega \subset \mathbb{R}^2$, and $L_g(\phi)$ and $A_g(\phi)$ are defined as

$$L_g(\phi) = \int_{\Omega} g \delta(\phi) |\nabla \phi| dx dy \quad (4)$$

$$A_g(\phi) = \int_{\Omega} g H(-\phi) dx dy \quad (5)$$

with δ as the univariate Dirac function, H as the Heaviside function, and g as the edge indicator function defined by

$$g = \frac{1}{1 + |\nabla G_{\sigma} * I|^2} \quad (6)$$

with I equal to an image and G is the Gaussian kernel with standard deviation σ . An advantage in employing a genetic algorithm, is that it is not necessary to know the mathematical model of the level set method as long as we have its implementation in a programming language. The interested reader is referred to the original references on the level set method such as [11], [12] for more details.

To implement the variational energy function, there are seven parameters to be specified [12]. The first and the second parameters, λ and ν , are the coefficient of the first and the second components of the external energy (3), respectively, where λ must be greater than zero and ν should be greater than zero to speed up shrinking the contour on the object boundary or less than zero to speed up expanding of the contour toward the object boundary. The third parameter, ε , is the width of the Dirac function and must be greater than zero. The fourth parameter, τ , is the time step of the level set method which, when its value is large, can speed up the algorithm, at the possible expense of the uncertainty of locating the boundary. The fifth parameter, μ , is the coefficient of the internal energy function (1), which must satisfy $\mu\tau < 1/4$ to maintain a stable level set method. The sixth parameter, ρ , is the input of the initial level set method where the area inside the initial contour is $-\rho$ and the outside is $+\rho$. The seventh parameter, σ , specifies the width of a Gaussian smoothing filter in order to remove noise in the input image.

C. Genetic Algorithm

A genetic algorithm (GA) [24] is a type of evolutionary system that simulates the process of natural selection over generations. In nature, a chromosome represents the features of an individual. Each chromosome consists of a number of genes, each representing a specific feature of an individual. In the field of molecular genetics, each gene consists of several alleles that are built using one of the four nitrogenous bases: adenine, cytosine, guanine, or thymine. In simulation, each chromosome of the GA is represented by a string of genes. Genes can be made using different types of alleles such as characters, digits, or numbers. All evolutionary methods simulate natural evolution, generally by creating an initial population, by evaluating the fitness of each individual related to other members in the population, by selecting individuals with a higher fitness value, by generating a new population using genetic operations (i.e. crossover and mutation), and finally by repeating this process from the evaluation step until a predefined termination criterion is reached. A brief explanation of each step in the GA approach follows below.

1) *Initial population*: Each individual (chromosome) is a solution for the system being designed. The number and the type of features from the under-design system are used to calculate the length of chromosomes, but there is no deterministic method to choose the number of individuals in the initial population. The size of the population will stay fixed during the run time of the GA. Random numbers are used with a normal distribution to produce the initial population. Randomness makes the GA a non-deterministic method that may end with different answers on different runs for the same problem.

2) *Selection*: In the current population, some individuals have a higher fitness level than others and so the GA positively biases its selection for them in generating a new population. Finding a good and efficient evaluation function is the most important aspect for designing a GA, while applying the function to evaluate individual chromosomes is the most time consuming. Therefore, a smaller population is chosen, although a larger population of chromosomes often has a higher probability of finding a solution, which is a global optimum.

3) *Crossover*: Crossover produces a new population. In this step, the GA combines elements (genes) of existing individuals in a current population (solutions) to create new solutions by inheriting some features of their parents (current solutions). Although this operation is important to produce a new population, we assign a low probability to some selected individuals to be present in the new population without any change. It gives them a chance to combine with some new individuals in the subsequent population. The probability of crossover is usually more than 85%. It should be taken into consideration that a copy of the best individual is always forwarded to the new population to keep the GA away from regression.

4) *Mutation*: Mutation is a random change in some genes to generate a new solution, which may be better than the previous solution. Since it is random and may yield a worse solution, it is applied with very low probability (say, less than 1% for each allele) in the GA. Mutation helps the GA to avoid becoming trapped at a local optimum.

This occurs when all individuals in a population are in the same region around the local optimum and crossover does not generate any new solutions in other areas.

5) *Repetition and termination criteria:* After generating each new population, the GA repeats the steps involving selection, crossover, and mutation to produce a new population, unless a termination condition is met. The GA uses different termination criteria such as a specific number of generations, finding an acceptable solution, or finding no change in fitness of the best individual, during several generations.

III. METHODOLOGY

A. Proposed Evaluation Function

We developed an evaluation function, which includes four measures to calculate geometric differences between “the object boundaries as determined by the level set method” and “the desired object boundaries.” To evaluate the resulting contour of the level set method, we compared it with a desired boundary selected by an expert (i.e. a radiologist). We also developed a semi-automatic method to help experts for drawing the desired boundary (to be explained in section C).

Assume X and Y are logic matrices with the same size as the image that is going to be segmented. X represent the desired boundary and Y the result of the level set method, where the logic 1 shows the points belong to the edge of object. Also, A and B are the same type of matrices which show the area surrounded by edges in X and Y , respectively. The number of contour overlap points (result of the level set algorithm) with the desired boundary is the first measurement used

$$s1 = |X \cap Y| / |X| \quad (7)$$

However, this was not always reliable, because there is high probability of selecting the wrong pixels on the desired boundary, as image edges are often blurry (e.g. abdominal organ edges in MR images and edges of lung airways in CT). For example, shifting the edge of one side of an organ by one pixel, results in 20% to 40% false-negative points. In addition to counting the number of overlap points, we calculate the percentage of the desired area covered by the contour area

$$s2 = |A \cap B| / |A| \quad (8)$$

Then, we determine the ratio of the parts of the contour that were outside the desired area to those inside

$$s3 = (|B| - |A \cap B|) / |A|. \quad (9)$$

Also, for the contour points that were not on the desired border, we calculate their distance to the nearest point on the desired border

$$Z = Y - (X \cap Y) \quad (10)$$

$$s4 = \sum_{\forall i \in Z} \min |i - j| \quad \forall j \in X. \quad (11)$$

The results of (7) and (8) are similar to the Jaccard similarity coefficient in the

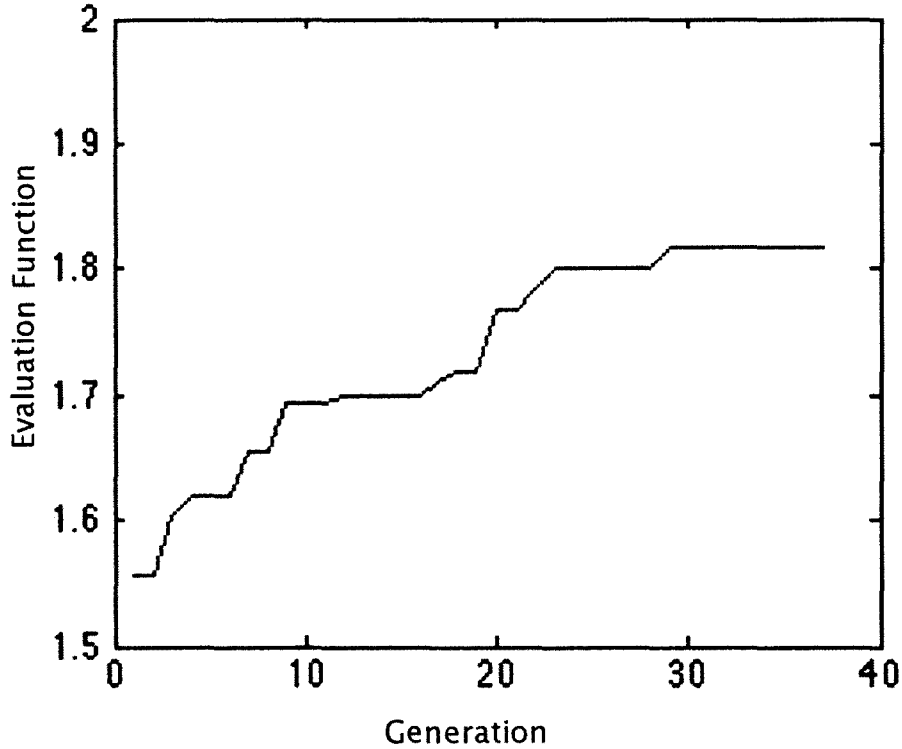


Fig. 2. An example of an evaluation function to show the progress of the genetic algorithm.

interval $[0,1]$ and are counted as positive points (advantage) for the current set of parameters of the level set algorithm. The result of (9), which is again similar to the Jaccard distance, is equal to or greater than zero, which often is in the interval $[0,1]$, and is counted as a negative point (disadvantage) for the current set of parameters of the level set algorithm. The distance between non-overlap points from the contour to the desired boundary (11) is a negative point (disadvantage) with no limitation in domain range, so we use its inverse as a positive point (advantage) in the interval $[0,1]$ (where for distance equal to 0, we calculate the inverse as 1). Our goal was to maximize the evaluation function (12) as shown in Fig. 2. We did not see any difference in progress of the GA while using different coefficients for s_1 , s_2 , s_3 , and s_4 for optimizing the level set algorithm as used for segmenting kidneys, so we gave equal weight to all components of (12):

$$f(\text{current parameters}) = s_1 + s_2 - s_3 + (1 / s_4). \quad (12)$$

B. Adjusting GA parameters dynamically (dGA)

While the choosing of a suitable probability for crossover and mutation, and

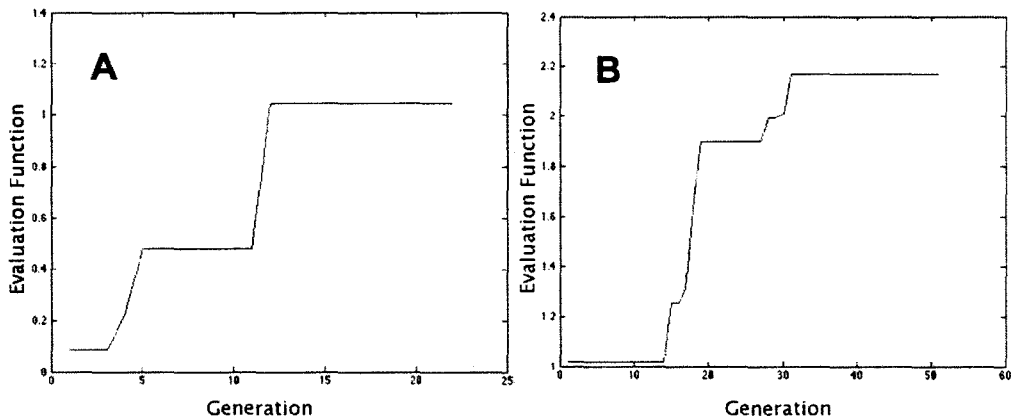


Fig. 3. Plot A shows the progress of the genetic algorithm with 19 individuals in the population. Plot B shows the progress of our dynamic genetic algorithm with 27 individuals in the population.

deciding on the number of points for crossover are crucial in the progress of the GA, there are, unfortunately, no specific rules described in the literature that would allow optimization. Choosing larger values for these three parameters (crossover probability, mutation probability, and the number of points for crossover) results in a more distorted new population, while smaller values diminish the progress of the GA. In this research, we used a string of 40 bits for each chromosome, which simulates seven parameters of the level set method (Table I). Another fixed parameter used was population size, which was set to 37, 27 or 19 chromosomes for different runs of the GA. Although the bigger population size covers more area in the solution domain, it needs a longer time to evaluate the population. We used 19 chromosomes to apply the GA on two slices of the MR or CT images with size 512x512 pixels. We increased the population size when applying GA on subsample of the image (approx. 100x100 pixels).

Other parameters, probability of crossover, probability of mutation, and number of points for crossover, affect convergence speed as well as distortion amount. Thus, the probability of crossover and mutation were initialized to 85% and 1%, respectively. If the GA calculation did not progress after five generations, the probability of crossover and the probability of mutation were increased by 1% and 0.5%, respectfully. A restriction was reached when the probability of crossover achieved 100% indicating the maximum probability of mutation could grow to 8.5%. The initial number of points for crossover was set to 4 randomly selected points between alleles and was increased by one, each time the probability of crossover was increased. An inverse change is applied when there is progress in the GA, where the initial amount became the minimum assignment to parameters. This variation of the GA is referred to as *dynamic genetic algorithm* (dGA). Fig. 3-A shows the result of applying a regular GA while Fig. 3-B shows the result of applying this dynamic change in maximizing the evaluation function. Although increasing these parameters results in lower average of population, it helps the GA

calculation to escape from local optima (i.e. the function was optimized to converge on a global maximum).

C. Selecting the Desired Boundary

One of the most time consuming image processing tasks for radiologists is measuring the area of organ/cysts by manually selecting the border of the area. The ultimate goal of this project is to develop a computational tool to help radiologists perform faster and more accurate organ or cyst cross sectional area measurements. But for evaluating GA chromosomes, we need to compare the result of the level set method, optimized using parameters derived from decoding GA chromosomes, to a desired border selected by a radiologist (CB). After evaluating several edge detection methods such as Sobel, Prewitt, Laplacian of Gaussian, Canny filter [1], etc., as well as high-pass filtering the image with a Fourier transform [1], we found the Canny filter, based on its automatic threshold, had the highest probability of finding the organ/cyst boundaries, but it needed to be manipulated by a radiologist for maximal accuracy.

We implemented a multi-step semi-automated algorithm in MATLAB (v7.4, The Mathworks, Natick, MA) using its Image Processing Toolbox to help the user (radiologist) select the boundary of the tissue of interest. Using the edge detection result, based on the Canny filter, the program first queries a user to draw a polygon around the region of interest excluding the edges of the unwanted organ/cysts. Second, it prompts the user to define the pixels that are part of the boundary, but not selected by the edge detection algorithm. Third, the user is able to delete the pixels that do not belong to the border but have been selected by the edge detection algorithm. Steps two and three are repeated once to allow correction of inaccuracies.

D. Termination condition for the level set method

We developed an efficient termination condition to determine a stopping point for the iteration of the level set method. This method is fast and accurate to within one pixel. As a contour-matrix contains floating-point numbers with two-digit precision, we used a rounding function to estimate pixel position. Thus, if the integer part of one element is fixed and the real part changes from 0.00 to 0.49 or from 0.50 to 0.99, the representative pixel of that element will not change. Also, one pixel may represent several elements of the contour-matrix. This means occasionally, although the contour-matrix is changing, the resultant boundary from that contour will not change. After every 40 iterations of the level set method, the boundary is reconstructed from the contour and compared with the boundary determined 40 iterations previously. If the difference (percentage of non-overlap points) is less than 2%, the level set method iteration is stopped.

E. Imaging

A variety of routine clinical MRI and CT data was used to evaluate the performance of our proposed method. A 3.0T GE Signa HD MRI system with an 8-channel torso array coil (GE Healthcare, Milwaukee WI) was used to scan subjects with polycystic disease containing several cysts in their kidneys and liver. The approach was tested primarily on T2 weighted fast recovery fast spin echo (FRFSE) images with fat saturation (8mm thickness and 1mm gap) and T2 weighted single-shot fast spin echo (SSFSE) images (4mm thickness and 0mm gap). However samples of steady state imaging (FIESTA; Fast Imaging Employing STeady-state Acquisition), short tau inversion recovery (STIR) for fat nulling, and dual echo in and out of phase, in axial and coronal planes, were used for testing. For all MR imaging sensitivity encoding with an acceleration factor of 2 (ASSET; Array Spatial Sensitivity Encoding Technique) was used to reduce imaging time and artifacts.

For assessment of the airway luminal diameter and area, CT images were acquired by using 64-channel multidetector CT scanners (LightSpeed VCT; GE Healthcare, Milwaukee, Wis). Whole-lung CT images with no intravenous contrast medium were obtained with the following parameters: detector collimation, 0.625 mm; field of view, 34.5 cm; pitch, 1.375; gantry speed, 0.4 second per rotation; automatic selection of the milliamperage setting (range, 128–300 mA); and noise index, 10. Axial reconstructions of 0.625mm slice thickness at 0.625mm reconstruction interval were provided for analysis. Images were provided in standard algorithm and lung algorithm format. Suitable axial slices and airways were chosen for assessment.

IV. RESULTS

The initial testing of our method involved assessment of healthy kidneys to determine the success of localizing the boundary between a healthy organ and its surrounding tissue. Two abdominal images (512x512 acquisition matrix), 14mm apart, were acquired from a healthy volunteer. The desired boundary of one of the two kidneys of each slice was specified by a radiologist (CB). A polygon inside the kidney was manually defined as an initial contour on each slice for applying the level set method. These two information components, the desired boundary and the initial contour, were consistent during the progress of the GA. We set the probability of crossover and mutation to 85% and 1%, respectively, and the number of points for crossover was set to 5. After 37 generations of the GA, a set of optimal parameters was found. Setting the level set method using this set of parameters resulted in finding the kidney boundary on different MRI slices from different subjects (patients) after 300 to 900 iterations, depending on how close the initial contour was to the true boundary. Note that this capability for generalization to the above degree is in sharp contrast to previous work where reproducibility on a single image was impossible to obtain [22].

It was noted that choosing a different initial contour did not influence the result of

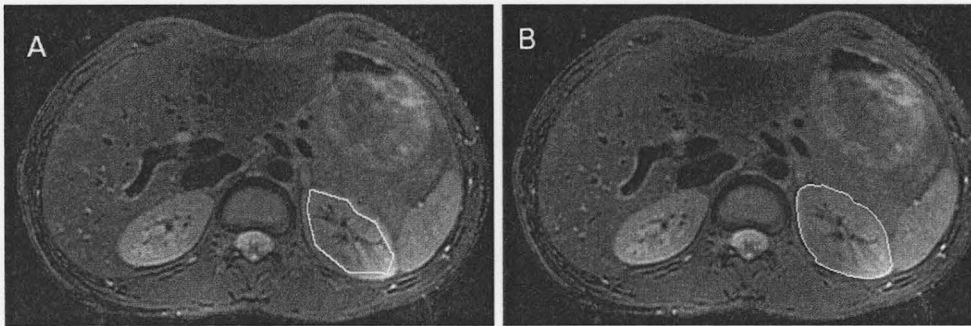


Fig. 4. The MR image on the left (A) shows the initial contour that was selected manually by nine mouse clicks and the right image (B) shows the result of the level set method after 400 iterations.

the level set method, but only the convergence time. The closer the initial contour to the desired area, the shorter the convergence time. One exception where the choice of the initial contour did have an effect on the output of the level set method is discussed at the second paragraph of the Conclusion section. Resulting contours from the level set method covered 97% to 99.75% of the desired area on different MR images (most were above 99% coverage). Although the resulting contour from the level set algorithm was 0.25% to 3% different from the desired boundary, the kidney shape remained. This small difference was not visually discernable and the resulting contours were acceptable to radiologists. Fig. 4 shows one example of an initial contour and the result of the level set method.

It took almost 1 minute for 100 iterations of the level set method on a 512x512 image using our sample computer (Apple iMac with 2.33 GHz Dual Intel Core and 3 GB memory). To reduce computation time, we restricted the application of the level set method by applying it on a rectangular region of interest (ROI) that included the organ of interest. Then, when applying the level set method in a ROI to find the kidney boundary, using the set of parameters already determined for kidneys, the percentage of covered area was substandard compared to the slower application on the whole image. Therefore, the GA was again used to find the best set of parameters for the smaller extracted images that only contained one kidney and a small surrounding area (ROI of approximately 110x110 pixels). Similar to the last run of the GA, we chose two slices of kidneys that were distal from each other and then cut a part of each slice. The rest of the work was exactly the same as previous runs of the GA. After 79 iterations, the GA converged on a new set of parameters. Then with the new application of the level set method using this set of parameters, the accuracy was the same as before, yet markedly faster. For example, Fig. 5-A shows a 109x107 ROI that was selected manually from a 512x512 abdominal MR image. Fig. 5-B shows the final contour on the kidney boundary reached after 400 iteration of the level set method. This took 15 seconds of computation time.

Radiologists need to monitor and determine temporal changes (if any) in cysts, and to rapidly know whether there is any enhancement following the injection of a

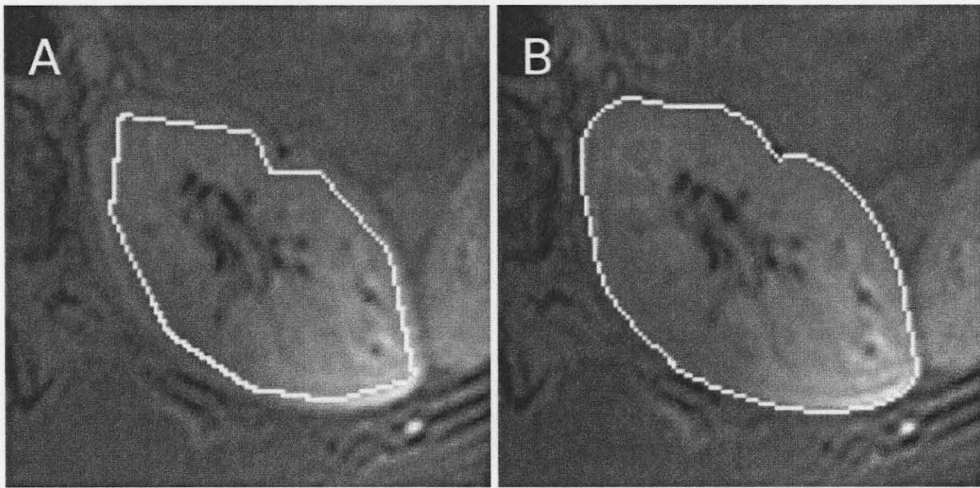


Fig. 5. The initial contour (A) and the result of the level set method (B) after 400 iterations (15 seconds of computation time).

contrast agent. Therefore it is an important requirement to find the border of a cyst, which is presumably comprised of one tissue type meaning that consistent image characteristics exist. To best define the boundary of cysts, we applied the level set method using the set of parameters found by applying the GA on two different slices of kidney. Initial results were not promising. However, by first applying the GA to optimize the level set method parameters, abdominal cyst boundaries could be easily identified.

We chose two slices of MR abdominal images from two patients with several cysts in their abdomen and then, as above, extracted a ROI for each analysis. For each slice, we specified the desired border and a polygon inside the cyst as an initial contour. The GA was then applied in the same way, with the same parameters used for two kidney slices. After 40 iterations, the GA converged on a new set of parameters. Applying the level set method using these new parameters resulted in finding cyst boundaries with 97% to 99.8% accuracy, with most being greater than 99%.

The result of applying the level set method on the whole image to find cyst borders was as good as applying it on an extracted ROI from the image when using the same set of parameters. This indicates we do not need to find a new set of parameters to apply on the whole image for finding edges of cysts in MR abdominal images. Fig. 6-A shows an 86x79 image of a cyst with the initial contour and Fig. 6-B shows the result of the level set method after 960 iterations, which took just 17 seconds to find.

Another application of our method that we tested involved measuring airway inner diameter on CT images. This is important for understanding the biophysics of gas flow in diseases in the lung [26]. As expected, none of the previously obtained sets of parameters worked well for this new kind of image. We applied a GA with population of 19 on two lung images (512x512) and after 23 iterations we found that this was still not adequate. Progress for the GA was assessed by comparing the result of the evaluation

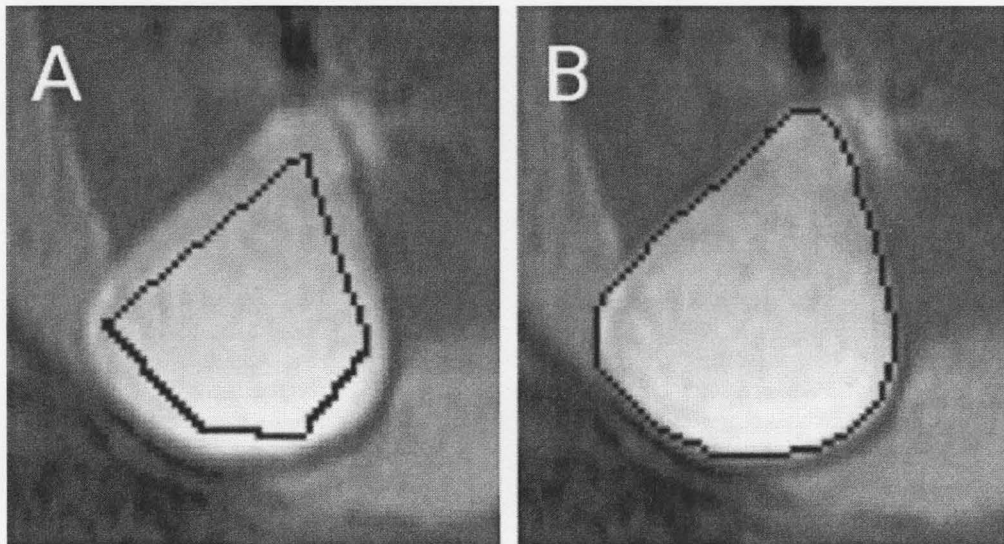


Fig. 6. A. The initial contour, B. The result of the level set method after 960 iterations (17 seconds of computation time).

function from the current GA run to the previous GA runs. The GA was stopped and we added eight randomly generated individuals to the current population, and then ran the GA again based on dynamically adjusting its parameters (dGA). After 52 generations, the dGA came up with a new acceptable set of parameters. Fig. 3-A shows the GA progress with a population of 19 individual after 23 generations. Fig. 3-B shows the second phase of the progress based on the dGA with a population of 27 individuals after 52 generations. Although we used the same set of parameters when applying the level set method on a selected part of lung images, we obtained accurate results on images approximately 80x80 pixels in size.

One of the problems we noted during lung CT image processing was voxel size. The smallest voxel for typical clinical protocols was $0.625\text{mm} \times 0.625\text{mm}$, in-plane, with a 1.25mm slice thickness. Greatest clinical interest was in evaluating airway diameter at the 6th to 10th airway branch levels, or diameters with size 3.6 down to 1.63 mm [27]. This low resolution imaging, not only does not show small changes in size, but also does not have enough area for manually selecting an initial contour. So we used a cubic resampling method to increase in-plane resolution by four times. Although the result showed acceptable measuring to radiologists, there was doubt about the fidelity of the underlying image. So, for some clinical data we produced a reconstructed image with a smaller field of view but same size (512×512) to have pseudo-higher resolution images. The voxel size of these new images was $0.188\text{mm} \times 0.188\text{mm}$ with 0.625mm slice thickness. Comparing the result of applying the level set method on these new high resolution images to the result of applying the level set method on resized images shows that resizing does not appear to cause any deviation in uniquely determining airway edges. Fig. 7 shows the result of finding the airway edge in a resized image and Fig. 8

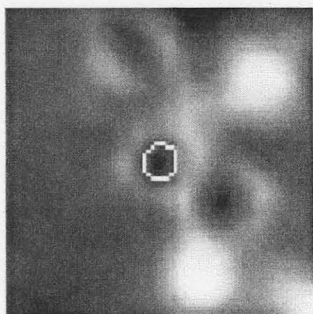


Fig. 7. Result of the level set method on resized lung CT image through a small airway (black).

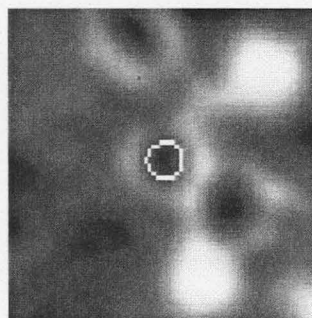


Fig. 8. Result of the level set method on high-resolution lung CT image, reconstructed from raw data.

shows the same in a high-resolution image. The small difference between these two results is the result of pixel size in these two images. The high-resolution image contains pixels of size 0.1875mm whereas the pixel size of the resized image is 0.1904mm.

V. DISCUSSION

A. Genetic Algorithm Considerations

Our results show that, using the proposed evaluation function, the GA can determine the optimal parameters for the level set method which can furthermore be used to accurately locate the edge of an organ in a CT or MR image, in a short period of time. Developing the dynamic genetic algorithms (dGA), allows one to escape from identifying local optima and therefore, enhance the convergence to a global optimum. According to the weakness that dGA brings to the average fitness of a population, we always start by using a regular GA, but apply the dGA if the expected progress for the best individual fitness can not be realized. We have also found that for the GA (and the dGA), better generalization occurs when two sample object boundaries are employed, as desired boundaries in the evaluation function. More issues on generality are discussed later in this paper.

Prior to our work, most GAs were used for optimizing parametric active contours (Snakes) for purposes of image segmentation. This reported research could be classified into two categories. The first category [13]-[17] applied GA in every iteration of the Snakes to find the optimum position of contour points. They called it Genetic Snakes. The main idea was illustrated by MacEchern *et al.* [13] whereas others [14]-[17] are different in either number of neighborhood points, which are considered as the search

domain for the GA, or in the definition of the Snakes energy function, which is used as the evaluation function for the GA. If the Snakes energy function is not characterized appropriately, the result of the GA is not reliable. Also, running the GA in every iteration of the Snakes is time consuming. However, the authors [13] mentioned that their method “yields a desirable convergence rate, with no time penalty if the GA is implemented in parallel.”

The second category of research [18]-[23] used the GA for finding the optimum coefficients of each component of the Snakes total energy function (e.g. internal energy, external energy, etc.). These coefficients weight the influence of each component of the total energy function. Some researchers [18]-[20] in this category used the GA to optimize the coefficients of the energy function for the Genetic Snakes (introduced within category one). The research presented in [19], [20] is based on [18] which used the GA for optimizing four coefficients of the total energy function that can be varied for three different values. This small number of choices for each coefficient leads to a relatively small size of the solution domain (i.e. $3^4 = 81$), which can be searched sequentially and shows no need for applying the GA. Also, in [18], no mention was made as to the form of the evaluation function used in the GA for optimizing these coefficients. Three key papers in this methodological category deserve more detailed explanation below:

Rousselle *et al.* [21] used the GA for a two-step optimization. First they used the GA to optimize five coefficients which weight the influence of each component of the Snakes total energy function (e.g. internal energy, external energy, etc.). The evaluation function of the GA is based on only intersection surface between a desired boundary and the result of the Snakes, which does not consider the over growing of the Snakes. Such a choice of the evaluation function results in a low probability of converging the GA to global optimum. As a second step, they used the GA to optimize the same coefficients at every iteration of the Snakes. This means they used the total energy function as the evaluation function to optimize the total energy function itself. This result tends to drive all coefficients toward zero for minimizing the total energy function. Although the sum of coefficients was set equal to one, this does not protect against the elimination of overly large components of the total energy function. Using the GA in every iteration of the Snakes is time consuming. Furthermore, they presented their result on only one manually produced noise-free image with two intensities (black and white) having high boundary gradient.

Xu *et al.* [22] used the GA to optimize three different kinds of parameters: coefficient and magnifier of each component of the Snake total energy function and preprocessing parameters to build the image energy function. First they applied a mutation operation on one gene of each chromosome and then used crossover for exchanging several genes between two individuals. Choosing the crossover points between the genes does not produce any new gene (parameter) for the next generation, so production of new genes is dependent on a mutation operation which is not a good strategy for the whole GA process. They also limited the maximum number of GA generations to 15 which resulted in non-repeatability of the GA for this application. They ran the GA three times and obtained a different result for each run. Finally they state their approach does not work in a general sense (i.e. fails when applied to images acquired

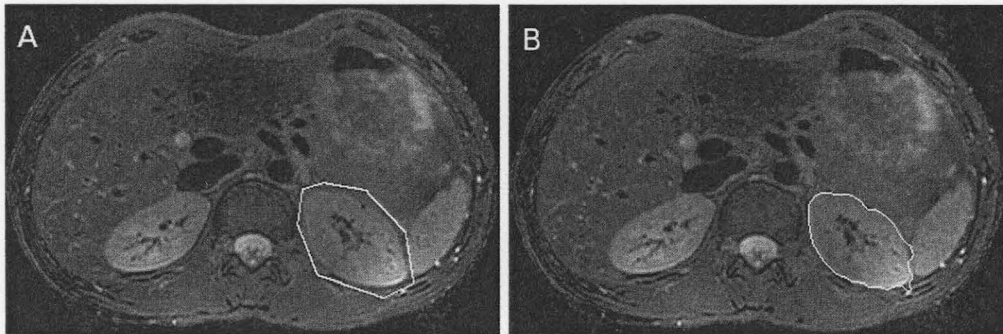


Fig. 9. Left image (A) shows the initial contour that covers one kidney and the right image (B) shows the result of the level set method after 3000 iterations.

from different subjects/patients with the same disease). Hence, in their approach, the resulting total energy function of Snakes, could not be used.

Finally Teixeira *et al.* [23] used the GA to optimize coefficients of Snakes total energy function as well as strength coefficients of their proposed adaptive-balloon force. They used real numbers as genes which results in the same problem as in [22] for producing new genes based on just a mutation operation. The evaluation function is based on the distance between the contour points and the center of gravity. With this evaluation function, the under- and over-segmenting points cancel each other. They mentioned that Snakes resulted in an average of 8% error where the standard deviation of error was 2.6%.

B. Level set method Consideration

Compared to other methods (i.e. Sobel, Prewitt, Laplacian of Gaussian, Canny filter, high-pass filter on Fourier transform, etc.) that are classically used for segmenting anatomical structures as visualized in medical images, we see the following significant benefits of using our approach, which includes the level set algorithm with optimized parameters: *First*, our method focuses on a specific organ/cyst whereas other procedures find the edge of all tissues in an image and so are more sensitive to noise; *Second*, other methods are sometimes restricted, i.e. they often employ a fixed or variable threshold; *Third*, although the procedure presented in this paper takes more time compared to others to find tissue edges, the user interaction time is less, particularly when considering the fact that results from other methods require user manipulation; *Fourth*, the GA algorithm with the Level set method, as described in this paper, works well on visceral images (e.g. kidney, liver, spleen), while other methods work reliably only on rigid structures such as the brain or knee; *Fifth*, as our method focuses on a specific tissue, and not the entire image, it has a higher potential for use in volume measurement and *Sixth*, the resulting contour always has the shape of the target tissue with an error approximately from 0.25%

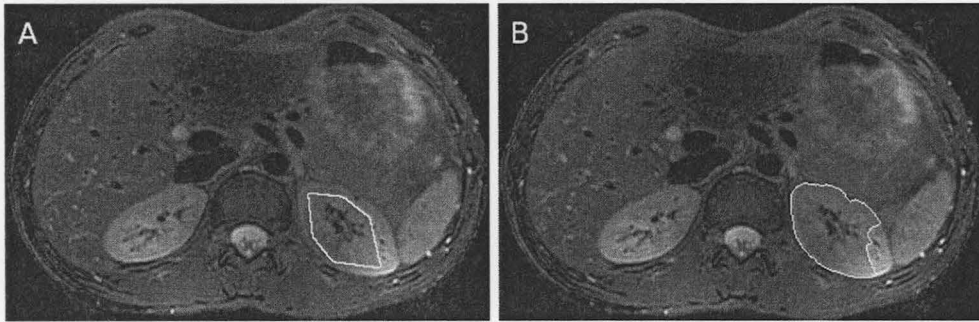


Fig. 10. Left image (A) shows that there are two different tissues between the initial contour and border of the kidney and the right image (B) shows the result of the level set method after 3000 iterations.

to 3% of the desired area.

VI. CONCLUSIONS

Using GA (or dGA), we optimized the set of parameters for the level set method, a geometric active contour, for use as a boundary detection method. To evaluate different sets of parameters, we developed an efficient evaluation function based on four measurement techniques that accurately find geometric differences between the result of the level set algorithm and the 'true' edge. To our knowledge this is the first time this approach has been attempted for the level set method as a geometric active contour.

In abdominal images, none of the organs have a smooth background, so using the shrinking version of the level set method with an initial contour that covers an organ is not practical. Fig. 9 shows one example of applying the level set method for shrinking an initial contour to the edge of a kidney in MR abdominal images that failed to converge on an actual border. A similar problem appears for organs that are composed of several types of tissues, when using the expanding version of the level set method, which used an initial contour that fits within the organ. The performance of the level set method is too sensitive to the subtle variations of a manually selected initial contour. If there is more than one tissue type between the initial contour and the border of the organ, there is higher probability that level set method does not converge on the organ border. Fig. 10 shows one example of this problem.

The fact that an organ is comprised of several tissue types and potentially has large connecting blood vessels (e.g. kidney, spleen, liver) is a problem for edge detection in some slices. An example of this problem can be seen in Fig. 11. In these cases, there is no guarantee that level set method will converge on the actual border and in fact, there is no obvious or certain 'rule of thumb' to manually select the border in these cases.

To obtain an accurate result in a shorter time, a different set of parameters is needed when applying the level set method on different tissues or different image modalities. This potentially makes the level set method difficult to set up for use in

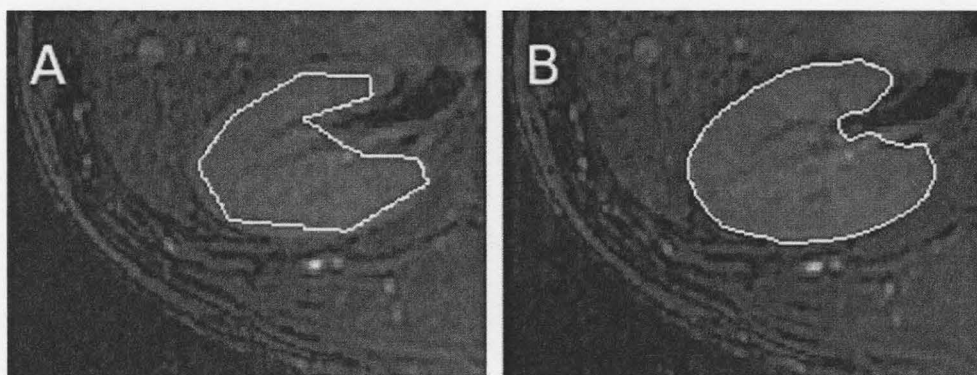


Fig. 11. Left image (A) shows the initial contour that is selected inside the kidney with some vessels connected to that kidney and the right image (B) shows the result of the level set method after 320 iterations.

different situations. Although the resultant contour is not sensitive to the initial (manually input) contour, it influences the computation speed. In some cases where an organ is composed of several tissues, the method will fail; for example, if there is more than one tissue type between the initial contour and the anatomically correct edge. This method takes almost five seconds for initializing the contour by clicking corners of a polygon inside the organ which can be done by a user with lower expertise than a radiologist, and then takes almost 10 to 20 seconds to draw the boundary. Comparing this time to the time that is needed to draw a boundary of an organ by a radiologist, which almost takes 2 to 3 minutes, and considering the fact that a boundary drawn by a human may be varying over time and affected by someone who is tired of processing thousands of images a day, shows the benefits of our method. Although several seconds is not a long time for finding the edge of an organ/cyst, it will be a considerably longer time if this method is applied to 3-D imaging datasets. As we implemented all algorithms in MATLAB, which is an interpreted programming language, we can further reduce the execution time by implementing this program in some languages such as C++, which has a compiler.

Our proposed evaluation function for the GA correctly assesses geometrical properties of the contour which find over- and under-segmenting as well as the distance to the optimal boundary of the object. In addition to the regular GA, using dGA (where needed) allows a determination of the global optimal parameters for the level set method which can furthermore be used to accurately locate the edge of an organ in a CT or MR image. In other words, using the GA (dGA), a set of optimal parameters is found for a specific organ in a specific modality (e.g. airways in CT), then the level set method with this set of parameters is able to segment the same organ in other images of the same modality with the maximum error of 3% where average error in [23] is 8%. This means there is no need to re-run the GA for every slice or every patient when needed, as was done by [22]. This ability to generalize from two samples to various slices and patients for the same modality and organ is one of the main advantages of our new technique.

ACKNOWLEDGMENT

We wish to thank the administration at St. Joseph's Healthcare for providing a research intensive environment. Help provided by Mr. Jay Neadles MRT (MR), from the Imaging Research Centre at St. Joseph's Healthcare is much appreciated. His expertise and advice were useful during the acquisition of the MR images used herein.

REFERENCES

- [1] R. C. Gonzalez and R. E. Woods, *Digital Image Processing*, 2nd Ed., Upper Saddle River, NJ, Prentice Hall, 2002, Chapter 10.
- [2] A. D. Elster and J. H. Burdette, *Questions and Answers in Magnetic Resonance Imaging*, 2nd Ed., Mosby Inc., 2001.
- [3] N. Saeed, "Magnetic Resonance Image segmentation using pattern recognition, and applied to image registration and quantization," *NMR Biomed.*, vol. 11, pp. 157-168, 1998.
- [4] M. Kass, A. Witkin, and D. Terzopoulos, "Snakes: Active Contour models," *Int'l J. Comp. Vis.*, vol. 1, pp. 321-331, 1987.
- [5] V. Caselles, F. Catte, T. Coll, and F. Dibos, "A geometric model for active contours in image processing," *Numer. Math.*, vol. 66, pp. 1-33, 1993.
- [6] S. Osher, J. A. Sethrian, "Fronts propagation with curvature-dependent speed: algorithms based on Hamilton-Jacobi formulations," *J. Computation Physics*, vol. 79, pp. 12-49, 1988.
- [7] V. Caselles, F. Catte, T. coll, and F. Dibos, "A geometric model for active contours in image processing," *Numer. Math.*, vol. 66, pp. 1-31, 1993.
- [8] R. Malladi, J. A. Sethian, and B. C. Vemuri, "Shape modeling with front propagation: a level set approach," *IEEE Trans. Pattern Anal. Mach. Intell.*, vol. 17, no. 2, Feb. 1995.
- [9] V. Caselles, R. Spario, and G. Spairo, "Geodesic active contours," *IEEE Int. Conf. Comp. Vision*, pp. 694-699, 1995.
- [10] T. F. Chan, L. A. Vese, "Active contours without edges," *IEEE Trans. Image Process.*, vol. 10, no. 2, Feb 2001.
- [11] J. A. Sethrian, *Level Set Methods and Fast Marching Methods*, Cambridge UK, Cambridge University Press, 1999, Chapter 17.
- [12] C. Li, C. Xu, C. Gui, and M. D. Fox, "Level Set evolution without re-initialization: A new variational formulation," *IEEE Computer Society Conference on Computer Vision and Pattern Recognition*, vol. 1, pp. 430-436, 2005.
- [13] L. A. MacEachern and T. Manku, "Genetic algorithms for active contour optimization," *IEEE Int. Sym. For Circuits and Systems*, Vol. 4, pp. 229-232, May 1998.
- [14] L. Ballerini, "Genetic Snakes for medical image segmentation," *EvoIASP'99 and EuroEcTel'99, Lecture Notes in Computer Science 1596*, pp. 59-73, 1999.

- [15] L. Ballerini, "Multiple Genetic Snakes for people segmentation in video sequences," SCIA, Lecture Notes in Computer Science 2749, pp. 275-282, 2003.
- [16] K. Mun *et al.*, "Active contour model based object contour detection using genetic algorithm with wavelet based image preprocessing," Int. J. Control, Automation, and Systems, vol. 2, no. 1, pp. 100-106, March 2004.
- [17] G. R. Rad, and M. Kashanian, "Extraction of the breast cancer tumor in mammograms using genetic active contour," Int. Conf. Biomedical and Pharmaceutical Engineering, pp. 30-33, Dec. 2006.
- [18] L. Ballerini, "Genetic Snakes for color image segmentation," EvoWorkshop, Lecture Notes in Computer Science 2037, pp. 268-277, 2001.
- [19] L. Ballerini, and L. Bocchi, "Multiple Genetic Snakes for Bone Segmentation," EvoWorkshop, Lecture Notes in Computer Science 2611, pp. 346-356, 2003.
- [20] A. R. Hussain, "Optic nerve head segmentation using genetic active contours," IEEE Int. Conf. Comp. and Comm. Eng., pp. 783-787, May 2008.
- [21] J. Rousselle, N. Vincent, and N. Verbeke, "Genetic algorithm to set active contour," CAIP, Lecture Notes in Computer Science 2756, pp 345-352, 2003.
- [22] Y. Xu *et al.*, "Optimization of active contour model parameters using genetic algorithms: segmentation of breast lesions in mammograms," SPIE Medical Imaging, vol. 4684, pp. 1406-1414, 2002.
- [23] G. M. Teixeira, I. R. Pommeranzembaum, B. L. Oliveria, M. Lobosco, and R. W. Santos, "Automatic segmentation of cardiac MRI using Snakes and genetic algorithms," ICCS, Lecture Notes in Computer Science 5103, pp. 168-177, 2008.
- [24] D. E. Goldberg, *Genetic Algorithm in Search, Optimization, and Machine Learning*, Boston, MA, USA, Addison-Wesley professional, 1989, Chapters 1-3.
- [25] R. Malladi and J. A. Sethian, "A unified approach to noise removal, image enhancement, and shape recovery". IEEE Trans. on Image Proc., vol. 5, pp. 1554-1568, 1996.
- [26] M. Sparrow, P. McFawn, T. Omari, and H. Mitchell, "Activation of smooth muscle in the airway wall, force production, and airway narrowing," Can J Physiol Pharmacol., vol. 70, pp 607-614, 1992.
- [27] D. E. Olson, G. A. Dart, and G. F. Filley, "Pressure drop and fluid flow region of air inspired into the human lung," J Appl. Physiol., vol. 28, pp. 482-494, Apr. 1970.

4.3 Summary of article

Using GA, we are able to optimize the setting of the LSM parameters in order to segment organ/cysts in MR and CT images. Before obtaining the result of this paper, we used a GA with just one sample image of an MRI kidney. The result of the GA based on one sample input failed to optimally characterize the LSM in order to segment many MR kidney images other than the sample image. Using two sample images, however, the GA could optimally characterize the LSM for segmenting kidneys in various MR images.

The step segmenting lung airways in CT image with optimized GA settings is only one of many to come in this research as provided in the subsequently enclosed articles. Specifically, we have continued by measuring some features of the lung using CT images in order to implement a lung disease recognition system. That means, executing the GA itself with a bigger population as well as feeding the GA with more sample input may result in a better parameter setting for the LSM, particularly for segmenting the kidney in MR images. We believe that there is no better determined set of parameters of the LSM for segmenting cysts, as they are made of only one tissue type.

The same belief holds for the set of parameters that the GA found for segmenting airway lumen in CT images. As we see in the images of lung airways (Fig. 7 and Fig. 8), the air in the lumen is always a black color in CT images which is surrounded by the lumen wall with a white color in CT images. The results of segmentation that our program has obtained on many lung CT images shows that the LSM with this set of parameters works very well on lung CT images. Even applying the LSM (characterized with the same parameters used for lung CT images) on a lung phantom CT images demonstrates very good results (refer to chapters 5 and 6). We also suggest that interested readers can check optimization possibility on other variations of the level set method using GA.

It is necessary to point out that the default path of this project was changed at this stage. When this project was started, the goal was to develop a method for automatically comparing the MRI serial images over time in order to find changes in number and size of cysts in kidneys and liver. There are several issues to be considered: first, using the current technology of MRI scanners (3.0 Tesla), the best resolution that can be obtained for abdominal images is a 4mm slice thickness which causes excessive error for registering images (specially for comparing small cysts); second, with the MRI scanner, many different images can be acquired (e.g. T1 weighted, T2 weighted, PD, SSFSE, SSFSE ASSET, Dual in-out of phase, FIESTA, STIR, FRFSE, LAVA, etc.) which show different gray intensities for the same tissue. This means, for using the LSM, we need to find an optimal set of parameters for every type of MRI acquisition. On the other hand, CT does not have this diversity in imaging, which facilitates the development of a method to assist the radiologist in measuring organs and comparing serial images in time as well as diagnostic diseases. Therefore, we focused on CT images (of the lung) for this thesis and were able to achieve good results.

Chapter 5:

Measuring Airway Luminal Diameter and Wall Thickness

5.1 Overview of article

In this chapter we present the second paper from our research, submitted to Medical and Biological Engineering and Computing, July 9, 2009. Before going to the article (section 5.2), a brief explanation with regard its position in the overall scheme of research along with some additional relevant information is presented here. Final section summarizes the research presented herein the chapter.

Lung airway characteristics are crucial while recognizing several lung diseases (some of which are described in chapter 7). The level set method (described earlier in chapter 4 and characterized by a set of optimal parameters) is employed to segment airway lumens. The generated contour for modeling the lumen shape is used as a starting point to measure lumen diameter and wall thickness.

The partial volume effect can be minimized by averaging the airway luminal diameter and wall thickness measurement over slices. The partial volume effect happens in low resolution (big voxel size) CT and MRI volumes. Voxels at the border of tissues contain a mixture of tissues which results in a pixel intensity whose average is a composite of signals from different tissues. The bigger the voxel size, the larger the partial volume effect.

The following article explains an enhancement to the airway lumen segmentation based on two segmentation methods, namely the seeded region growing algorithm and level set method, which both focus on a specific object in the image as opposed to the more common method of finding edges of all object/tissues in the whole image. These methods were developed to find the centerline of airways in order to measure the subsequent bifurcation angle, an issue which will be in chapter 6.

5.2 Article

A Multi-step Algorithm for Measuring Airway Luminal Diameter and Wall Thickness on Lung CT Images

Mohammadreza Heydarian, Michael D. Noseworthy, Markad V. Kamath, Colm Boylan, and W. F. S. Pohlman

Abstract—Accurate measurements of airway diameter and wall thickness are important parameters in the understanding of numerous pulmonary diseases. Here we describe an automated method to measure small airway luminal diameter and wall thickness over numerous contiguous CT images. Using CT lung images from 22 patients and an airway phantom, a seeded region growing algorithm was first applied to identify the lumen of the airway. This result was applied as an initial region for boundary determination with the level set method. Once found, subsequent algorithmic expansion of the luminal border was used to calculate airway wall thickness. This algorithm evaluates the neighbor slices of the airway automatically and measures the airway luminal diameter and wall thickness. Our approach also detects airway bifurcations. Our new approach provides rapid, automated, and accurate clinically important lung airway measurements and is useful to radiologists who use CT images for pulmonary disease assessment.

Index Terms: CT, level set method, lung airway, seeded region growing algorithm.

I. INTRODUCTION

The bronchial wall thickness and airway luminal diameter are extremely important in the pathogenesis of Asthma. Wall thickness and luminal diameter are also important in the assessment of numerous other pulmonary diseases (e.g. Bronchiectasis and COPD). In addition the assessment of wall thickness and luminal diameter may be valuable as a marker of response of the airways to therapy. Because of the complexity of the airways and the time limitations imposed on radiologists only gross changes in the airways are usually documented in radiological reports beyond research protocols. In addition manual analysis of the airways using various measurement tools has typically been prone to inaccuracy and lack of reproducibility. As a consequence much information regarding the airways on a CT examination is never extracted nor properly utilized. The application of image segmentation algorithms would provide an alternate and novel approach [1,2].

Airway lumen segmentation [3-24] and wall thickness measurements [4,6,8-13,17,21,24] have previously been attempted, with limited success. Although CT segmentation methods take advantage of the lower airway Hounsfield unit (HU), relative to the airway wall, most methods for segmenting lumen [3-14,17,23] are directly or indirectly based on a fixed threshold, which may cause inaccuracies due to over growing ('the leaking problem') or under growing the lumen. The most common approach for wall thickness measurement is based on the full-width at half-maximum (FWHM) method [4,6,21] which typically overestimates wall area [6,21].

Segmentation algorithms can be classified into two categories: low-to-intermediate level and high-level [26]. The first category, which operates at the pixel level, includes five popular methods: gray intensity histogram analysis, texture analysis, edge enhancement and linking, region growing, and contour following. The second category, which is anatomical segmentation, needs prior knowledge, which is usually supplied by an expert.

The level set method (LSM) [27,28], a geometric active contour model [29], is one reasonable choice of segmentation methods as it focuses on a specific object, rather than the whole image, and there is no need for a fixed or variable threshold. However, similar to other variations of the LSM, the new variational formulation of the LSM [28] that we are using for this project requires the specification of several parameters as well as the determination of an initial region inside the object for initiation. Unfortunately, there is no one set of parameters that is suitable on all types of images. In other words, every kind of image needs a specific set of parameters. Also, there seem to be no 'rules of thumb' for generalization. To offset this problem, it is possible to use a genetic algorithm (GA) [30] as a heuristic search method to optimize parameters of the level set method in order to obtain more accurate results within a short time. We have previously reported the details on the optimization of the LSM in a previous study to automatically segment kidney cysts from normal kidney tissue and segment airway lumen [31]. To provide the LSM with an initial region inside the lumen, a seeded region growing algorithm (SRGA) [1] was used with a dynamic low threshold to avoid over growing. The SRGA output is a

region that is close to the actual border of the lumen, which results in less iterations of the LSM for accurate convergence on the lumen boundary.

Often when performing airway segmentation on lung CT images, the airway wall cannot be separated from an adjacent vessel (**Fig. 1**). This occurs because the pixel intensity range of the vessel overlaps considerably with that of the airway wall. Hence for accurate analysis, the section of airway wall abutting an adjacent vessel must be excluded from analysis by some means. To measure airway wall thickness, taking this complexity into account, we developed a new method based on a statistical measurement of the expansion of the lumen boundary. By locating the seed for the SRGA on neighboring slices, we enabled the automatic tracking of airways across neighboring slices. In this paper, we demonstrate a new one-click automated multi-step method for segmenting lung lumen and measuring airway wall thickness over numerous contiguous slices, which take into account bifurcations and arterial signals.

II. MATERIALS AND METHODS

A. Imaging

Routine clinical lung CT data were used to evaluate the performance of our method. Images were chosen from patients suffering from asthma and COPD as well as patients with thoracic problems requiring CT scanning but otherwise having healthy lung tissue. The images were acquired by using 64-channel multidetector CT scanners (LightSpeed VCT; GE Healthcare, Milwaukee, WI). Whole-lung CT images with no intravenous contrast medium were obtained with the following parameters: detector collimation, 0.625 mm; field of view, 34.5 cm; pitch, 1.375; gantry speed, 0.4 second per rotation; automatic selection of the milliamperage setting (range, 128–300 mA); and noise index=10. Axial reconstructions of 0.625mm slice thickness at 0.625mm reconstruction intervals were provided for analysis.

One of the problems we noted during lung CT image processing was voxel size. The smallest in-plane voxel size for typical clinical protocols was 0.625x0.625mm (based on the chosen field of view and reconstruction method used by scanner), with a 0.625mm slice thickness. The greatest clinical interest is in evaluating airway diameter around the 6th to 10th airway branch levels, or diameters with size 3.6mm down to 1.63mm [32,33]. This native resolution is not able to differentiate small size changes, and also does not have enough area for LSM contour initialization. So we used a cubic resampling method to increase in-plane resolution to approximately 0.2mm (albeit with a broader point spread function). Although the result showed acceptable measurements to radiologists, there was doubt about the fidelity of the underlying image. So, for some clinical data we produced a reconstructed image with a smaller field of view but same size (512x512) in order to have pseudo-higher resolution images. The voxel size of these new images was 0.188x0.188 mm with 0.625mm slice thickness. Comparing the result of applying the LSM on these new pseudo-high resolution images to the result of applying the LSM on

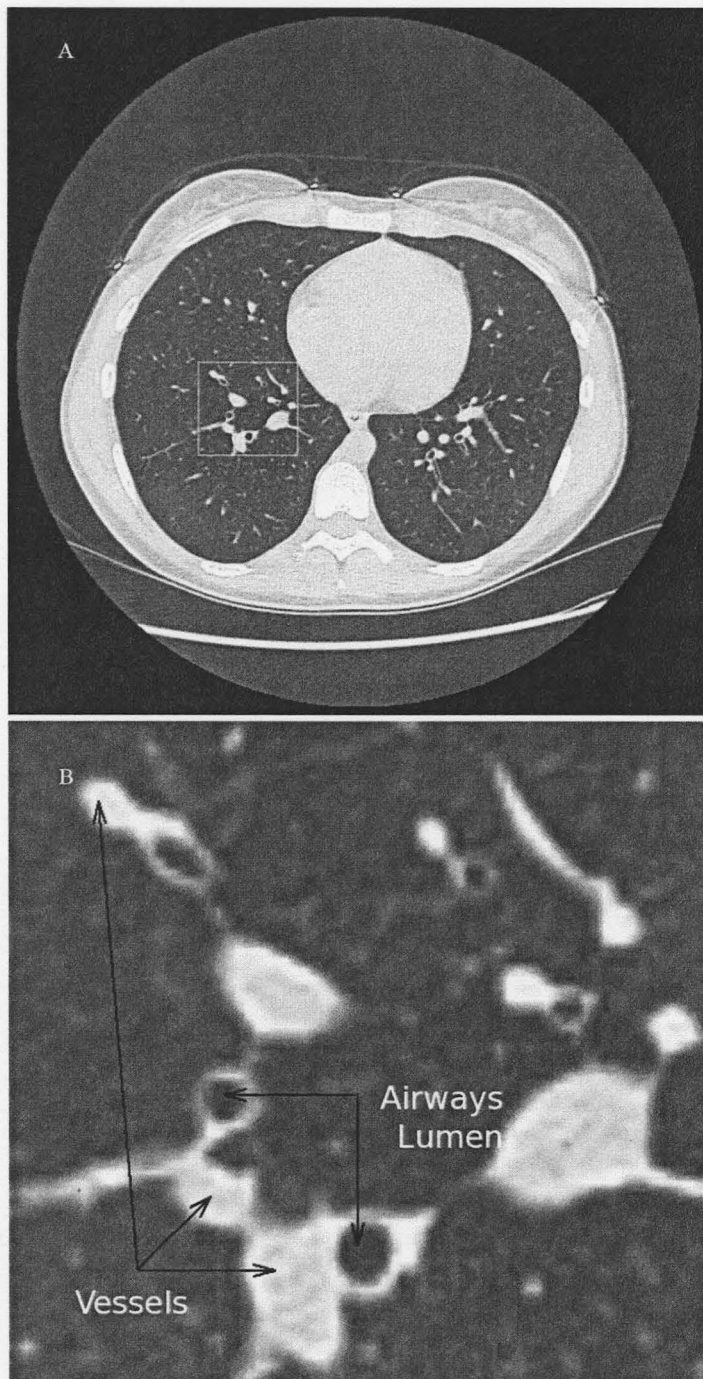


Fig. 1: (a) shows the whole lung, (b) shows part of the lung illustrating vessels connected to the airway.

resized images (by our algorithm) shows that resizing does not appear to cause any deviation in uniquely determining airway edges.

B. Mathematical Background

The level set method is a shape detection method, which isolates a particular shape of an object inside the image. The object must correspond to a region whose pixels have different grayness intensity from neighboring regions [34]. Introduced by Malladi [35], the use of level set methods for shape recovery makes it insensitive to noise at boundaries but enables convergence on the object boundary. The algorithm naturally executes topological change and stops based on the image gradient. The idea is to define a filter for finding the image gradient, the results of which show no change in the gradient away from boundaries and sharp changes near boundaries [34]. Using the level set method, numerical computation for curves and surfaces on a fixed Cartesian grid can be performed with no need to parameterize these objects. A variational formulation of the LSM was introduced by Li *et al.* [28], which has high potential to be used as boundary detection approach in medical images. Although this method is mathematically sound and may work with a variety of images, it requires the specification of a set of seven parameters, for which there is no possible ‘rules of thumb’ for finding the optimal parameters for each kind of image. We [31] used a genetic algorithm to optimize this variational formulation of the LSM [28] through setting of its parameters.

A seeded region growing algorithm (SRGA) groups pixels into a region based on various selection criteria. The algorithm needs a position as a starting seed and a threshold as part of the selection criteria. Next, the algorithm finds the distance between each neighbor pixel of the previously selected region (i.e. a seed for starting) to the mean of that area and if the distance is less than the threshold, this pixel will be added to the current region. When the distance of all neighbor pixels is bigger than a threshold, the algorithm is terminated. Algorithm 1 shows fundamental of a SRGA in a pseudo code where $I(x,y)$ is the intensity of pixel in position (x,y) and $avg(currentArea)$ is the average of intensity of all pixels in previously selected area by SRGA, which is initialized by the selected seed point.

Algorithm1:

newArea = {*seed*}

repeat

currentArea = *newArea*

neighborPixels = *neighborsOfCurrentArea*

for all (*x,y*) ∈ *neighborPixels*

if $\text{abs}(I(x,y) - \text{avg}(\text{currentArea})) \leq \text{threshold}$ *Then*

add (*x,y*) *to* *newArea*

endif

endfor

until *newArea* == *currentArea*

C. Dynamic Calculation of the Threshold for the Seeded Region Growing Algorithm

For the purpose of generalization, we did not set any fixed threshold for the SRGA. Instead, we used a dynamic threshold calculated as twice the standard deviation of the previously selected area plus the standard deviation of the body background (i.e. the air surrounding the patient) as noise. Equation (1) shows this threshold is calculated:

$$T_i = 2\sigma(A_{i-1}) + \sigma(\text{background}) \quad 1 \leq i \leq 10 \quad (1)$$

where T_i is the threshold and A_{i-1} is the area containing the selected pixel based on T_{i-1} at previous step of region growing. For initialization purposes, the algorithm adds all eight neighbors of the seed (clicked point for first slice) to the initial region (A_0).

$$A_0 = \text{dilation}(I, \text{seed}) \quad (2)$$

where I is the underlying image. As some reconstructed CT images do not contain the body background, we set an average of the standard deviation of the body background from several CT images (approximately 14).

$$T_i = 2\sigma(A_{i-1}) + 14 \quad 1 \leq i \leq 10 \quad (3)$$

At each step of the SRGA, all neighbor pixels of the previously selected region

$$\text{neighborPixels} = \text{dilation}(A_{i-1}) - A_{i-1} \quad (4)$$

were compared to the mean of that region (A_{i-1}) and if the distance was equal to or less than the calculated threshold in (3), the pixel will be added to the current region. By the end of each step (up to step 10), the mean and standard deviation of the current region was calculated and used for setting the new threshold. From step 11, the threshold calculated from step 10 was used. The Euclidean distance (which, in this case, is a simple difference) between the intensity of pixels and the mean of a previous region was used for this work. Equation (5) shows how the new area is selected based on the dynamic threshold:

$$\begin{aligned}
A_i &= A_{i-1} \cup \{(x,y) \mid (x,y) \in (\text{dilation}(A_{i-1}) - A_{i-1}) \quad \text{and} \quad \text{abs}(I(x,y) - \text{avg}(A_{i-1})) \leq T_j\} \\
\text{where} \quad &1 \leq i, \\
&1 \leq j \leq 10, \\
&\text{if} \quad i \leq 10 \quad \text{then} \quad i = j
\end{aligned} \tag{5}$$

When using the result of the SRGA as the initial contour for the LSM, it is not critical that the SRGA find the exact region of interest, however over-segmentation is an aspect that may occur. To protect the SRGA from growing over the region of interest, a smaller threshold is calculated which is not recalculated after 10 steps of growing. Also, to avoid over growing, the algorithm checks the area of the resulted region and if it is larger than the largest expected, then the SRGA will be performed again from the seed, but will reduce the number of steps for calculating the dynamic threshold. Note that this largest expected area may occur when the lumen is not perpendicular to the slice plane and, at a 60 degree angle, the elliptical shape of the lumen is twice the normal cross-sectional size. Our experience shows that if the SRGA passes the lumen border, the region will grow covering more than two-thirds of the image, which is much larger than the biggest luminal area. So the calculated threshold can be fixed such that the largest expected area is no more than twice the biggest lumen area (actual size in mm^2). Using metadata from the DICOM file, the actual size of a voxel can be calculated, so that the algorithm works well on all images with any resolution (voxel size). Algorithm 2 shows the pseudo code for this method:

Algorithm2:

```

function    f = SRGA(I,seed)
    steps = 10;    /* max    step */
    A0 = dilation(I,seed);
    i = 1;    /* current    step */
    repeat
        repeat
            if    i ≤ steps    then
                T = 2σ(Ai-1) + 14;
            endif
            Ai = Ai-1 ∪ {(x,y) | (x,y) ∈ (dilation(Ai-1) - Ai-1)    and
                                abs(I(x,y) - avg(Ai-1)) ≤ T};
        until    Ai == Ai-1
        steps = steps - 1;
    until    |Ai| < largestLumenArea
    return    Ai

```

D. Lumen Diameter Measurement

Using the result of the SRGA as the initial contour, the level set method was able to find the accurate border of the lumen in a very short time [31]. If one considers a pipe that is transected in any direction, the minimum diameter of the resultant elliptical shape is equal to the diameter of the original pipe. Using this property, we measured the luminal diameter (explained below). Having the luminal border, the algorithm finds the center of the luminal area, then it finds the nearest pixel on the border to this central point. This is the radius that belongs to the smallest diameter of the luminal border. If the number of pixels on the minimum diameter is even, then the central point cannot be positioned exactly at the middle of diameter, so the first minimum radius may be smaller than half of the diameter. For accuracy, even one pixel count is important in the measurement of the lumen diameter, so we need to find the length of the other radius of this diameter. Thus the algorithm looks for the other pixels on the lumen border on the opposite direction to the first radius in order to find the nearest one.

E. Wall Thickness Measurement

Most airway walls are connected to vessels and the intensity intervals of pixels which belong to them (wall and vessel) have a large overlap (see **Fig. 1**). Therefore, none of the existing segmentation algorithms are able to accurately distinguish an airway luminal wall from the vessel connected to it. Radiologists estimate the wall thickness through measuring the minimum wall thickness at the edges where the wall is not connected to any vessel. In this paper a fitting method has been developed to find the minimum thickness of the airway luminal wall. The method involves converging the LSM on the boundary of the lumen, and then expanding the border by one pixel, so that all pixels on the new border belong to the wall. If the minimum intensity of pixels on this border is called k , then using the histogram of this border, the algorithm counts the number of pixels that are in the interval $[k, k+40]$.

$$k = \min(I(x,y)) \quad \text{where } (x,y) \in \text{currentBorder} \quad (6)$$

$$\text{templ} = \text{sizeof}(\{(x,y) \mid (x,y) \in \text{currentBorder} \quad \text{and} \quad I(x,y) \leq k + 40\}) \quad (7)$$

The algorithm will use this number of pixels (*templ*) for deciding on the selection of the outer border of the wall. Then the algorithm expands the border (using a dilation algorithm [1]) by one pixel at each step of this fitting algorithm and measures the number of pixels on the new expanded border for which their intensity is less than $k+40$ (i.e. pixels in interval $[0, k+40]$). **Fig. 2** shows all the steps for expanding the lumen boundary while **Fig. 3** shows the corresponding histogram for each step of expanding the boundary. If the number of pixels on the new expanded border (which are in a defined interval) is close (say, at most, 35% different) to the number from the first border on the wall, it indicates this border is located at the other (outer) side of the wall and thus the number of expanding steps times the pixel size shows the wall thickness. When part of the expanded

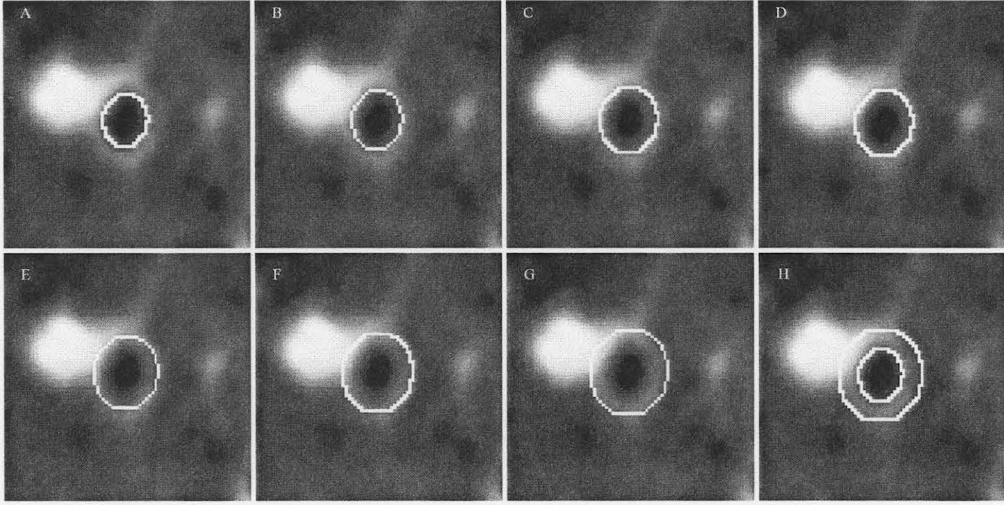


Fig. 2: (a, b, c, d, e, f, g) show the expanding level of a lumen contour by one pixel, respectively, while (h) shows the inner and outer border of airway wall.

border reaches the other side of the wall, the number of pixels whose intensity is in the initial interval $[0, k+40]$ is near to the *temp1*, and the algorithm determines the smallest wall thickness which is our goal. The reason that 40 was chosen for the interval width is that the number k may be affected by noise in CT images, so we considered the interval width to be close to two times of the standard deviation of background (which is an estimation of noise). We tested numbers 30, 40, and 50 and found 40 provided the best results (based on experience with the phantom we developed). Algorithm 3 shows the pseudo code for this method.

Algorithm3:

$border_0 = dilation(I, lumenArea) - lumenArea$

$k = \min(I(x, y)) \quad \text{where } (x, y) \in border_0$

$temp1 = sizeof(\{(x, y) \mid (x, y) \in border_0 \text{ and } I(x, y) \leq k + 40\})$

$i = 0$

repeat

$i = i + 1$

$border_i = dilation(AreaOfBorder_{i-1}) - AreaOfBorder_{i-1}$

$temp2 = sizeof(\{(x, y) \mid (x, y) \in border_i \text{ and } I(x, y) \leq k + 40\})$

until $(abs(temp2 - temp1) \leq round(0.35 * temp1) \text{ or } (temp2 > temp1))$

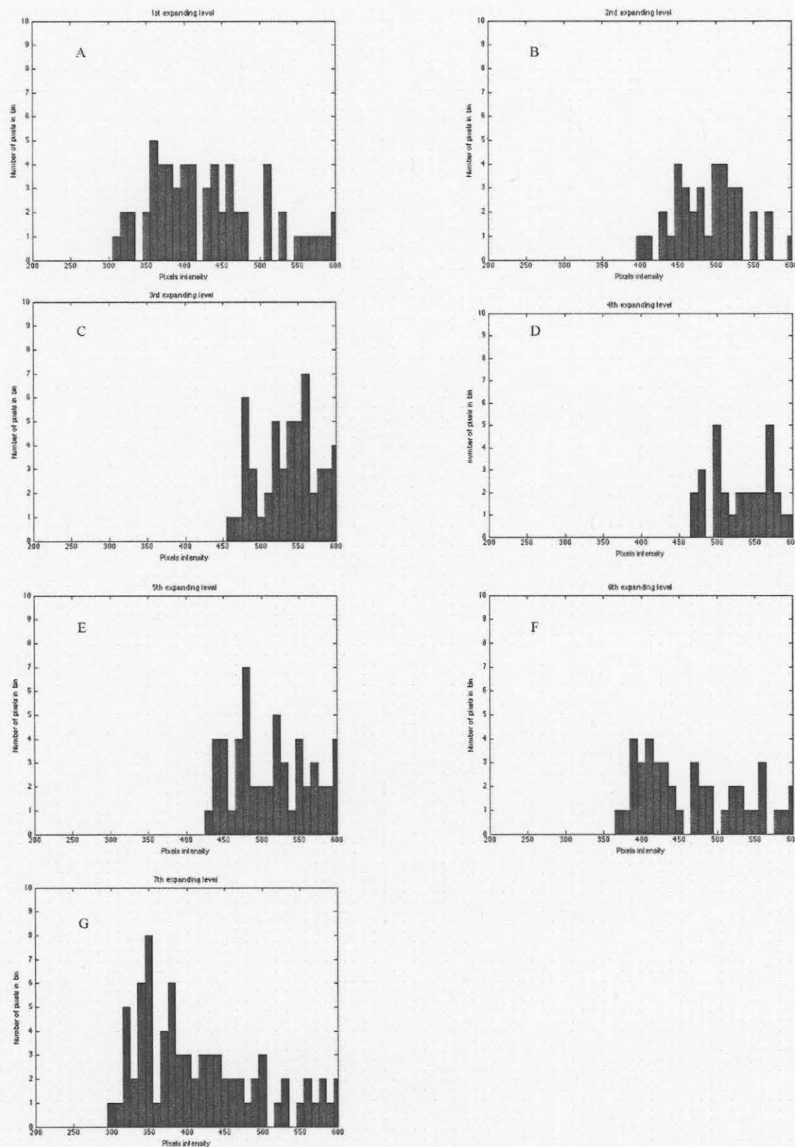


Fig. 3: (a, b, c, d, e, f, g) show the corresponding histogram of pixels on the border illustrated in figures 2 a-g, respectively.

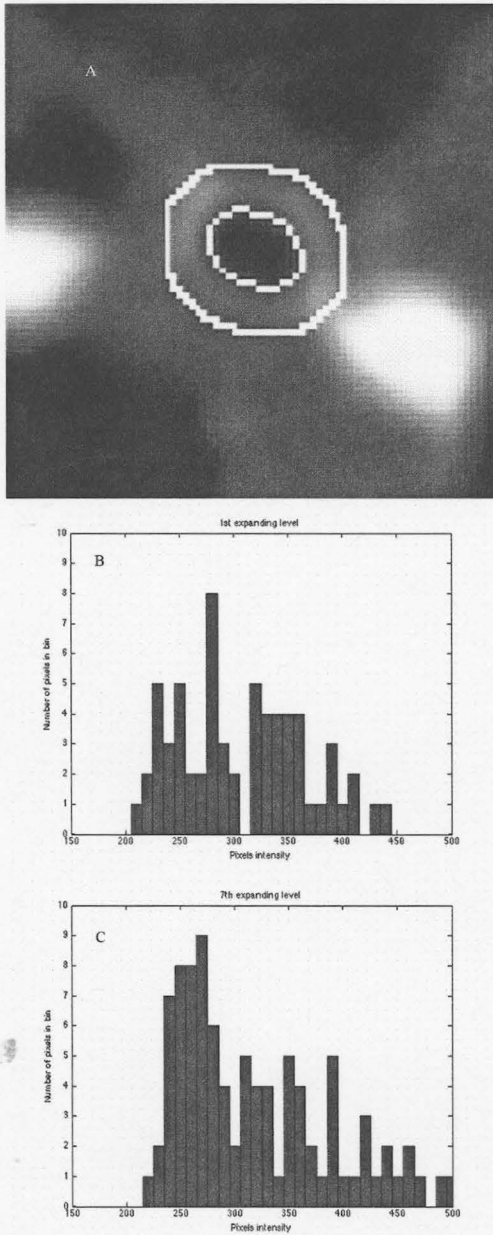


Fig. 4: (a) shows the inner and outer border of the airway wall. Both (b,c) are histograms from pixels in the inner and outer boundary of the luminal wall, respectively.

Fig. 4 shows the first and last contours (along with their histograms) which are used for measuring the wall thickness.

Counting the number of expansions of the border for measuring the wall thickness is accurate if the lines between pixels in interval $[0, k+40]$ and the lumen center are parallel to the X or Y axis. Also there may be several pixels on the previous expanded border which fit in the interval $[0, k+40]$, but not enough to fire the termination rule as explained in Algorithm 3. Thus, for more accurate measurement, we find the distance between each pixel that is in interval $[0, k+40]$ to the nearest pixel on the first (inner) border of the airway wall. Then the average of these distances gives the final wall thickness. This reduces the effect of using difference-rate (35%) in algorithm 3 to find the difference between number of pixels (which are in the mentioned interval) on the inner and the outer border of the wall. To ignore the pixels adjacent to the inner border of wall, the algorithm just considers the pixels on the expanded borders after the second expansion. **Fig. 5** shows all pixels on the expanded borders (after the second expansion) which are in the interval $[0, k+40]$ as well as all pixels on the first (inner) border of airway wall. Algorithm 4 shows the pseudo code:

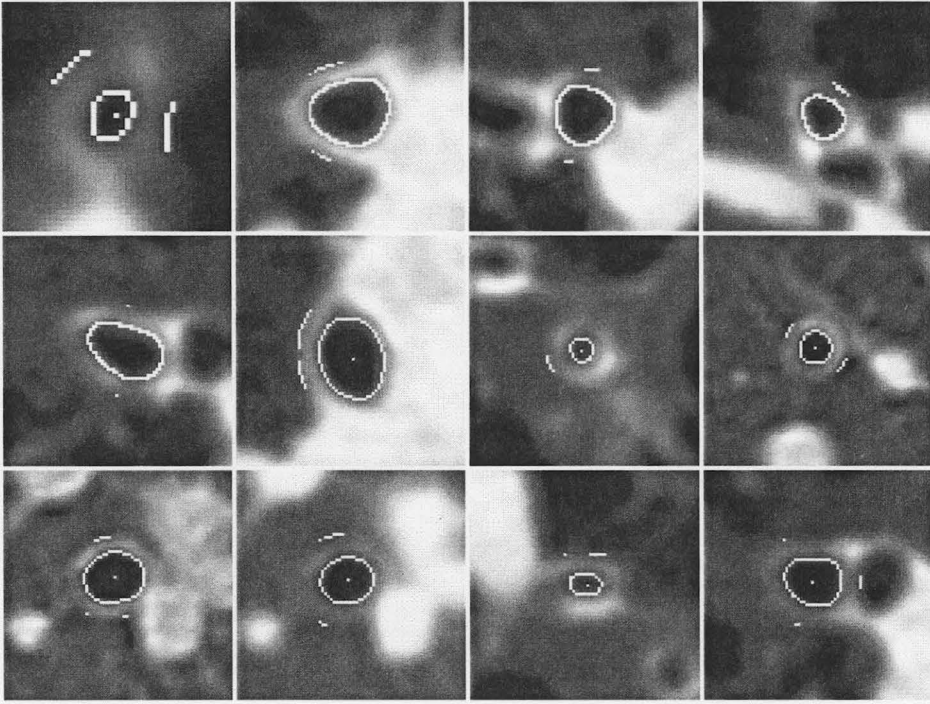


Fig. 5: Results of different slices acquired from different patients showing all pixels on expanded borders (after the third expansion) which are in the interval $[0, k+40]$ as well as all pixels on the first (inner) airway border wall (where k is the minimum intensity of inner border wall pixels).

Algorithm4:

$temp = \{(x, y) \mid (x, y) \in border_j, 3 \leq j \leq i \text{ and } I(x, y) \leq k + 40\}$ /* i from Algorithm3 */

$m = \text{sizeof}(temp)$

for $t = 1 : m$

$dist_t = \min(\text{euclideanDist}((x_t, y_t), (p, q)))$ where $(p, q) \in border_0$ and $(x_t, y_t) \in temp$
end

$wallThickness = \text{avg}(dist_t)$ for $t = 1 : m$

F. Trace Airway Cross Slices and Bifurcation Detection

Measuring airway luminal diameter and wall thickness over many slices of the airway allows us to identify abnormal wall thickening and abnormal widening or the absence of tapering of the airway as is seen in Bronchiectasis. In addition this process allows for identification of any error in measurement on any of these. A heuristic method was created for tracing airways automatically. For finding the lumen boundary, the algorithm simply needs a pixel position to start the SRGA, so it is necessary to locate a position inside the lumen for the next slice when tracing the airway. To do that, the center of the current segmented lumen is used as the starting point for the next slice. In addition to locating the starting point, the termination condition is another important part of this tracing algorithm. The algorithm checks two termination rules to detect bifurcation. If it continues to apply the SRGA on the next slice which contains the bifurcation, the SRGA converges on the area which covers almost two-thirds of the whole image because the starting point (i.e. the center of the previous lumen) will be located on the lumen wall and will grow through the connected vessel and other area with similar intensity. This will happen even if the SRGA uses the threshold calculated from the first step of the growing. Also, rarely, the tracing algorithm may find just one of the branches where the area is almost half (or at most 80%) of the area of the lumen from the previous slice. So, the algorithm checks these two conditions to locate the bifurcation. The measurements of the last few slices (at bifurcation area) are excluded from calculating the mean and standard deviation for measuring the airway luminal diameter and wall thickness over the slices. This part of the project is on going and we are attempting to implement an algorithm to follow both branches at each bifurcation in order to measure the bifurcation angle automatically.

III. RESULTS

A. Patient CT Images

Applying the proposed method for dynamically calculating the threshold for the SRGA, the previously reported ‘leaking’ problem typically present during lung airway segmentation, was eliminated. Using this dynamic threshold, the SRGA was able to find a boundary almost near to the actual border of the lumen (i.e. the border defined by a radiologist, CB). This boundary was used as an initial contour for the LSM to find the accurate luminal border. Although restarting the SRGA for dynamically calculating the threshold is time consuming, there is consequently less iteration time required for the LSM to converge on the lumen border providing an overall faster segmentation. Less than 10% of cases needed to restart the SRGA for dynamically calculating the threshold. Using our sample computer (Apple iMac with 2.33 GHz Dual Intel Core and 3GB memory) that we used to implement and test this method, it takes less than one second for the SRGA to terminate on a region inside the lumen. In the case of restarting the SRGA

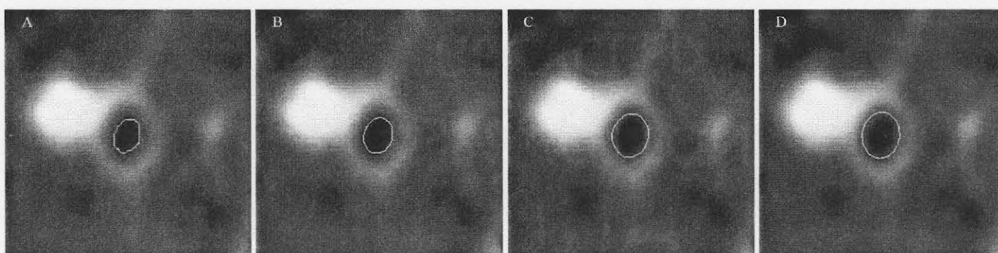


Fig. 6: (a) initial contour for LSM, (b, c, d) contours after 100, 420, and 800 iterations of the LSM, respectively.

for dynamically calculating the threshold, it takes almost one second for each restart. In the worst case, nine restarts were required to find a bifurcation in the tracing operation).

When characterizing the LSM [28] with an optimized set of parameters [31], it always converged to the boundary of the lumen in CT images accurately. **Fig. 6** shows the evolution steps of the LSM for a lumen CT image. Using this accurate boundary, the algorithm was able to find the lumen diameter. Based on the fact that when cutting a circular cylinder in any plane, the small diameter of consequent ellipse is equal to the diameter of the cylinder, the algorithm does not need to reconstruct the 3D image to force the airway to be perpendicular to the plane (so this diameter measurement method is fast and accurate).

An approximation on how long it takes for the algorithm to find the lumen boundary on CT images depended on both the image size and also the size of the lumen (in addition to number of LSM iteration). The bigger image and the bigger lumens required more time for each iteration of the LSM. For example, it took almost 1 minute for 100 iterations of the LSM on a 512×512 pixel image using our sample computer and implementing the method in MATLAB. To reduce computation time, we restricted the application of the level set method by applying it on a rectangular region of interest (ROI) that included the lumen of interest. The algorithm selected this ROI automatically based on the position of the seed from the seeded region growing algorithm. For example, on the same computer, the LSM took approximately 8 to 20 seconds for converging on a lumen boundary after 400 to 1200 iterations, respectively, with application on a 81×81 pixel image.

Practically, the most difficult and challenging part of assessing airways on CT images is measuring wall thickness. Our proposed fitting method measures the wall thickness similar to the technique that radiologists use for scaling it. This method is simple, fast, and repeatable which are acceptable end results for radiologists. **Fig. 2** shows all steps of expanding the lumen boundary in order to measure the wall thickness. **Fig. 3** shows the corresponding histograms to all steps of expanding the boundary. **Fig. 4** shows the first and last contours (along with their histograms), which are used for measuring the wall thickness. **Fig. 5** shows all pixels on the expanded borders (after the

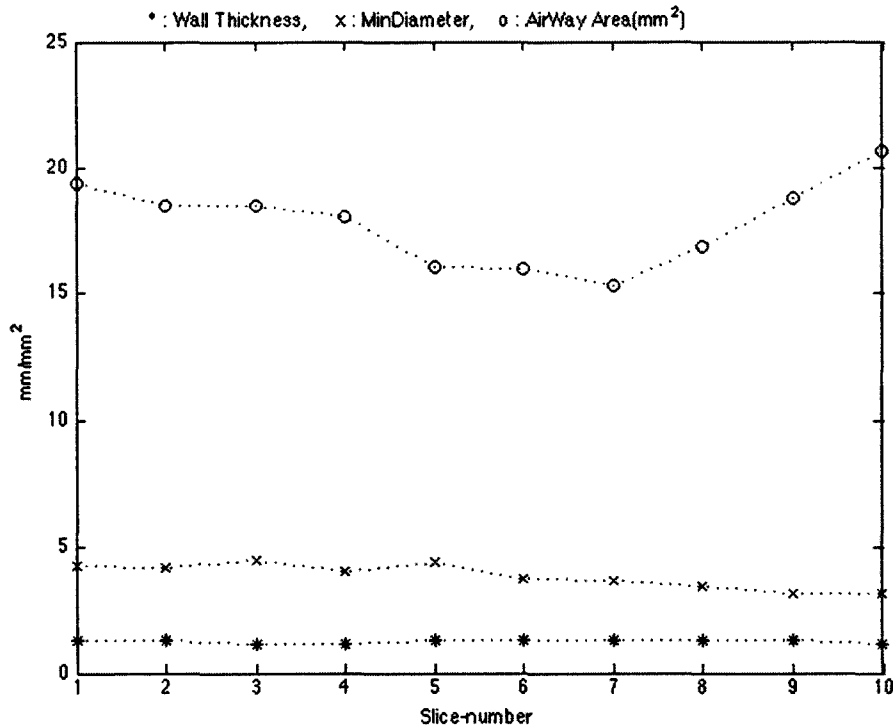


Fig. 7: The top curve shows lumen area (mm^2), middle curve shows lumen diameter (mm), and the bottom curve shows the airway wall thickness (mm).

third expansion) which are in the interval $[0, k+40]$ as well as all pixels on the first (inner) border of airway wall. We applied our method on clinical lung CT images from 22 patients, each containing several series of axial images (e.g. Standard ALG, Lung ALG, etc.) where each series includes 14 to 400 images (according to the slice thickness and gap between the slices). Using our sample computer, it required less than one second to find the wall thickness with our method. The smallest diameter and wall thickness that our algorithm measured are 0.63mm and 0.52mm, respectively. Visual assessment by a radiologist (CB) confirmed the acceptability of our results.

Because of possible effects that noise and partial volume problems may bring to the result of measurements of the lumen diameter and wall thickness, it is not practical to rely on one measurement. Repeating measurements on neighboring slices is necessary to reduce the error. Also the way the lumen diameter changes over one airway branch is meaningful for recognizing some diseases. Using our tracking method, the algorithm follows one branch of an airway automatically and measures the lumen diameter and wall thickness over many slices. We applied this part of our method on five clinical lung CT images, which contain images without a gap between them and with the maximum

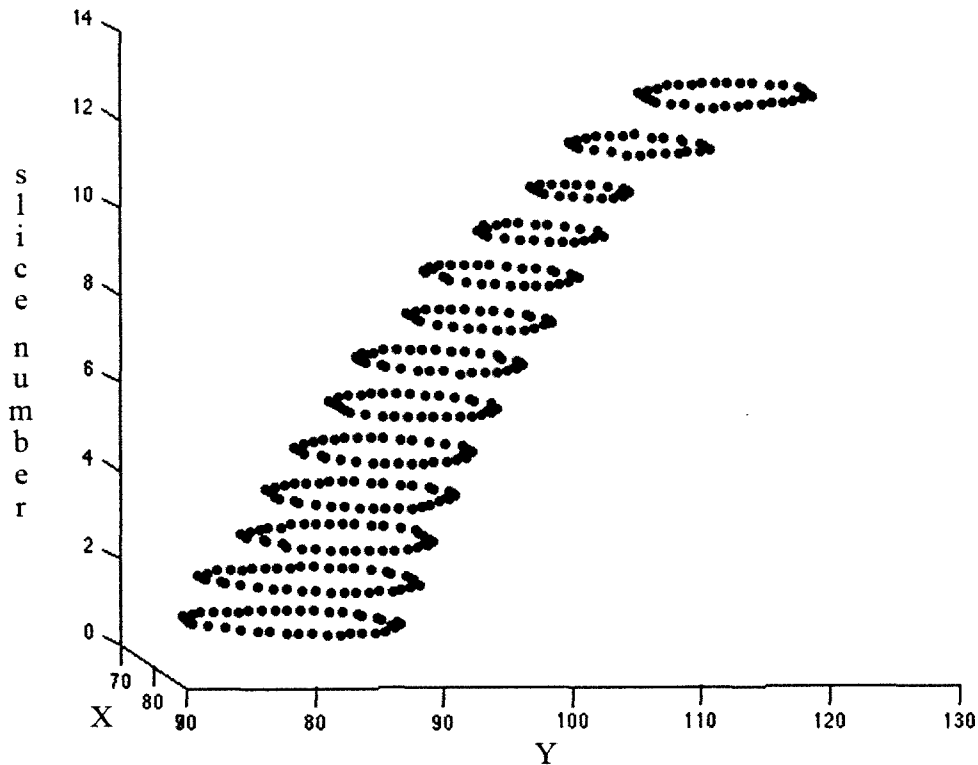


Fig. 8: 3D view of pixels on the lumen boundary over slices.

1.25mm of the slice thickness. **Fig. 7** shows a plot resulting from the luminal measurements over one complete airway (10 slices with 0.625mm thickness) from a patient with Chronic Obstructive Pulmonary Disease (COPD). The area calculated here is the area of elliptical shape of the lumen in the slice plane and is used just for visualizing changes in the lumen area. **Fig. 8** shows a 3D view of pixels on the boundary of lumen over several slices.

B. Measurements on a Phantom

To validate the accuracy of our method for measuring lumen diameter and wall thickness, a phantom was constructed by placing different size glass pipettes and one plastic syringe at varying angles in Styrofoam (**Fig. 9**). This phantom simulates the airways (tubes) and the lung parenchyma (Styrofoam) to which we can apply the LSM, characterized by the set of optimized parameters for lung CT images. Before making the phantom, we measured the inner and outer diameter of the pipettes and syringe using a digital caliper. Unfortunately we found the syringes are not completely symmetric cylinders and the inner and outer diameter varies from top to bottom. Thus, although the

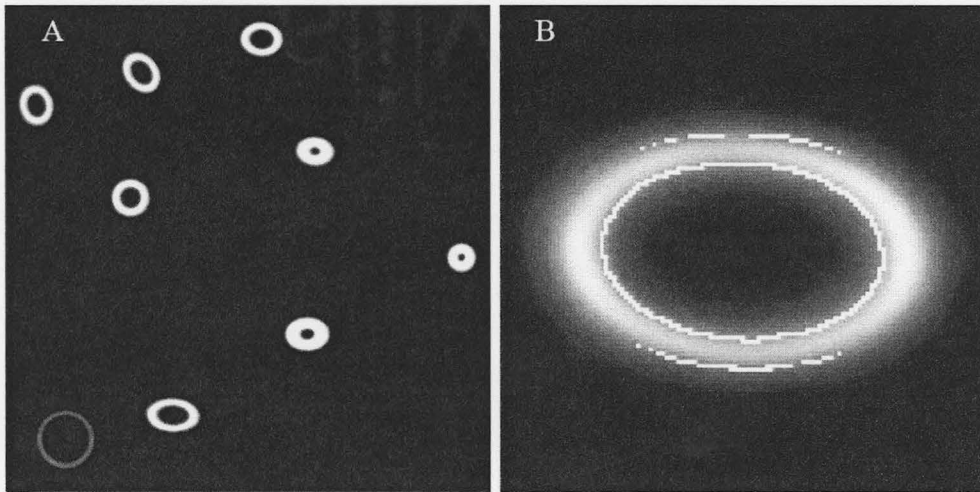


Fig. 9: (a) shows one axial slice of the phantom, through the Styrofoam, (b) shows the result of lumen segmentation and wall thickness measurement.

density of plastic syringes is more similar to lung airways when scanned by the CT scanner, we used glass pipettes in order to construct a more accurate phantom. Care was taken to not deform/compress the plastic syringe when caliper jaws were used during measurement of inner and outer diameters which would have led to computational inaccuracies. Also, in order to measure the wall thickness of the plastic syringe at several positions on the side of the syringe wall, we cut the syringe in places which resulted in thickness variation from 0.82mm to 1.05mm. As our method always finds the minimum thickness of the wall, we put the minimum size (0.82mm) as the wall thickness in Table I. Our results show the measurements using the caliper and the LSM calculation are close to each other (See Table I). Measurements using CT always underestimated the inside diameter of the glass pipettes, while at the same time overestimating their wall thickness by almost one pixel size (i.e. 0.25mm in our case after resizing the original CT image). There was only one exception while measuring wall thickness of plastic syringe (Type#4 in Table I), which was only a very slight underestimate of wall thickness. According to the pixel size of the phantom CT image, the difference between these two was almost equal to one pixel size, which represents an uncertainty factor of $\pm 0.25\text{mm}$ in the X-Y plane. In other words, our method has subvoxel accuracy, considering the actual CT scanner voxel (sensor) size ($0.625\text{mm} \times 0.625\text{mm} \times 0.625\text{mm}$).

IV. DISCUSSION AND CONCLUSIONS

It is often difficult, even for well trained radiologists, to evaluate temporal differences between two images taken in a time sequence, which is barely discernable to the naked eye. It is considerably more difficult to detect, localize and identify changes in successive temporal image sequences while working with 3D data sets which may often contain hundreds of images. Also, for a physician/radiologist who typically examines tens of thousands of images per day, the process of repeated measurement of lumen diameter and its wall thickness over slices and also assessment of changes over time are not only tiresome but also prone to inaccuracies. Thus, we assist a radiologist in identifying a boundary and subsequently measuring the diameter and wall thickness of lung airways which helps to speed up the process of recognition of diseases and identification of temporal variations.

A. Lumen Segmentation Considerations

There is much research on measuring airway luminal diameter and wall thickness as well as many works on finding the relationship between these measurements and lung diseases. Jong *et al.* [25] reviewed such work until 2005, providing a useful list of references. All of these measurement methods start with segmenting the airway lumen, which has lower Hounsfield unit (HU) comparing to the airway wall. Most methods for segmenting the lumen [3-14,17,23] are, directly or indirectly, based on a fixed threshold, that is one of the causes of over growing (the leaking problem) or under growing when segmenting the lumen. Some of them [3-10, 12-14] use the SRGA which is highly sensitive to its fixed threshold which causes the over growing or under growing when choosing a higher or lower threshold, respectively. The SRGA also suffers from noise in the image. As well, the presence of an injected contrast agent and system acquisition parameters (e.g. X-ray energy level) can modulate image features (i.e. intensity of pixels).

Other work used methods such as Maximum Likelihood method [11], Laplacian of Gaussian [17], fuzzy connectivity methods [18-20], and fuzzy classifier [23] for segmenting lung lumen which need to be manually edited [17] and/or, directly or indirectly, are based on a fixed threshold or fuzzy membership [11,17-20, 23] that has the same problem as mentioned for the SRGA. Some other methods such as energy based reconstruction [15], selective marking and depth constrained (SMDC) connection cost [16], and GVF Snake [22] were used for segmenting upper airways and are not able to track airways with small luminal diameter at levels over seven. Although some recent work [12,13], in addition to use fixed thresholds (e.g. -900 and 0), assigned a partial membership to the pixels that are between two fixed thresholds, this is another way of using a fixed threshold between two others. In other words, they assigned pixels with HU less than -900 to lumen and pixels with HU bigger than 0 to wall, then giving partial membership to the pixels between these two thresholds based on dividing their intensity by -900, which is similar to selecting one threshold equal to -450. Also recently, Odry *et*

TABLE I

Shows the measurement of glass pipettes and one plastic syringe inner diameter and wall thickness in both methods, using caliper and the algorithm on CT images.

	Size Using Caliper (mm)		Size Using CT (Pixel Size = 0.2539mm)			
	Name of Pipette	Inside Diameter	Wall Thickness	Inside Diameter		Wall Thickness
Size (mm)				Standard Deviation	Size (mm)	Standard Deviation
Type#1 Angle#1	5.50	0.73	5.17	0.04	0.94	0.01
Type #1 Angle#2	5.63	0.66	5.16	0.04	0.94	0.05
Type #1 Angle#3	5.55	0.79	5.34	0.07	0.96	0.08
Type #1 Angle#4	5.56	0.72	5.37	0.06	0.84	0.05
Type #2 Angle#1	5.97	1.02	5.52	0.09	1.29	0.11
Type #3 Angle#1	3.51	1.84	3.18	0.12	2.08	0.11
Type#4 Angle#1	12.01	0.82	11.72	0.02	0.78	0.01

al. [24] used a parametric active contour, Snakes, to segment the lumen and wall areas. However, this was applicable only on the lumens perpendicular to the plane and works only on unraveled images.

While most reported methods in the literature use some algorithms based on (directly or indirectly) a fixed threshold for segmenting the luminal airways, our two-step method is not based on a fixed threshold. Different thresholds are reported in the literature (e.g. - 500 HU in [36] and -577HU in [37]). Our proposed method dynamically calculates the threshold which always ends with a value less than the actual threshold for segmenting the lumen on the current CT slice. Using this smaller threshold, the SRGA results in under segmenting the lumen, which is our goal. (This is because the result of the SRGA will be used as an initial contour for the LSM and should therefore be inside the lumen). The second step of our method, the LSM, uses the result of the first step as an initial contour and expands this contour to the actual border of the lumen. For the first step of this method, we benefit from the SRGA speed. It rapidly expands one pixel (seed) to the area which is close to the actual boundary. At the second step, we benefit from the LSM accuracy, where the LSM is characterized using the optimized parameters from the GA [31]. This step protects the segmentation method from over growing (the so called ‘leaking problem’) and under growing. Although the LSM is slow compared to the SRGA, we see the following significant benefits of using the LSM with optimized

parameters: *First*, it protects the segmentation method from the leaking problem and under-segmentation; *Second*, it is not restricted to a fixed or variable threshold; *Third*, it is not sensitive to noise; and *Fourth*, the resulting contour always produces the shape of the lumen in the slice plane.

B. Wall Thickness Considerations

While the segmentation of an airway lumen is the first step in processing lung images, finding its wall thickness is the second and the most difficult part. The most commonly reported method for measuring wall thickness is based on Full-Width at Half-Maximum (FWHM) method [4,6,21]. By comparing the result of this method to the anatomical measurement of the same subjects, Nakano *et al.* [6,21] showed that their method (i.e. manually tracing the lumen perimeter [21] and manually removing the rays beyond the wall [6,21], before using FWHM method) ends up with overestimation of wall area and underestimation of lumen area. Reinhardt *et al.* [11] proved that FWHM methods might be suitable for airways with thick walls, but not for thin. The FWHM technique needs to place a lumen center point, where the X-ray attenuation values along rays distributed through the lumen wall from the centre are measured. The ray attenuation will increase and then decrease when it passes the wall from the lumen side to the lung parenchyma side. Using X-ray attenuation values along rays distributed through the lumen wall, some other works tried to use a circular and/or elliptic estimation [8-11,17], or fixed threshold and partial membership [12,13], for finding wall area/thickness.

Methods based on FWHM need to simulate casting X-rays from the lumen center toward the wall and then measure the ray attenuation values (positioning center point was done manually or needed another segmentation method to find the lumen area and then based on that, find the center point). Next, based on a fixed threshold [4,6] (e.g. excluding rays bigger than 2.5mm [4], or eliminating the rays which are smaller than *threshold1* or greater than *threshold2* [6]), or manually [21], they need to remove the rays beyond the wall in vessel area, before using the FWHM method. Finally, the result of these types of measurements is the average of all measurements on the rays. The result may be affected by the partial volume problem and/or errors in removing the rays beyond the wall. Also these methods need to reconstruct the images to make the airway perpendicular to the plane, otherwise the wall is highly affected by the partial volume problem at the direction of the airway angle.

Other methods for wall thickness measurement use circular and/or elliptical estimation [8,9,10] of airway which needs to use a fix threshold to remove the rays through the vessel (e.g. excluding rays bigger than $\frac{3}{4}$ lumen diameter in [10]). These estimating methods need to reconstruct the 3D images which is time consuming and cause more measurement errors. Reinhardt *et al.* [11] used a Maximum Likelihood algorithm to segment luminal and wall area which is not reliable when considering the overlap of intensity of pixels from airway wall and connected vessel. Berger *et al.* [17] manually edited the result of segmenting the lumen and wall area based on the 'Laplacian Of Gaussian' segmentation method. Some recent work [12,13], in addition to using fixed thresholds, assigned a partial membership to the pixels that are between two fixed

threshold, which is another way of using a fixed threshold between two others. In other words, they assigned pixels with HU bigger than 0 to the wall, then gave partial membership to the pixels between 0 and -700 based on dividing their intensity by -700, which is similar to selecting one threshold equal to -350. This method is not reliable because the fixed thresholds are too sensitive to noise implying that such fixed thresholds are not generally applicable to all lung CT images. In another recent work, Odry *et al.* [24] used parametric active contour, Snakes, to segment lumen and wall area which is applicable only on the lumens perpendicular to the plane and works on unraveled image. As the authors of [24] mentioned, and could be seen from the illustrated figures in [24], their method suffers from under- and over-segmentation while the contour converges to the outer border of wall around the artery vessel. Other methods suffer from various weakness (i.e. manually positioning seed, manually editing rays trough vessel, using fixed threshold, inaccuracy around vessel); however, our simple fitting method accurately (based on visually validation from radiologist and validation by phantom) measures wall thickness very quickly.

Our method for measuring wall thickness is based on the similarity of voxels which belong to the inner and outer boundary of the wall. In other words, when expanding the lumen boundary by one pixel, all pixels on the expanded boundary (new contour) belong to the wall (inner border), then we expand the contour several times, until it reaches the outer border of the wall. We assume that these pixels (on the outer border) have the same property the pixels had at the inner border of the wall. In addition to being simple, fast, and accurate, another advantage of our method is that it simulates the manner in which radiologists measure wall thickness. In other words, the clinical approach to measuring wall thickness is to look for the thinnest wall around the lumen which leads to the part that is least affected from the partial volume problem and any neighboring blood vessel.

C. Tracing Airway Considerations

Measuring airway luminal diameter and wall thickness may be affected from some side effects (i.e. partial volume problem, noise, artifacts, etc.), thus it will be beneficial to do the measuring over slices and then calculate the average over several neighboring slices. Also recognizing several diseases is another benefit of this multi-slice measurement. Finding a loss of normal tapering of the lumen when progressing distally is a sign of bronchiectasis which is a feature of many disease entities involving the airways (e.g. cystic fibrosis, tuberculosis, tracheobronchomegaly). This may also be seen in cases of lung fibrosis where there is secondary traction on the airway (e.g. idiopathic pulmonary fibrosis or UIP).

D. Summary

In summary: *first*, our two-step method for segmenting the airway lumen benefits from both the speed of the SRGA and the accuracy of the LSM. Also by measuring the smaller diameter of the elliptical shape of the lumen, when the airway is not perpendicular to the plane, there is no need for time consuming reconstruction of 3D CT

images, in order to ensure a perpendicular airway to the plane. *Second*, our fitting method for measuring wall thickness is simple, fast, accurate, and emulates a clinical approach used by radiologists. It also does not suffer from partial volume effects with the connected vessel. *Third*, our automatic method for tracking airways makes these (above) measurements more accurate. Furthermore, averaging several measurements over neighboring slices reduces the confounding effect of noise, partial volume, and potential artifacts. Also measurements over one branch can be used for recognizing some diseases. These whole steps for measuring airway luminal diameter and wall thickness over slices need the least amount of user interaction, which means, after selecting one slice from CT images, it just needs two user-defined inputs: one mouse click (seed for region growing algorithm) and one input number ± 1 (tapering direction). The rest of the subsequent processing is completely automatic. Further verification of this work using formaldehyde-fixed animal lung will be the starting point of future work.

ACKNOWLEDGEMENTS

Funding for this work was provided through a fellowship to Mr. Mohammadreza Heydarian. Dr. Kamath was supported in part by a Natural Sciences and Engineering Research Council (NSERC; Canada) Discovery Grant.

References

- [1] R.C. Gonzalez and R. E. Woods, *Digital Image Processing*, 2nd Ed., Upper Saddle River, NJ, Prentice Hall, 2002, Chapter 10.
- [2] A. Oppelt, *Imaging Systems for Medical Diagnostics: Fundamentals, Technical Solutions and Applications for Systems Applying Ionizing Radiation, Nuclear Magnetic Resonance and Ultrasound*, Wiley, 2006.
- [3] M. Sonka, G. Sundaramoorthy, and E. Hoffman, "Knowledge-Based segmentation of intrathoracic airways from multidimensional high resolution CT images", *Medical Imaging, Proc. SPIE*, vol. 2168, pp.73-85, 1994.
- [4] Y. Nakano *et al.*, "Computed Tomographic measurements of airway dimensions and emphysema in smokers", *Am J Respir Crit Care Med*, vol. 162, pp. 1102-1108, 2000.
- [5] T. Law and P. Heng, "Automated extraction of bronchus from 3D CT images of lung based on genetic algorithm and 3D region growing", *Medical Imaging, Proc. SPIE* vol. 3979, 2000.
- [6] Y. Nakano *et al.*, "Development and validation of human airway analysis algorithm using multidetector row CT", *Medical Imaging, Proc. SPIE* vol. 4683, 2002.
- [7] X. Zhou *et al.*, "Automatic segmentation and recognition of anatomical lung structures from high-resolution chest CT images", *Computerized Medical Imaging and Graphics*, vol. 30, pp. 299-313, 2006.

- [8] B. Odry *et al.*, “Automated airway evaluation system for multi-slice computed tomography using airway lumen diameter, airway wall thickness and broncho-arterial ratio”, Medical Imaging, Proc. SPIE vol. 6143, 2006.
- [9] O. Weinheimer *et al.*, “About objective 3-D analysis of airway geometry in computerized tomography”, IEEE Trans. Medical Imaging, vol. 27, No. 1, Jan. 2008.
- [10] J. Lee *et al.*, “Human airway measurement from CT images”, Medical Imaging, Proc. SPIE vol. 6515, 2008.
- [11] J. Reinhardt, N. D’Souza, and E. Hoffman, “Accurate measurement of intrathoracic airways” IEEE Trans. Medical Imaging, vol. 16, NO. 6, Dec. 1997.
- [12] J. K. Leader, *et al.*, “Quantification of airway morphometry: the effect of CT acquisition and reconstruction parameters”, Proc. of SPIE vol. 6511, 65111R, 2007.
- [13] B. Zheng, *et al.*, “Automated detection and quantitative assessment of pulmonary airways depicted on CT images”, Med. Phys. 34 (7), pp. 2844-2852, July 2007.
- [14] M. F. McNitt-Gray, *et al.*, “Development and testing of image-processing methods for the quantitative assessment of airway hyperresponsiveness from high-resolution CT images”, Thoracic Imaging, vol. 21(6), pp 939-947, November/December 1997.
- [15] C. Fetti and F. Preteux, “Quantitative 3D CT bronchography”, IEEE Int. Symp. Biomed. Eng., 2002.
- [16] C. Fetti, F. Preteux, C. Beigelman, and P. Grenier, “Pulmonary airways: 3-D reconstruction from multislice CT and clinical investigation”, IEEE Trans. Medical Imaging, vol. 23, NO. 11, Nov. 2004.
- [17] P. Berger *et al.*, “Airway wall thickness in cigarette smokers”, RSNA Radiology, pp. 1055-1064, June 2005.
- [18] J. Tschirren, E. Hoffman, G. McLennan, and M. Sonka, “Intrathoracic airway trees: segmentation and airway morphology analysis from low-dose CT Scans”, IEEE Trans. Medical Imaging, vol. 24, NO.12, Dec. 2005.
- [19] J. Tschirren, E. Hoffman, G. McLennan, and M. Sonka, “Segmentation and quantitative analysis of intrathoracic airway trees from CT images”, Proc. American Thoracic Society, vol. 2, pp. 484-487, 2005.
- [20] K. Palagyia, J. Tschirrena, E. A. Hoffman, and Milan Sonka, “Quantitative analysis of pulmonary airway tree structures”, Computers in Biology and Medicine, vol. 36, pp. 974-996, 2006.
- [21] Y. Nakano *et al.*, “The prediction of small airway dimension using computed tomography”, Amr J Res Crit Care Med, vol. 171, pp. 142-146, Jan. 2005.
- [22] I. Cheng, S. Nilufar, C. Flores, and A. Basu, “Airway segmentation and measurement in CT images”, IEEE Proc. 29th Annual Int Conf EMBS, Aug 2007.
- [23] F. Rizi *et al.*, “A hybrid fuzzy based algorithm for 3D human airway segmentation”, IEEE 2nd Int Conf Bioinfo Bio Med Eng, p. 2295-2298, May 2008.
- [24] B. L. Odry, *et al.*, “Active contour approach for accurate quantitative airway analysis”, Proc. of SPIE vol.6916, 691613, 2008.
- [25] P. Jong, N. Muller, P. Pare, and H. Coxson, “Computed Tomographic imaging of the airways: relationship to structure and function”, Eur Respir J, vol. 26, NO. 1, pp. 140-152, 2005.

- [26] N. Saeed, “Magnetic Resonance Image segmentation using pattern recognition, and applied to image registration and quantization”, *NMR Biomed.*, vol. 11, pp. 157-168, 1998.
- [27] S. Osher, J. A. Sethrian, “Fronts propagation with curvature-dependent speed: algorithms based on Hamilton-Jacobi formulations”, *J. Computation Physics*, vol. 79, pp. 12-49, 1988.
- [28] C. Li, C. Xu, C. Gui, and M. D. Fox, “Level Set Evolution Without Re-initialization: A new Variational Formulation”, *IEEE Computer Society Conference on Computer Vision and Pattern Recognition*, vol. 1, pp. 430-436, 2005.
- [29] V. Caselles, F. Catte, T. Coll, and F. Dibos, “A Geometric Model for Active Contours in Image Processing”, *Numer. Math.*, vol. 66, pp. 1-33, 1993.
- [30] D. E. Goldberg, *Genetic Algorithm in Search, Optimization, and Machine Learning*, Boston, MA, USA, Addison-Wesley professional, 1989, Chapters 1-3.
- [31] M. Heydarian, M. Noseworthy, M. Kamath, C. Boylan, W. Poehlman, “Optimizing the level set algorithm for detecting object edges in MR and CT images”, *IEEE Trans. Nuclear Science*, Vol. 56, No. 1, pp.156-166, Feb. 2009.
- [32] D. E. Olson, G. A. Dart, and G. F. Filley, “Pressure drop and fluid flow region of air inspired into the human lung”, *J Appl. Physiol.*, vol. 28, pp. 482-494, Apr. 1970.
- [33] K. Horsfield, G. Dart, D. E. Olson, G. F. Filley, and G. Cumming, “Models of the Human Bronchial Tree”, *J Appl. Physiol.*, vol. 31, no. 2, pp. 207-217, Aug. 1971.
- [34] J. A. Sethrian, *Level Set Methods and Fast Marching Methods*, Cambridge UK, Cambridge University Press, 1999, Chapter 17.
- [35] R. Malladi and J. A. Sethian, “A Unified Approach to Noise Removal, Image Enhancement, and Shape Recovery”. *IEEE Trans. on Image Proc.*, vol. 5, pp. 1554-1568, 1996.
- [36] M. McNitt-Gray *et al.*, “Development and testing of image-Processing methods for the quantitative assessment of airway hyperresponsiveness from high-resolution CT images”, *J Computer Assisted Tomography*, vol. 21, NO. 6, pp 939-947, Dec 1997.
- [37] G. King *et al.*, “An analysis algorithm for measuring airway lumen and wall areas from high-resolution Computed Tomographic data”, *Am J Respir Crit Care Med*, vol. 161, pp. 574-580, 2000.

5.3 Summary of article

A manual verification of measurements derived from the algorithms is the most important issue of this paper. An objective method to find the error is to measure the anatomy of lung on pathology samples. Knowing the actual airway luminal shape and size, one can provide the GA with a more accurate boundary. This is one of the more important suggestions for future work. Also, differing airway lumen boundary determinations due to the actual anatomical measurements, will affect the result of wall thickness measurements.

With the absence of pathological lung samples, another important point is using appropriate material for making a lung phantom substitute. On the first attempt, a phantom was fabricated using plastic syringes in Styrofoam. It provided a good contrast as well as similar Hounsfield Unit (HU) interval to the actual HU interval of the lung CT. In other words, Styrofoam has the same HU property as does parenchyma and plastic syringes have the same HU property as lumen. However, plastic syringes are flexible and usually have different inner boundary shapes and diameters along the length of the syringe. Also these syringes usually have different wall thickness at different positions along the length of the syringe. **Fig. 10** shows our first phantom. **Fig. 11** shows a photo of a syringe that was cut in the middle. The different thicknesses along different sides of the syringe can be noted.

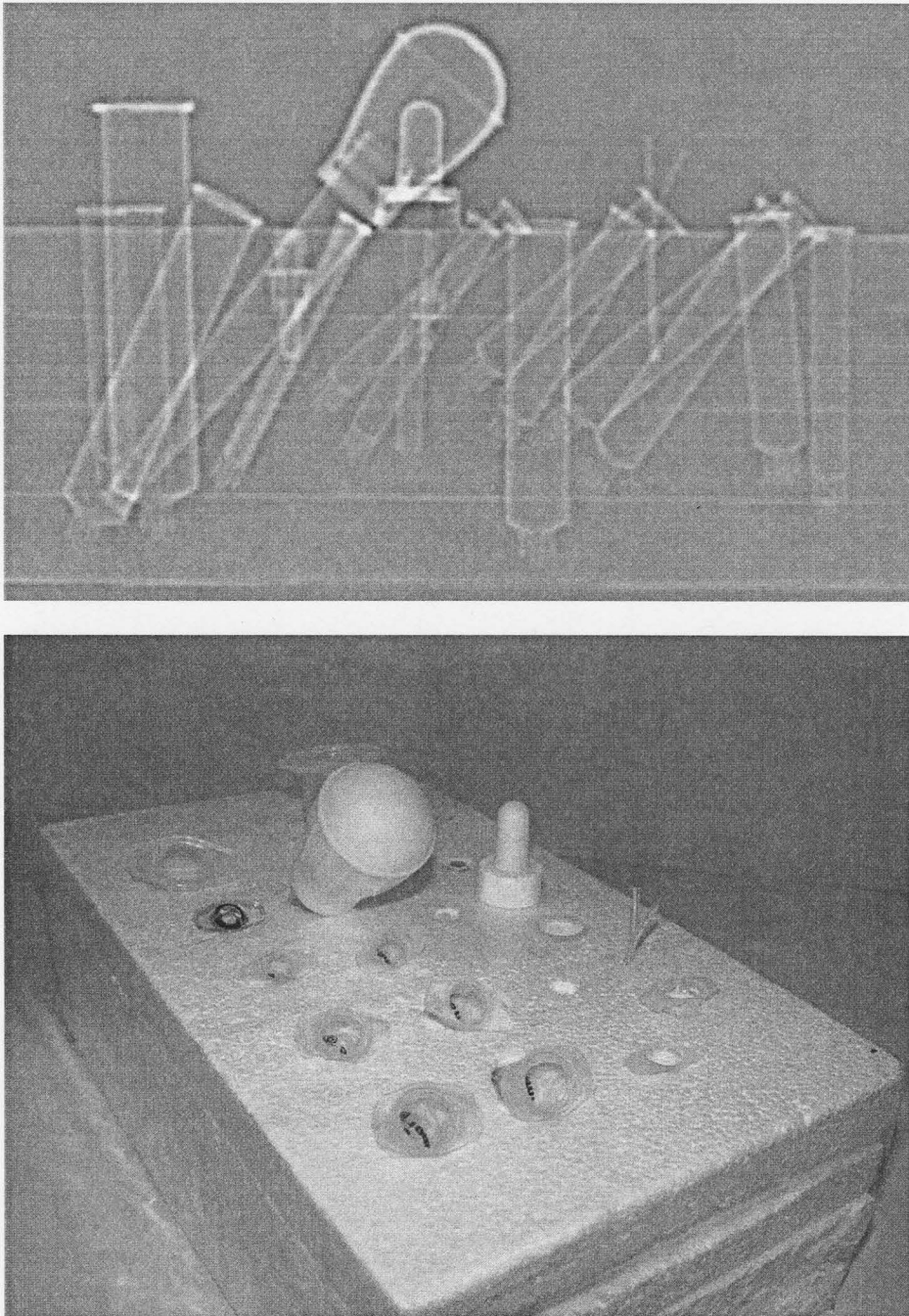


Fig. 10: (Top) shows an x-ray of our phantom from coronal view, (bottom) shows a photo of our phantom.

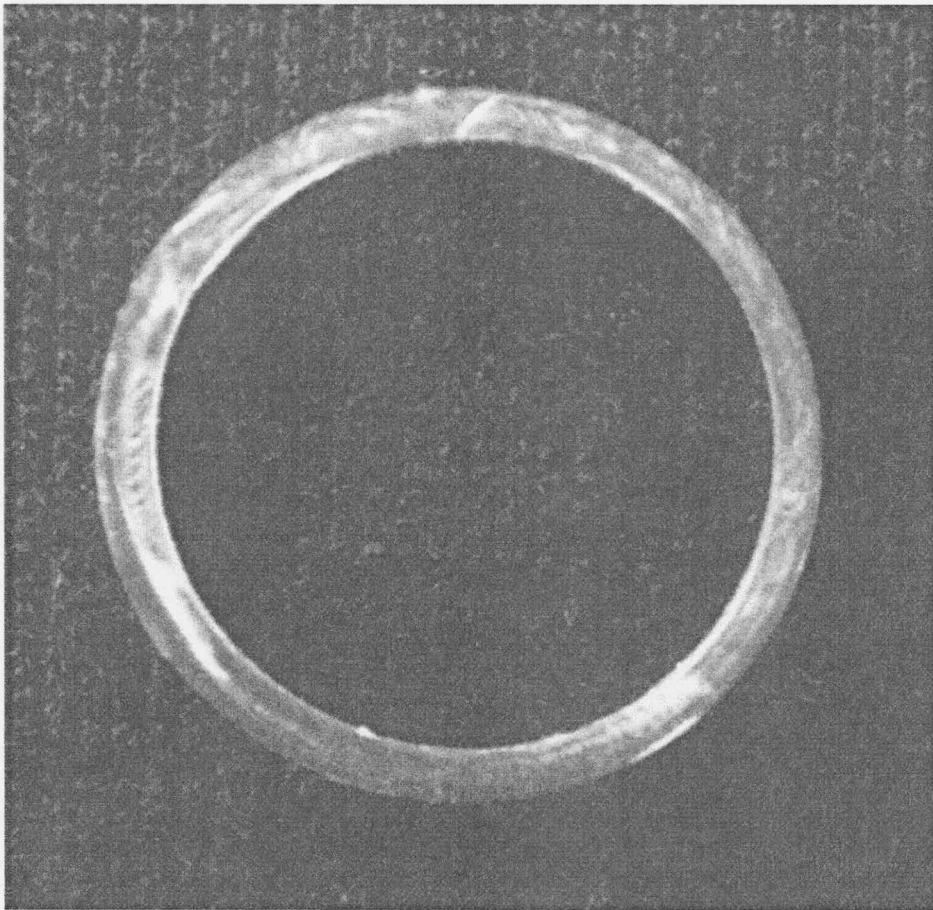


Fig. 11: shows a photo of a syringe that was cut in the middle.

Chapter 6: Measuring Angle of Lung Airway Branches

6.1 Overview of article

In this chapter the third paper based on the current research being submitted to Annals of Biomedical Engineering is presented. This article is a continuation of lung airway characterization described in chapter 5 as the second article resulted from this Ph.D. project.

6.2 Article

A Morphological Algorithm for Measuring Angle of Airway Branches in Lung CT Images

Mohammadreza Heydarian, Michael D. Noseworthy, Markad V. Kamath, Colm Boylan,
W.F.Skip Poehlman

Abstract

Accurate measurement of human lumen bifurcation angle in the bronchial tree may be an important parameter for evidence of pulmonary diseases. Here we describe a new, rapid, and accurate automated method for recognizing and following airway bifurcation over numerous contiguous CT images. Based on morphological properties of airways and specific changes to airway properties while traveling through the bifurcation, our method is able to track airways through several levels of bifurcations. Then, based on the center of the lumen area found by a segmentation algorithm, our method estimates the centerline of each branch and calculates the angle between two branches of a bifurcation. Applying the method on an airway phantom, we obtain accurate results in a short period of time. This new approach provides a rapid, automated, and accurate lung airway angle measurement. Our method will prove useful to radiologists who use CT images for pulmonary disease assessment.

Keywords: seeded region growing algorithm, level set method, CT, lung airway, lumen.

I. INTRODUCTION

Accurate measurement of human lumen airway angles has the potential to assess numerous pulmonary diseases (e.g. asthma and COPD) and assist in the evaluation of pulmonary disease therapy. To assist this process which can be carried out automatically on lung CT images, we need to develop an accurate and automatic angle measurement technique. Typically, the airway angle is measured ‘by hand’ using imaging vendor-provided software and a workstation. With numerous contiguous slices, this method becomes very time consuming for the radiologist and it is also prone to fatigue related inaccuracies. An ideal alternative approach is to use image-processing methods combined with mathematical constructs describing anatomical airways.

Some work has been done on automatically measuring the angle of airways branches [2-4] or the direction of the airway comparing to “the perpendicular line to the slice plane” [5]. To measure the bifurcation angle, it is necessary to deal with structural properties of the airway tree as well as the mathematical concepts of estimating the lumen centerline based on the curve resulting from the specification of the center of the segmented lumen over relevant slices. There is much research on segmenting lung lumen. While most of these segmentation methods use a 2D/3D Region Growing Algorithm (e.g. [6-9]), which is very sensitive to its threshold setting, other laboratories use different methods such as fuzzy connectivity [10] or Snakes [11] to segment airway lumen. In our previous work [12] (see chapter 5), we developed an accurate segmentation technique to specify luminal border in lung CT images. This method generates a relatively accurate segmentation without the leakage problem (over segmentation). In this paper, we demonstrate a new one-click automated multi-step method for measuring airway bifurcation angles over several levels of branches.

II. MATERIALS & METHODS

A. Imaging

Routine clinical lung CT data were used to evaluate the performance of our method. Images were chosen from patients suffering from asthma and COPD as well as patients with thoracic problems requiring CT scanning but otherwise having healthy lung tissue. The images were acquired by using 64-channel multidetector CT scanners (LightSpeed VCT; GE Healthcare, Milwaukee, WI). Whole-lung CT images with no intravenous contrast medium were obtained with the following parameters: detector collimation, 0.625 mm; field of view, 34.5 cm; pitch, 1.375; gantry speed, 0.4 second per rotation; automatic selection of the milliamperage setting (range, 128–300 mA); and noise index=10. Axial reconstructions of 0.625mm slice thickness at 0.625mm reconstruction intervals were provided for analysis.

B. Mathematical Background

The level set method (LSM) [13,14], a geometric active contour model [15], is a reasonable choice for segmentation, as it focuses on a specific object, rather than the whole image, and there is no need for a fixed or variable threshold. However, the variation of the LSM, which we use for segmenting lung airway lumen, requires the specification of several parameters as well as the determination of an initial region inside the object for initiation [14]. Unfortunately, there is no single set of parameters that is suitable on all types of images. In other words, every kind of image needs a specific set of parameters. Also, there seem to be no ‘rules of thumb’ for generalization. To offset such a problem, it is possible to use a genetic algorithm (GA) [16] as a heuristic search method to optimize parameters of the level set method in order to obtain more accurate results within a short period of time [12]. To provide the LSM with an initial region inside the lumen, a seeded region growing algorithm (SRGA) [1] was used with a dynamic low threshold (see chapter 5) to avoid over growing. The SRGA output is a region that is quite close to the actual border of the lumen, which results in fewer iterations of the LSM for accurate convergence on the lumen boundary.

A seeded region growing algorithm (SRGA) groups pixels into a region based on various selection criteria. The algorithm requires a position within the region of interest as a starting seed and a threshold as part of the selection criteria. Next, the algorithm finds the distance between each neighboring pixel of the previously selected region (i.e. a seed for starting) to the mean of that area and if the distance is less than the threshold, this pixel will be added to the current region. When the distance of all neighbor pixels is bigger than a threshold, the algorithm is terminated. In our previous work (see chapter 5), we introduced a dynamically calculated threshold for protecting the SRGA from over growing within the lumen area. Algorithm 1 shows the fundamental growth of a SRGA in pseudo code where $I(x,y)$ is the intensity of a pixel in position (x,y) and $avg(currentArea)$ is the average intensity of all pixels in a previously selected area by the SRGA, which is initialized by a seed point.

Algorithm1:

newArea = {seed}

repeat

currentArea = *newArea*

neighbourArea = *neighboursOf CurrentArea*

 for all $(x,y) \in \text{neighbourArea}$

 if $I(x,y) - avg(currentArea) \leq threshold$ Then

 add (x,y) to *newArea*

 endif

 endfor

until *newArea* == *currentArea*

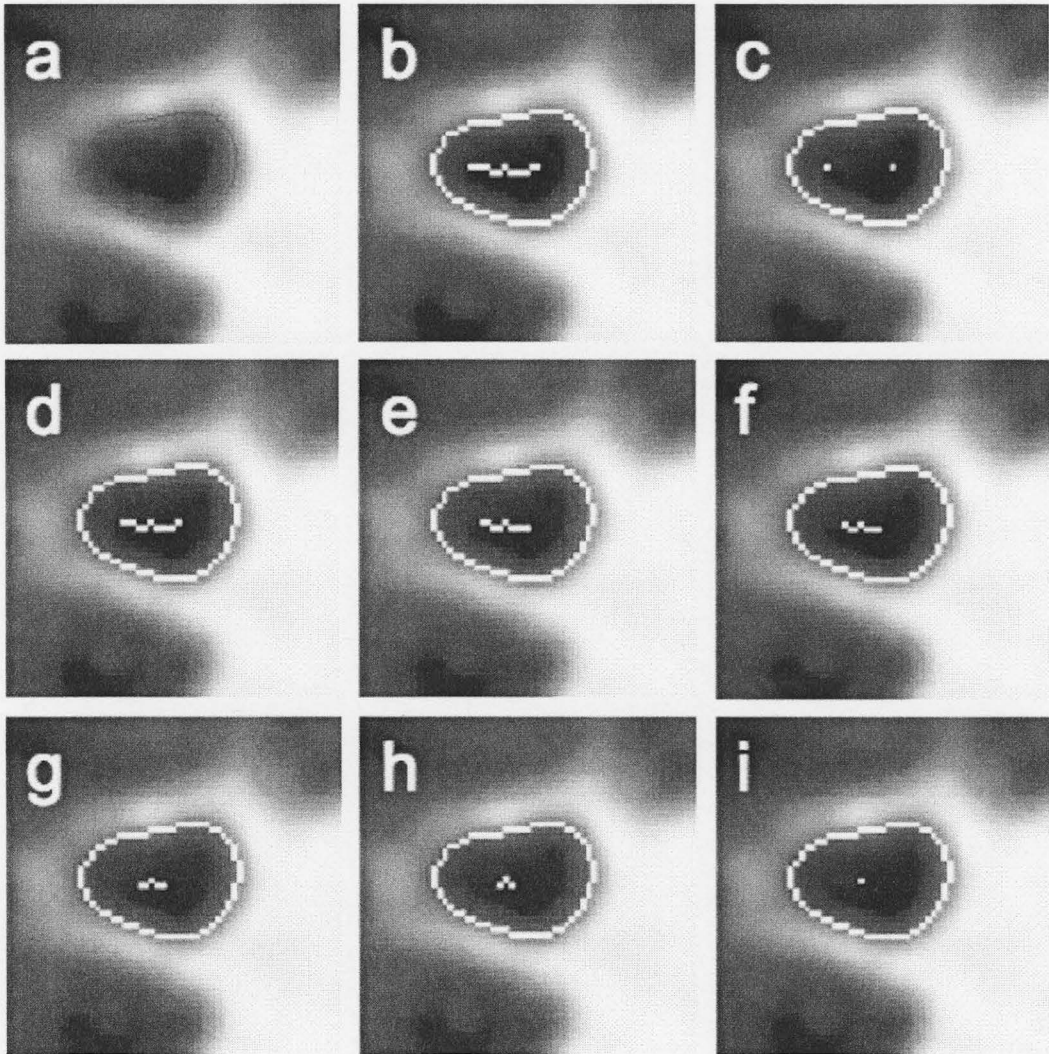


Figure 1: Shows different steps on lumen center specification: (a) result of level set method, (b) result of thinning function, (c) end points of part c, (d, e, f, g, h, i) result of several steps for deleting end points.

C. Lumen Center Specification

Using the result of the SRGA as the initial contour, the level set method is able to find the accurate border of the lumen in a very short time. Briefly, consider the fact that when cutting a circular cylinder in any plane, the center of the resultant elliptical shape is in the position of the cylinder centerline. Thus the current algorithm described herein finds the luminal center without any need for reconstructing the image in order to manipulate the airway perpendicular to the plane.

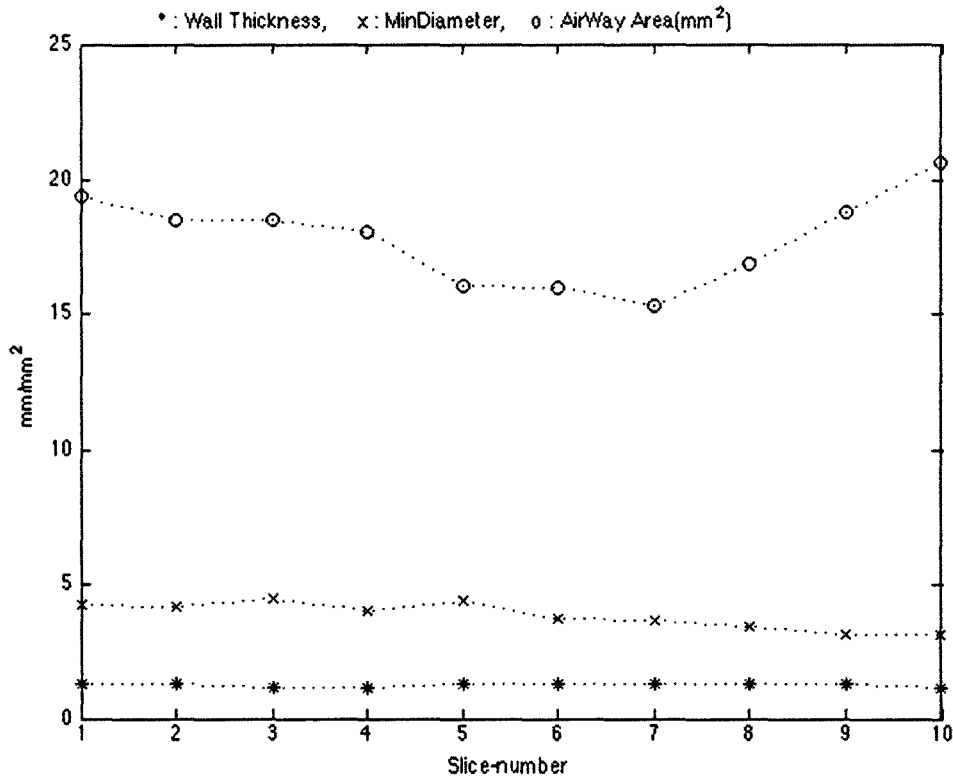


Figure 2: Top curve shows the lumen area (mm^2), middle curve shows the lumen diameter (mm), and the bottom curve shows the airway wall thickness (mm).

Having the luminal border and using a thinning algorithm [1], our technique finds the thin shape of the lumen, which typically is a line with at least one point (pixel) on it. Then for objects greater than two points, the program removes the end-points of the thin object. This process results an object with one or two points on it. In the case of two points, the program always chooses the top/left point. The remaining point is the center of the lumen. **Fig. 1** shows these steps to find the center point of the lumen.

We also developed another method to find the center point which is faster, but we did not find it as accurate as the previous method. In this method, the algorithm finds four points at each side of the lumen border. By averaging top and down points and also averaging left and right points, the algorithm finds the center point.

D. Trace Airway Cross Slices and Bifurcation Detection

A heuristic method was created (see chapter 5) for tracing airways automatically. For finding the lumen boundary, the algorithm simply needs a pixel position to start the SRGA, so it is necessary to locate a position inside the lumen for the next slice when tracing the airway. To do that, the center of the current segmented lumen is used as the

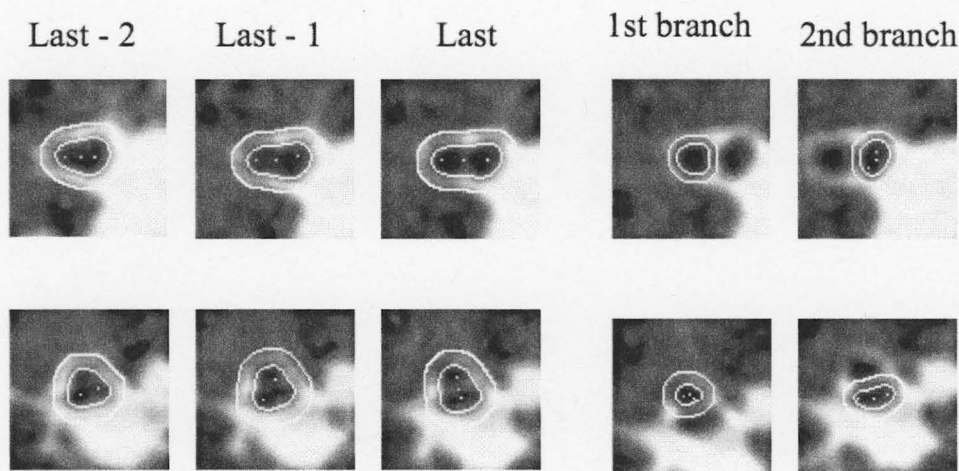


Figure 3: Shows several steps of localizing the center of both branches at a bifurcation.

starting point for the next slice. In addition to locating the starting point, the termination condition is another important part of this tracing algorithm. As seen in **Fig. 2**, the lumen area (usually) becomes bigger when reaching a bifurcation whereas before this point it (usually) gets smaller. In other words, in the curve obtained by plotting the lumen area as a function of the distance travelled, there is a 'valley' before the bifurcation. In some diseases, however, the lumen diameter and area are expanding toward the bifurcation; in this case, the ratio of progress for this measurement is much larger when near the bifurcation. So we find the ratio of the current lumen area to the one which was measured from the slice 2mm (three slice with 0.625mm thickness) away. A ratio that is bigger than 1.2 is taken as a sign for reaching a bifurcation and therefore the next step for finding each of the branches starts at this point (explained in next section). The algorithm begins checking this ratio after passing five slices.

The algorithm described in this paper also checks two other termination rules to detect a bifurcation. If it continues to apply the SRGA on the next slice which contains the bifurcation, the SRGA converges on the area which covers almost two-thirds of the whole image because the starting point (i.e. the center of the previous lumen) will be located on the lumen wall and will grow through the connected vessel and other area with similar intensity. This will happen even if the SRGA uses the threshold calculated from the first step of the growing. Also, rarely, the tracing algorithm may find just one of the branches where the area is almost half (or at most 80%) of the area of the lumen from the previous slice. So, the algorithm checks these two conditions to locate the bifurcation. The measurements of the last few slices (at the bifurcation area) are excluded from calculating the bifurcation angle over the slices.

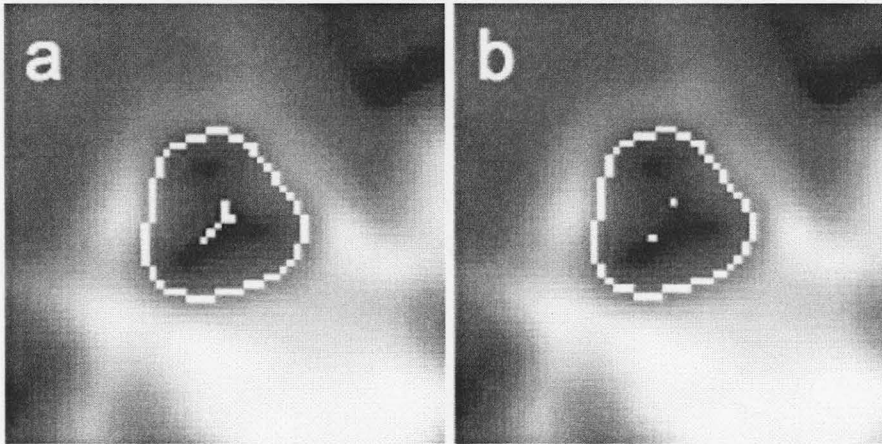


Figure 4: Shows a case that the result of thinning lumen boundary has more than two end-points.

E. Finding the Center of Branches at a Bifurcation

To localize the center of both branches, we developed a morphological method based on the result of segmentation from the previous slice. Similar to the method that we used to locate the center of the current lumen (purpose of which is to locate a seed on the lumen at the next slice), the algorithm finds the thin object of the current segmented lumen. Near a bifurcation, the shape of the lumen area will change to a dumbbell shape, whose thinning object is a line with usually a slight curve. The algorithm uses both endpoints of this line as the starting points for the SRGA on the next slice. If the results of the SRGA from both endpoints do not overlap, this signifies that the next slice contains a bifurcation and the algorithm will use these two endpoints as the starting points for each branch. On the other hand, if an overlap did occur, the algorithm continues in a similar manner as it did for the previous slices (using the lumen center point for starting the SRGA on the next slice). **Fig. 3** shows the result of this step of the algorithm for two different cases. In some rare cases, the result of the thinning algorithm may not be a line as seen in **Fig. 4**. In these cases, our algorithm finds two end points with the most distance between them, and continues the algorithm with these new points. For finding the center point in these cases, the algorithm will delete all end points.

A slight modification of our method seems to offer more accuracy. For the modification, the algorithm finds the maximum distance between the center point of the current lumen area and the pixels on the current lumen border which is used as half of the maximum diameter (of the current lumen area). Then the difference is found between this maximum diameter and length of the thin object. The thin object is extended by $1/7$ of this difference, where $1/7$ was empirically obtained through trial and error efforts. For extending the thin object line, the algorithm uses the direction of the thin object endpoints by checking the points before the endpoints at both sides. In order to protect the system

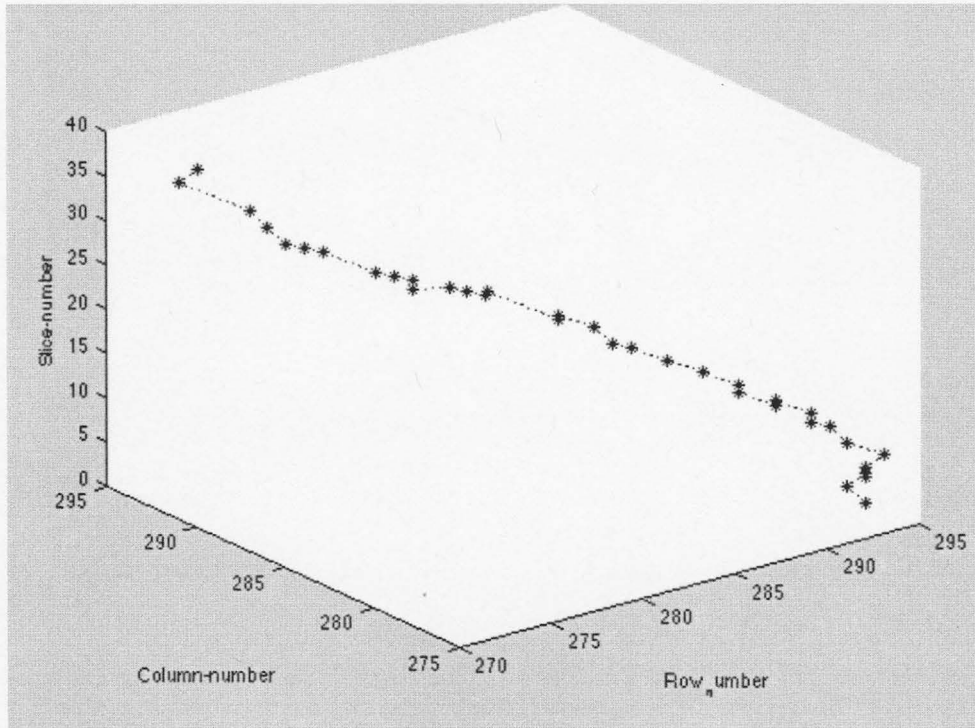


Figure 5: Shows the position of lumen center points in X-Y axis.

from introducing an error associated with this modification, the algorithm protects the thin object from becoming over extended, by checking whether the end points are still inside the lumen boundary (i.e. it is possible that the expansion direction of the thin object is not in the same direction as the maximum diameter and therefore it may go beyond the lumen boundary). Also, the distance between the new endpoints and the lumen border in the extending direction is checked. If this distance is less than one half of the extended length (again a factor that is empirically obtained) or the end point(s) are outside the lumen boundary, the last added endpoint(s) would be removed until this condition changes.

F. Estimating the center line of an airway

The algorithm, as described above, is able to locate the center points of a lumen through each branch. By using the linear regression method (*polyfit* function in Matlab), the algorithm is able to define a line fitted on the center points of a branch. Once we have the estimated line for both branches of one bifurcation, the angle between these two lines is calculated. To estimate the line, we need to reformat the position of the center points to the actual position in a millimeter scale:

$$xValues = xValues * xVoxelSize$$

$$\begin{aligned} yValues &= yValues * yVoxelSize \\ zValues &= zValues * zVoxelSize \end{aligned} \quad (1)$$

where $xValues$, $yValues$, and $zValues$ are records of lumen center pixel positions in directions x , y and z , respectively, and $xVoxelSize$, $yVoxelSize$, and $zVoxelSize$ are the size of a voxel in directions x , y and z , respectively. **Fig. 5** shows the position of the center points in X-Y dimension where the X- and Y-axis are based on the number of pixels in each direction. Then the linear regression method is applied on the position values of each dimension to find the coefficients of the line-equation in all three dimensions:

$$\begin{aligned} a &= polyfit(t, xValues, 1); \\ b &= polyfit(t, yValues, 1); \\ c &= polyfit(t, zValues, 1); \end{aligned} \quad (2)$$

where t is a vector of natural numbers from 1 to $length(xValue)$. Considering the fact that the center points near the bifurcation are not reliable and airways have a curve while near to the bifurcation, we need to ignore the center points near to the next bifurcation area. Thus we eliminate the last 40% of the center points, so the vector t contains the natural numbers from 1 to $0.60 * length(xValue)$. The resulting line equation can be shown as below:

$$\begin{aligned} x &= a * t + xI \\ y &= b * t + yI \\ z &= c * t + zI \end{aligned} \quad (3)$$

where xI , yI , and zI are the distance of the line from the center of the axis (0,0,0) and are not important in calculating the angle between the two lines as seen in (4) below. **Fig. 6** shows the result of estimating a centerline in a three dimension plane. The angle between two estimated lines could be calculated as:

$$\theta = \arccos\left(\frac{a_1 a_2 + b_1 b_2 + c_1 c_2}{\sqrt{a_1^2 + b_1^2 + c_1^2} \times \sqrt{a_2^2 + b_2^2 + c_2^2}}\right) \quad (4)$$

III. RESULTS

A. Patient CT images

The proposed method is able to automatically measure the angle of bifurcations at several levels in lung CT images. This measurement is a result of automatically tracing an airway as well as the bifurcation detection and then following branches in the cross sectional lung CT images (slices). **Fig. 7(a)** shows a 3D view of tracing an airway as well as one of its branches. **Fig. 7(b)** shows a 3D view of tracing an airway and both of its branches. Visualizing the result of the segmentation which shows the lumen border in 3D dimensions is very useful to radiologists in order to estimate any airway tapering and the bifurcation angle. Having the lumen border at every slice, the algorithm is able to find the center of the lumen area for each slice (explained in part E of II). Based on the fact that

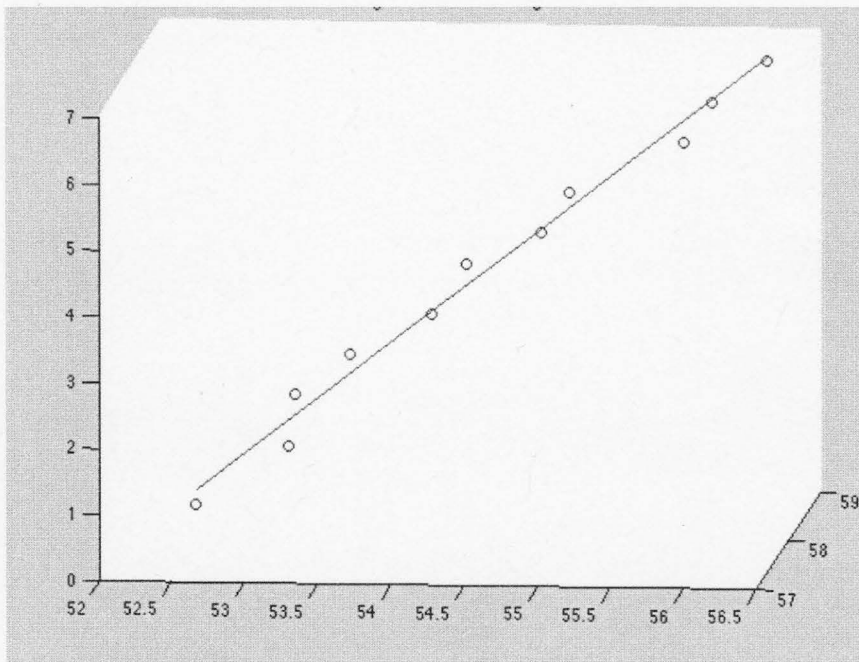


Figure 6: Shows the result of estimating lumen center-line as a straight line.

when cutting a circular cylinder in any plane, the center of the resultant ellipse is the same as the center of the cylinder, the algorithm does not need to reconstruct the 3D image to make the airway perpendicular to the plane (so this method for finding the center of lumen is fast and accurate). **Fig. 8** shows the result of estimating the center points as a line for both branches of a bifurcation. Using (4) for measuring the angle, the algorithm does not need to find the intersection of these two lines, and also does not need to consider the distance of each line to the center of X-Y-Z axis. Applying this algorithm on clinical lung CT data from patients, the algorithm is able to follow several levels of airways while finding the bifurcations and tracking them. The algorithm stacks bifurcation position, the slice number, and the position of branch center points for each bifurcation, so it can recursively trace all branches at different levels. This method is simple, accurate, and repeatable which results with useful information for radiologists.

B. Measurements on Phantom

To validate the accuracy of our method for measuring the bifurcation angle, a phantom (**Fig. 9**) was constructed by placing different size plastic Y-shape pipes at varying angles in Styrofoam. **Fig. 10** shows a CT slice of this phantom near to the bifurcation area of most of the pipes. This slice shows Y-shape pipes with different sizes (i.e. diameter, length) and angles which are placed in different directions. This phantom

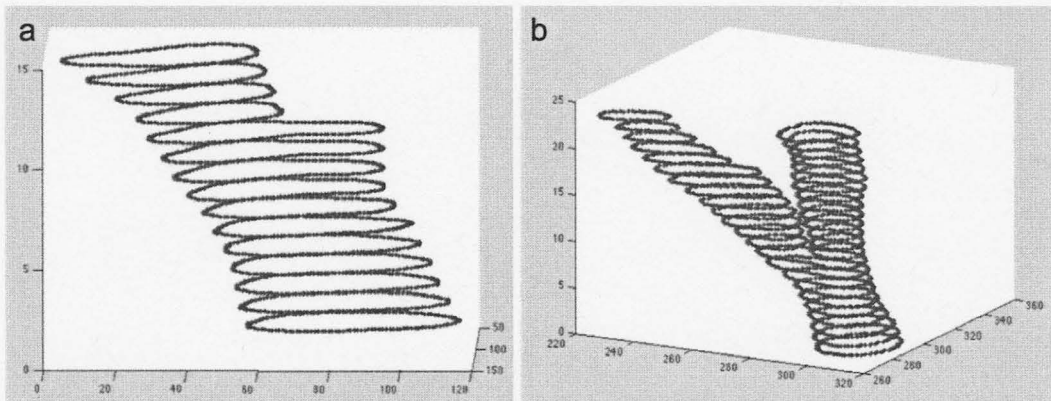


Figure 7: (a) 3D view of the result of tracing and segmenting airway lumen through one of the branches at a bifurcation, (b) 3D view of the result of tracing and segmenting airway lumen through one of the branches at a bifurcation.

simulates the lung airways to which we can apply our previously reported segmentation method (see chapter 5) followed by the morphological angle measurement method. Before making the phantom, we measured the angle of plastic Y-shape pipes using a protractor (angle-finder-ruler), which has ± 1 degree reading error.

Our results show that the measurements using the protractor and our method are close to each other (See **Table I**) when we use 12 or more slices of the CT images. **Table I** is based on measurements of those Y-shape pipes which are covered with more CT slices. In addition to these pipes, for the Y-shape pipes with smaller length or the ones that are in such a direction that less axial slices are needed to cover them, we prepared the result of angle measurement in the form of **Table II**. This is the result of scanning a phantom made of four different Y-shape pipes where three types of them have 60-degree angle (types 1-3) and one type has 120-degree angle (type 4). That part of the phantom with 60-degree angle comes in three different sizes of inner diameter (i.e. 3.0mm, 5.0mm, and 6.0mm). In **Table II** we calculated the deviation of the measurement by this method with that obtained through a manual measurement (as reference) for all pipes while taking into account the different number of slices. Also we calculated the average deviation from the reference angle for each type of pipes separately. The result shows that for measuring the angle based on our method on CT data, we need almost 7 slices (0.75mm thickness) to obtain an acceptable measurement.

Additional observations can be made from the results in this table. First, we see that the angle measurement on pipes with smaller inner diameter is more accurate. Second, the angle measurement based on center points as a result of applying thinning method on lumen boundary is more accurate than angle measurement based on center points as a result of applying center points finder based on top-down-left-right points of lumen.

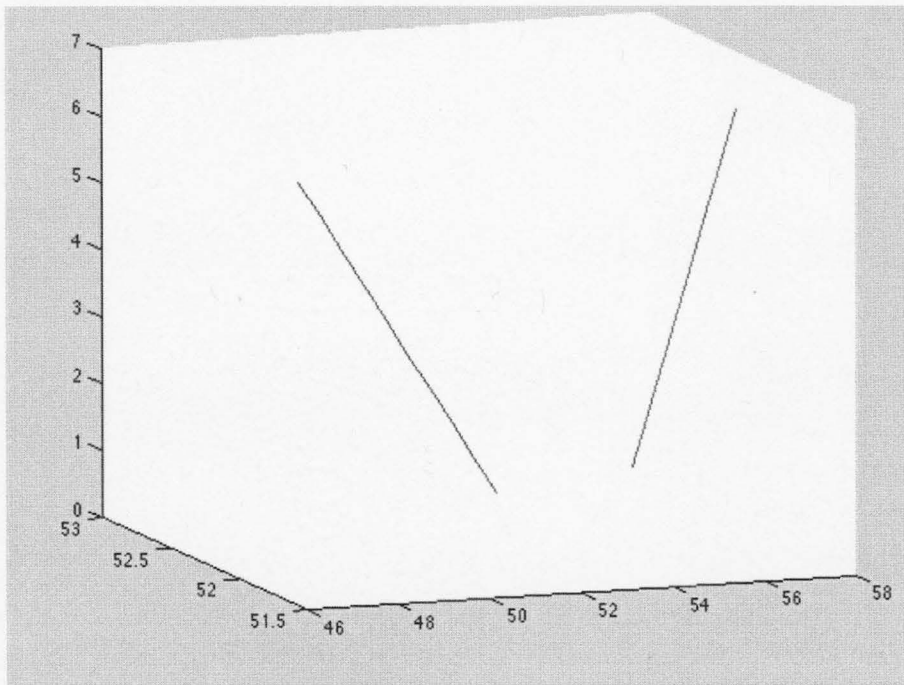


Figure 8: shows the result of estimating center-line for both branches of a bifurcation.

IV. DISCUSSION and CONCLUSIONS

It is difficult for radiologists to measure the angle of bifurcation in lung CT images. It is considerably more difficult to detect, localize and identify changes in successive temporal image sequences while working with 3D data sets which may often contain hundreds of images. It has been estimated that a radiologist often examines several thousand images/day. In such a context, the assessment of changes over time are not only tiresome but highly prone to inaccuracies. Thus, one can assist a radiologist in identifying a boundary of lumen and subsequently measuring the airway bifurcation angle which will help identification of temporal variation and help to speed up the process of diagnosis of diseases.

All lung assessment methods start with segmenting the airway lumen (e.g. [6-11]), which has lower Hounsfield unit (HU) comparing to the airway wall. Jong *et al.* [17] reviewed such work on lung characterization and relationship between features and diseases until 2005, providing a useful list of references. We used an accurate method [12] (see chapter 5) with no leaking (over segmenting) problem to segment the lumen.

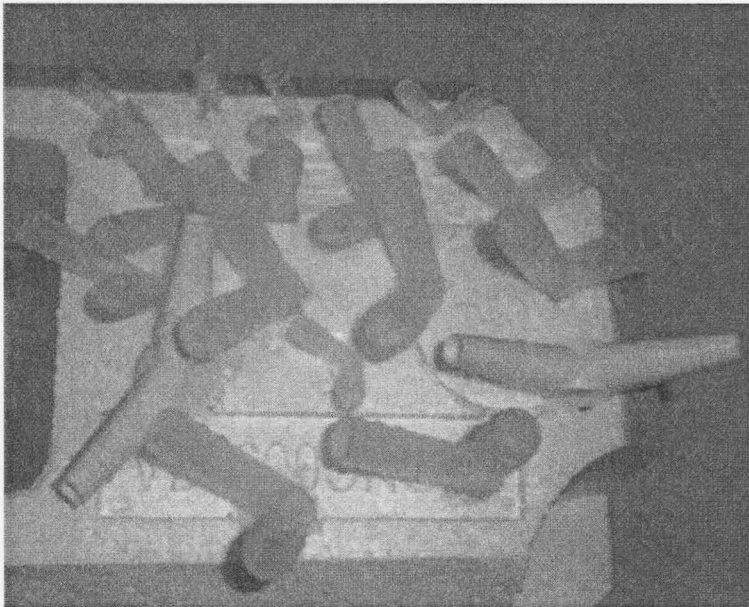


Figure 9: Shows a photo of phantom.

We are able to apply this method on neighboring slices automatically. Our results demonstrate accurate identification of the centerline of the airways.

There is some research work on measuring airway angles. Wood *et al.* [2,3] used 3D seeded region growing algorithm (SRGA) to segment airway lumen from its wall. Then by averaging x-, y-, and z-values of pixels at each cluster, their algorithm reduced the segmented area to central axis. By finding the nearest point to the three central axis which are forming a bifurcation, their algorithm identifies the branching point. Then by connecting the branching points, it is able to calculate the bifurcation angle. Since lung airways are generally not straight (i.e. they have curves at the end of each branch), this method may not be sufficiently accurate. On the other hand, our method does not need to find the branch point where it calculates the bifurcation angle based on the line estimation of each branch separately. It also considers 60% of the center points of each branch. By comparing two different methods for finding the center point of the lumen (see part C of II and Table II), we found the morphological method is more accurate than the averaging method. As well, the method that we used for segmenting airway lumen [12] (see chapter 5) is more accurate than the 3D SRGA, which is very sensitive to the selected threshold. Another problem, while using SRGA, is the leaking problem which results in producing some false branches and will corrupt the result of any angle measurements.

Kitaoka *et al.* [4] simulate lung airways using several equations which does not require real lung CT image to work. It is also for simulating non-disease lung which can be used to compare the result of angle measurements methods on non-disease lung CT

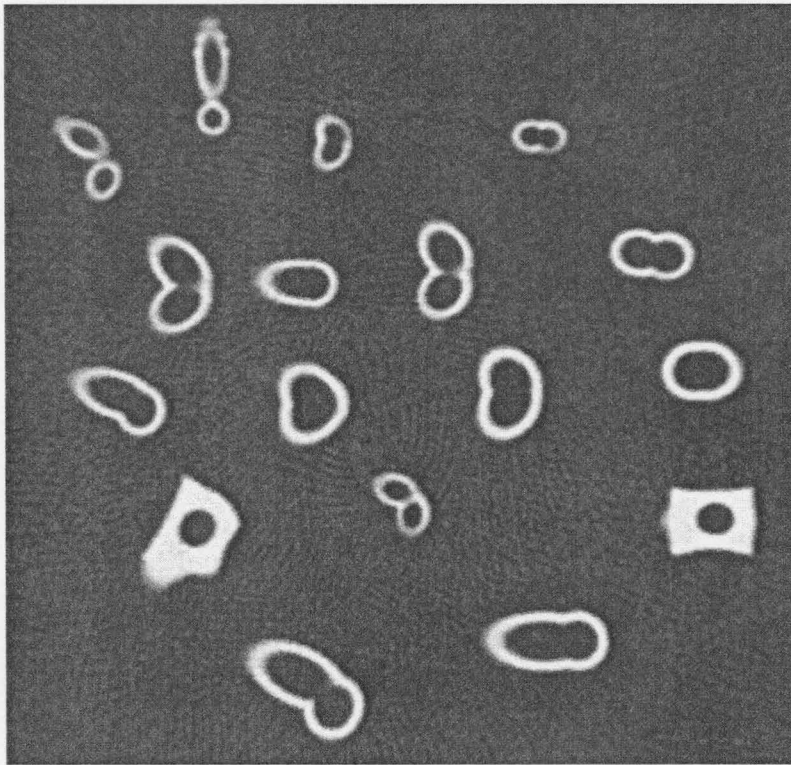


Figure 10: Shows a CT slice of this phantom, where this slice positioned near to the bifurcation area of most of pipes.

images. In another related work, King *et al.* [5] found the direction of airway at each point based on two adjacent slices. They found the angle between the airway and the line perpendicular to the slice plane.

Finding the airway centerline may be affected from some side effects (i.e. partial volume, noise, artifacts, etc.), thus it will be beneficial to include as many slices as possible (except those near the bifurcation) and then estimate the centerline over several neighboring slices. This is one advantage of our method compared to [2,3]. Also using our previous method for segmenting the lumen [12] (see chapter 5), our algorithm ends up with a more accurate lumen boundary and consequently more accurate airway centerline and accurate angle measurement.

In summary: *first*, our method for estimating centerline benefits from both the speed of the SRGA and the accuracy of the LSM. Also based on the fact that the center point of the elliptical shape of the lumen (when the airway is not perpendicular to the plane) is the center of circular airway lumen, there is no need for time-consuming reconstruction of 3D CT images, in order to ensure a perpendicular airway to the plane. *Second*, by using (4) for measuring the angle, our algorithm does not need to find the intersection of the

branches to the centerline. *Third*, by comparing two different methods for finding the center of the lumen, we found that the morphological method is more accurate. *Fourth*, these whole steps for measuring bifurcation angle need a minimal amount of user interaction. Thus, after selecting one slice from CT images, the algorithm needs just two inputs: one mouse click (the seed for region growing algorithm) and one input number ± 1 (tapering direction). The rest of the subsequent processing is fully automatic.

ACKNOWLEDGEMENTS

Funding for this work was provided through a fellowship to Mr. Mohammadreza Heydarian. Dr. Mark Kamath and Dr. Skip Poehlman's participation was supported in part by Natural Sciences and Engineering Research Council (NSERC; Canada) Discovery Grants to both.

References

- [1] R.C. Gonzalez and R. E. Woods, *Digital Image Processing*, 2nd Ed., Upper Saddle River, NJ, Prentice Hall, 2002, Chapter 10.
- [2] S. Wood, J. Hoford, E. Hoffman, E. Zerhouni, and W. Mitzner, "Quantitative 3-D reconstruction of airway and pulmonary vascular tree using HRCT", SPIE vol. 1905, pp. 316-323, 1993.
- [3] S. Wood, E. Zerhouni, J. Hoford, E. Hoffman, and W. Mitzner, "Measurement of three-dimensional lung tree structures by using computed tomography", American Physiological Society, pp. 1687-1697, 1995.
- [4] H. Kitaoka, R. Takaki, and B. Suki, "A three-dimensional model of the human airway tree", *Journal of Applied physiology*, vol. 87, Issue 6, 2207-2217, Dec. 1999.
- [5] G. G. King, N. L. Muller, K. P. Whittall, Q. Xiang, and P. D. Pare, "An Analysis Algorithm for measuring Airway Lumen and Wall Area from High-Resolution Computed Tomographic Data", *Am J Respir Crit Care Med*, Vol. 161, pp. 574-580, 2000.
- [6] Y. Nakano *et al.*, "Development and validation of human airway analysis algorithm using multidetector row CT", *Medical Imaging, Proc. SPIE* vol. 4683, 2002.
- [7] X. Zhou *et al.*, "Automatic segmentation and recognition of anatomical lung structures from high-resolution chest CT images", *Computerized Medical Imaging and Graphics*, vol. 30, pp. 299-313, 2006.
- [8] O. Weinheimer *et al.*, "About objective 3-D analysis of airway geometry in computerized tomography", *IEEE Trans. Medical Imaging*, vol. 27, No. 1, Jan. 2008.
- [9] J. Lee *et al.*, "Human airway measurement from CT images", *Medical Imaging, Proc. SPIE* vol. 6515, 2008.

- [10] J. Tschirren, E. Hoffman, G. McLennan, and M. Sonka, “Intrathoracic airway trees: segmentation and airway morphology analysis from low-dose CT Scans”, IEEE Trans. Medical Imaging, vol. 24, NO.12, Dec. 2005.
- [11] B. L. Odry, *et al.*, “Active contour approach for accurate quantitative airway analysis”, Proc. of SPIE vol.6916, 691613, 2008.
- [12] M. Heydarian, M. Noseworthy, M. Kamath, C. Boylan, W. Poehlman, “Optimizing the level set algorithm for detecting object edges in MR and CT images”, IEEE Trans. Nuclear Science, Vol. 56, No. 1, pp.156-166, Feb. 2009.
- [13] S. Osher, J. A. Sethrian, “Fronts propagation with curvature-dependent speed: algorithms based on Hamilton-Jacobi formulations”, J. Computation Physics, vol. 79, pp. 12-49, 1988.
- [14] C. Li, C. Xu, C. Gui, and M. D. Fox, “Level Set Evolution Without Re-initialization: A new Variational Formulation”, IEEE Computer Society Conference on Computer Vision and Pattern Recognition, vol. 1, pp. 430-436, 2005.
- [15] V. Caselles, F. Catte, T. Coll, and F. Dibos, “A Geometric Model for Active Contours in Image Processing”, Numer. Math., vol. 66, pp. 1-33, 1993.
- [16] D. E. Goldberg, *Genetic Algorithm in Search, Optimization, and Machine Learning*, Boston, MA, USA, Addison-Wesley professional, 1989, Chapters 1-3.
- [17] P. Jong, N. Muller, P. Pare, and H. Coxson, “Computed Tomographic imaging of the airways: relationship to structure and function”, Eur Respir J, vol. 26, NO. 1, pp. 140-152, 2005.

TABLE I: Shows the result of angle measurements on Y-Shape pipes with 6.0mm inner diameter while considering all, or some percentage of slices.

	100% of slices		80% of slices		60% of slices		40% of slices		20% of slices	
P i p e #	Number of slices for branch1 and branch2	Angle based on Method 1 and Method 2	Number of slices for branch1 and branch2	Angle based on Method 1 and Method 2	Number of slices for branch1 and branch2	Angle based on Method 1 and Method 2	Number of slices for branch1 and branch2	Angle based on Method 1 and Method 2	Number of slices for branch1 and branch2	Angle based on Method 1 and Method 2
1	30,30	59.60 59.43	24, 24	59.86 59.44	18, 18	59.73 59.23	12, 12	59.45 58.30	6, 6	58.52 52.19
2	29, 28	60.08 59.66	22, 22	59.84 59.73	17, 17	59.91 59.40	12, 11	59.75 59.20	6, 6	53.86 55.75
3	25, 25	59.46 59.43	20, 20	59.06 59.36	15, 15	59.34 59.23	10, 10	56.94 58.74	5, 5	53.53 55.29
4	30, 30	59.59 59.56	24, 24	59.75 59.56	18, 18	59.55 59.74	12, 12	59.51 59.69	6, 6	59.14 59.40

TABLE II: Shows the result of angle measurements where the actual angle for types 1-3 are 60 degree (with 3.0mm, 5.0mm, and 6.0mm inner diameter for types 1,2, and 3, respectively) and for type 4 is 120 degree. Method-1 uses thinning function and Method-2 uses top-down-left-right method for finding lumen center.

Different Y-shape pipes at various direction	Methods for finding lumen center	Number of slices (0.7mm thick) to be considered for angle measurement							
		12	dev.%	10	dev.%	7	dev.%	5	dev.%
Type 1 Direction1	Method 1	60.05	0.09	59.58	0.69	58.80	2.00	58.62	2.29
	Method 2	59.26	1.23	58.92	1.79	57.28	4.53	55.78	7.02
Type 1 Direction2	Method 1	59.26	1.22	59.46	0.89	56.77	5.37	56.54	5.76
	Method 2	59.32	1.13	58.89	1.84	57.39	4.34	56.48	5.86
Type 1	Method 1	60.27	0.46	60.28	0.48	59.48	0.87	58.96	1.73
Direction3	Method 2	59.09	1.51	58.81	1.97	58.86	1.89	57.15	4.74
Deviation on Type1	Method 1		0.59		0.69		2.74		3.26
	Method 2		1.29		1.87		3.59		5.87
Type 2 Direction1	Method 1	59.58	0.70	59.77	0.38	57.59	4.01	52.32	12.80
	Method 2	59.54	0.76	59.35	1.07	57.53	4.11	53.39	11.02
Type 2 Direction2	Method 1	59.51	0.80	59.69	0.50	57.65	3.91	54.11	9.80
	Method 2	58.71	2.14	58.87	1.88	57.41	4.31	55.63	7.28
Type 2	Method 1	59.16	1.39	57.46	4.23	53.72	10.46	49.81	16.97

Direction3	Method 2	60.81	1.37	60.60	1.00	58.41	2.64	57.97	3.37
Type 2 Direction4	Method 1	58.47	2.54	58.34	2.76	57.70	3.82	56.77	5.37
	Method 2	59.54	0.76	59.46	0.90	57.70	3.82	57.11	4.80
Type 2 Direction5	Method 1	59.26	1.23	59.62	0.63	60.01	0.02	57.45	4.24
	Method 2	59.40	0.99	59.53	0.78	59.17	1.37	57.30	4.50
Deviation on Type2	Method 1		1.33		1.70		4.44		9.84
	Method 2		1.20		1.13		3.25		6.19
Type 3 Direction1	Method 1	59.04	1.60	57.45	4.24	54.44	9.26	53.65	10.58
	Method 2	58.42	2.63	58.43	2.61	58.25	2.91	56.23	6.27
Type 3 Direction2	Method 1	59.66	0.56	57.98	3.36	62.44	4.08	53.43	10.94
	Method 2	59.38	1.02	58.35	2.75	57.71	3.81	55.20	7.99
Type 3 Direction3	Method 1	59.80	0.33	59.38	1.02	58.84	1.92	57.29	4.51
	Method 2	58.52	2.45	57.58	4.03	53.85	10.25	49.26	17.88
Type 3 Direction4	Method 1	60.38	0.63	59.84	0.25	59.96	0.05	58.37	2.71
	Method 2	59.82	0.29	60.02	0.05	59.81	0.31	57.92	3.45
Type 3 Direction5	Method 1	61.16	1.94	61.37	2.30	61.90	3.17	64.14	6.90
	Method 2	59.58	0.70	59.74	0.43	58.57	2.38	57.84	3.59
Deviation on Type3	Method 1		1.01		2.23		3.70		7.13
	Method 2		1.42		1.97		3.93		7.84
Type 4 Direction1	Method 1	118.7 3	1.06	118.69	1.09	119.7 6	0.19	118.6 1	2.31
	Method 2	119.2 7	0.60	118.96	0.86	120.4 4	0.37	119.2 1	1.31
Type 4 Direction2	Method 1	118.4 7	1.27	118.26	1.45	121.1 5	0.96	N/A	N/A
	Method 2	120.3 5	0.29	119.48	0.43	120.7 8	0.66	N/A	N/A
Deviation on Type4	Method 1		1.17		1.27		0.58		2.31
	Method 2		0.45		0.64		0.52		1.31
Ave. on Dev. %	Method 1		1.05		1.62		3.34		6.62
Ave. on Dev. %	Method 2		1.19		1.49		3.18		6.03

6.3 Summary of article

Similar to the part discussed for second paper, to find the precision of this measurement, one needs to measure the anatomy of lung with pathology. This is a suggestion for future work. The limitation with simulating the lung using the phantom explained here in this paper is that it is impossible to make a phantom to show all properties of real lung. One property is that all lung airways have a curvature where the simulated airways are completely straight. The other property is that all healthy lung airways have tapering through the next level of branching which can not be simulated using existing Y-shape pipes.

Chapter 7: Conclusion and Future Work

7.1 Introduction

Medical imaging plays an important role in diagnosis of certain diseases. Radiologists who use imaging technology are trained to observe and recognize normal and pathological variations of anatomical structures, obtained through various forms of medical imaging technologies. Medical imaging devices such as MRI and CT, nowadays, produce very high quality images (of sub-millimeter isotropic voxel resolution) of internal body structures. These technological advances provide radiologist/physicians the ability to localize and classify even minute abnormalities in organs (lesions). Although higher quality images apparently increase the probability of accurate diagnosis, the process takes more time for the radiologist to interpret all the available information. For instance, when a voxel thickness is reduced from 5 mm to 1 mm and its X-Y dimensions are reduced from $2\text{mm} \times 2\text{mm}$ to $0.5\text{mm} \times 0.5\text{mm}$, the number of slices is increases five times and number of pixels in each slice is increases four times.

In general, medical equipment industry which builds these medical imaging devices (i.e. MRI, CT) embeds image-processing utilities which performs rudimentary processing as resizing and filtering, in the commercial software sold to the customer. Several multi-purpose packages (i.e. AFNI, ITK/VTK, Osirix) are also available for fundamental processing such for resizing, filtering, basic segmentation, and limited registration (e.g. are designed for specific organs such as the brain). None of these packages were suitable for the current project, so it became necessary to design and develop new software-package for automatically characterizing lung CT images. Several novel suggestions originating from the radiologist were incorporated into the software. A number of other ideas are included in suggestions for future work.

To aid radiologists in measuring airway luminal diameter and wall thickness, the program queries the user to select a slice number and then asks the user to click on the interested lumen area (not necessarily the exact center). The user is next asked to specify the direction of airway tapering in addition to selecting a slice number and clicking on the area of interest within the lumen. In addition to showing the result of lumen diameter and wall thickness measurements, this program shows the image with the lumen boundary being highlighted. Also it provides those points on the outer wall border which are used for the measurement of wall thickness. Further, it plots the measurements over slices and gives the average and standard deviation of measurements of all slices over that branch. An example for this is provided in figure 9 in Chapter 5.

The program also illustrates lumen boundary pixels on a black and white 3D plot after tracing a branch or after tracing a bifurcation. This output helps the user to see the results of the program in a simple illustration which makes it easier to find any errors and/or any lung abnormality by visualization. Also this illustration helps in extending the program by showing the position of the lung that has some specific properties and/or abnormalities.

7.2 Knowledge Base Systems for Diagnosis of Lung diseases

Much research has been done on finding the relation between the quantitative assessment of lung airways (using CT images and/or histological examination of excised lungs) and lung diseases. While (to our knowledge) all of these methods characterize the lung condition manually or semi-automatically processing CT images, software reported in this thesis has been developed with minimal user interaction than previously required to characterize lung CT images. The next step is to characterize a group of lung CT images which involve patients who have been diagnosed with a specific disease. Through a radiologist (CB), access to St. Joseph's Healthcare database can be obtained in order to gather a specific group. A very small control group has been established involving a normal population. A confounding situation exists here because there is no practical manner in which to scan healthy volunteers by CT scanner without the risk of X-ray exposure. The only method to establish a normal group is to look at all lung CT images to collect patients with thoracic problems requiring CT scanning but otherwise having healthy lung tissue. Currently, CT images of 17 patients suffering from asthma are available although no control group data exists. Therefore it is not possible to confirm the hypothesis on the relation between lung CT properties and specific diseases, and consequently it's not practical to develop a knowledge base system for automatically recognizing some lung diseases, as was originally anticipated.

Developing a knowledge base system (or an expert system), based on the result of lung-characterization program, will allow us to more accurately assess and diagnose these diseases more confidently and at an earlier stage. It is expected that through the use of current software, one will be able to demonstrate changes in various measured parameters before and after a drug therapy. This will be particularly important in the assessment of therapeutic response to airway modifying agents or therapies (thermoplasty) in the treatment of asthma and chronic obstructive pulmonary disease (COPD).

To illustrate the application of the software to classify the CTs of patients suffering from asthma, the procedure outlined in the present thesis was applied to 17 patients suffering from asthma. **Table I** shows the result of measuring inner luminal diameter and luminal wall thickness for two or three slices per case. These slices and the lumen in each slice were selected by a Radiologist (CB) from CT images with 1.25mm thickness, 0.7mm × 0.7mm for X-Y dimension (0.175mm after resizing), and 10 mm to 20 mm gap between slices. The ratio of 1/6 could be set as a threshold for the diagnosis a lung disease. If the thickness to diameter ratio (TDR) can be set to 1/6 or less as being healthy, then a TDR that is larger than 1/6 shows a possibility of a disease. **Fig 1** provides a plot based on the TDR column of Table I. **Fig 2** shows the average of deviation from 1/6 for each case. As we see in **fig 2**, $avg(TDR) - (1/6)$ in most of the cases is larger than zero which is positive evidence for our hypothesis. To unambiguously prove this kind of hypothesis, it is necessary to examine data from healthy subjects.

TABLE I
Results of luminal diameter and wall thickness measurements and their computed ratio.

Case #	Slice #	Wall thickness (mm)	Airway Lumen Diameter (mm)	Airway External Diameter (mm)	Thickness to Diameter Ratio (TDR)	TDR-(1/6)	Average of TDR-(1/6) per case
1	13	1.3825	3.5888	6.3538	0.2176	0.0509	
	14	0.8120	1.8692	3.4932	0.2325	0.0658	0.0584
2	11	0.6753	3.3344	4.6849	0.1441	-0.0225	
	13	0.8095	1.9157	3.5346	0.2290	0.0623	0.0199
3	12	1.4152	2.5874	5.4178	0.2612	0.0945	
	14	0.7366	0.6306	2.1038	0.3501	0.1835	0.1390
4	21	0.9834	2.2065	4.1733	0.2356	0.0690	
	22	0.9483	2.9642	4.8607	0.1950	0.0284	0.0487
5	11	0.6054	3.0793	4.2902	0.1411	-0.0255	
	12	0.6756	4.6547	6.0060	0.1125	-0.0542	-0.0399
6	19	0.5262	5.7145	6.7670	0.0778	-0.0889	
	20	1.4113	3.4912	6.3138	0.2235	0.0569	
	21	0.7975	2.4543	4.0493	0.1970	0.0303	-0.0006
7	18	0.9466	4.9819	6.8751	0.1377	-0.0290	
	19	1.1061	4.7365	6.9487	0.1592	-0.0075	-0.0182
8	18	0.7656	4.5938	6.1250	0.1250	-0.0417	
	19	0.9685	3.0066	4.9436	0.1959	0.0292	0.0584
9	68	1.0197	4.7005	6.7399	0.1513	-0.0154	
	69	1.303	3.0195	5.6255	0.2316	0.0650	0.0584
10	70	1.1106	5.6505	7.8717	0.1411	-0.0256	
	71	1.1613	5.8932	8.2158	0.1413	-0.0253	
	76	0.9215	4.1064	5.9493	0.1549	-0.0118	-0.0209
11	12	2.2999	2.1474	6.7472	0.3409	0.1742	
	13	0.7660	2.5443	4.0762	0.1879	0.0212	0.0584
12	19	0.5274	3.4254	4.4803	0.1177	-0.0489	
	20	1.4685	1.665	4.602	0.3191	0.1524	
	21	0.7241	2.1268	3.5749	0.2025	0.0359	0.0465
13	10	0.6864	3.496	4.8688	0.1410	-0.0257	
	11	1.1027	2.1239	4.3293	0.2547	0.0880	0.0584
14	18	1.3906	2.5451	5.3263	0.2611	0.0944	
	19	1.2035	2.086	4.493	0.2679	0.1012	0.0584
15	18	2.9031	2.0095	7.8157	0.3714	0.2048	
	19	1.8899	2.6305	6.4103	0.2948	0.1282	
	20	1.786	1.4265	4.9985	0.3573	0.1906	0.1745
16	8	0.7022	1.9692	3.3735	0.2081	0.0415	
	9	0.8992	0.87109	2.6695	0.3368	0.1702	0.0584

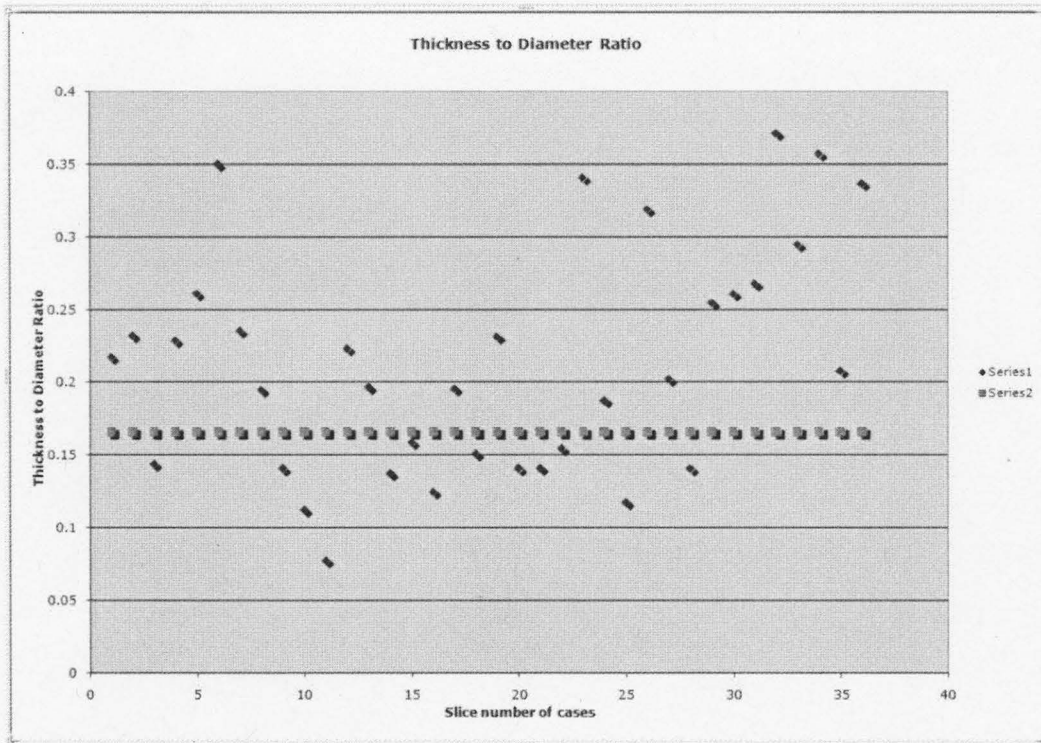


Figure 1: A plot of the dispersion of the Thickness to Diameter Ratio from Table I.

7.3 Suggestions for Future Work

In this PhD research, the focus has been on developing segmentation-based algorithms for quantitative analysis of CT and MRI images. This included segmenting and characterizing of the airways in the lung. Such segmentation procedure was fundamental for further measurements such as airway luminal diameter, bronchial wall thickness and bronchial bifurcation angle measurements. These measurements are of critical importance in the understanding of a number of lung diseases including asthma and COPD. As the approach used here has been shown to be accurate with phantom studies, further verification of these algorithms using formaldehyde-fixed animal lung will need to be performed. Further developments of the software can take a number of possible pathways.

The current algorithm is now only able to trace a part of the bronchial tree. In other word, this algorithm is only able to track airways which have at most, an angle of 60 degrees to the perpendicular line drawn to the slice plane. Thus the algorithm needs to be extended in order to segment the entire bronchial tree, where it will be able to perform

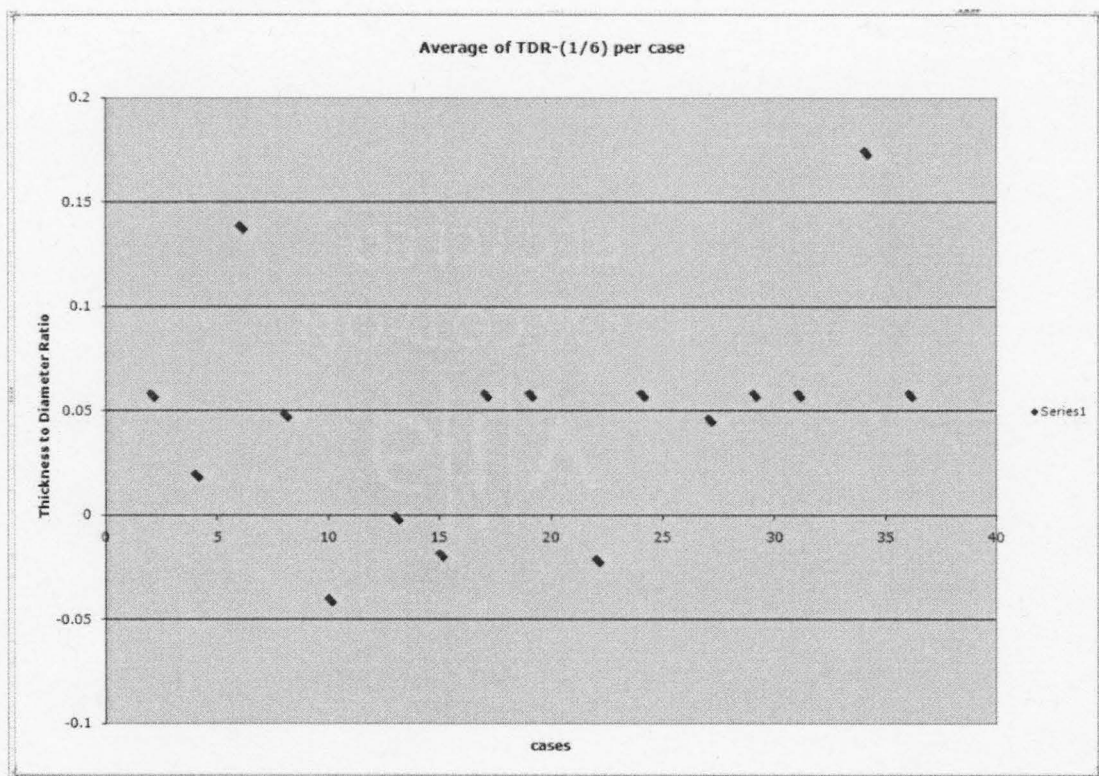


Figure 2: shows the average of deviation of TDR from 1/6 for each case.

additional measurements and statistical calculations. Such an algorithm would need CT lung data in 3D.

Three other enhancements remain to be implemented:

- a. The analysis system could be of much help to the production radiologist with the display and presentation of calculated luminal characteristics (diameter, wall thickness, ratio of interest, wall tapering, etc.) on the Apple/Osiris-based working environment used by practicing radiologists. This needs to be carefully done disrupt the normal working procedures of the radiologist, which seem to be unique for each radiologist. This is an interesting and non-trivial study in itself in the field of human-computer interaction (HCI).
- b. An independent study for evaluating the reproducibility of measurements obtained on the same data at different times by the same radiologist and by multiple radiologists need to be performed to characterize intra- and inter- observer errors.
- c. A third enhancement would be to compare the same subject's progress in time in response to a medical intervention in time. Such a development would help the radiologist track the progress or regression of a disease over time.

For comparing the luminal diameter and wall thickness, a measurement needs to be taken using the Full-Width at Half-Maximum (FWHM) technique on both, phantom

and animal lung models. In previous reports, the FWHM method is involved, where researchers used a fixed threshold and/or manually edit away the casted rays to the luminal wall. Thus, to minimize the user interaction, it is necessary to modify FWHM method in order to eliminate the requirement of a fixed threshold or any manual editing.

Following an analysis of results of using the current algorithm using a histological examination of animal lung, and also by extending the program as described above, it would be very useful to implement a diagnostic Expert System. This is an artificial intelligence technique, which implements rules that are used by physicians for disease recognition. When complete, the user of this expert system will be able to assess the probability of any specific disease or whether there is evidence of any disease. In both cases, the expert system should present the logic and list those rules that were used as well as uncertainty factors.

Following suggestions may be considered for further development of the software described herein:

- a. Implementation and execution of the software in C++.
- b. Parallel and clustered computing may be attempted to provide almost real time feedback to the radiologist in order to expedite his/her diagnosis and increase his/her productivity.
- c. As part of software integration, it is also necessary to provide an 'easy to use' interface
- d. Reconstructing the lung in 3-D using isometric voxels with new memory management procedures would enable processing of larger datasets of lung images, looking for specific disorders.

7.4 Summary

While the current version of the software needs to be validated using histological examination of a human/animal lung, our results using the phantom combined with the visual assessment by a radiologist have confirmed its potential in a clinical setting. Further, the reproducibility of the procedure as applicable to various sets of test data gives us confidence that the algorithm can be used for inter- or intra- subject comparison purposes.

The MATLAB environment for implementing and evaluating the present software, results in much higher run time during execution, which can be shortened by compiler based languages such as C or C++. But at this step of project, the run time of algorithm is deemed acceptable for measuring lumen diameter and wall thickness over one branch or measuring angle for several branches. The bigger the area of the image being examined, longer it takes to perform segmentation. Currently, it takes 10 to 20 seconds for segmenting the lumen and measuring lumen diameter and wall thickness (using Apple iMac with 2.33 GHz Dual Intel Core and 3 GB memory). This means that tracing a branch with 20 slices (0.7mm thickness) takes 3.3 minutes to 6.6 minutes and measuring an angle takes approximately 7-13.2 minutes. While characterizing the smaller

airways (after 6th level of airway branching) the actual time on the sample sets of images is about 7 minutes to measure the angle.

The development of these tools will allow the user (a senior Radiologist) to provide logistical support for ongoing clinical trials in Respiriology and Thoracic Surgery at McMaster University. This type of quantitative assessment of a CT examination is considered by the health care professionals to be an advanced health technology related to digital imaging. The completed software solution for quantitative analysis of lung CT has strong potential for commercialization in the future. These systems will be particularly attractive to picture archiving and communication systems (PACS) vendors or may be marketable as a plug-in for PACS systems in the future. It is also likely that quantitative assessment of a CT examination performed on a lung has the potential to become routine in clinical and research practice in the near future.